Investigations of Parameters Impacting Transmembrane Electrophoresis for Improved SDS Depletion of Proteome Samples for Mass Spectrometry

by

Nicole Unterlander

Submitted in partial fulfilment of the requirements
for the degree of Master of Science

at

Dalhousie University
Halifax, Nova Scotia
June 2018

Table of Contents

List of Tables

List of Figures

Abstract

Sodium dodecyl sulfate (SDS) is a favoured reagent for proteomic sample preparation but detrimental to down-stream analysis by liquid chromatography and mass spectrometry (LC-MS). This group previously introduced a novel electrophoretic device termed transmembrane electrophoresis (TME), which depletes SDS to levels permitting LC-MS (≤100 ppm) while maintaining high protein yield (Kachuk *et al*. *J. Proteome Res.* **2016**, p2634). Initially, TME required lengthy runs (1 hour), and frequent pausing/manual mixing to prevent overheating. As such, this thesis presents TME modifications to allow operation at higher currents, which increases the rate of SDS depletion. Changing different membrane parameters provides lower resistance thereby decreasing Joule heating. Operation at constant current (instead of constant voltage or power) is determined to be optimal by minimizing heat production. Increasing beyond 50 mA demands additional strategies for temperature management. Here, TME operation with a stir bar to agitate the sample cell is presented as a fully automated alternative to pausing/manual mixing. Constant stirring is shown to significantly reduce sample temperatures, allowing operation at higher constant current (70 mA). In doing so, the time required for SDS depletion below 100 ppm is reduced to ≤15 min. Reduced temperatures also translate to higher sample yields ≥95%. The stir bar also reduces concentration polarization and membrane fouling phenomena which reduces resistance and increases depletion rates. Finally, the application of the improved TME platform to bottom-up and top-down workflows is assessed in comparison to two popular depletion methods, acetone precipitation and filter-aided sample preparation (Wiśniewski *et al*. *Nat. Methods* **2009**, p359). All methods successfully deplete SDS from a proteome mixture to ≤10 ppm, though TME provides consistently higher sample yields (≥95%). TME also gives higher peptide spectral matches per protein when analyzed by LC-MS, and favours the identification of low molecular weight proteins, which are often underrepresented in proteomics studies.

List of Abbreviations Used

2-DE	Two-dimensional gel electrophoresis
ANOVA	Analysis of variance
BCA	Bicinchoninic acid
BHb	Bovine hemoglobin
BSA	Bovine serum albumin
BUP	Bottom-up proteomics
CE	Capillary electrophoresis
CID	Collision induced dissociation
C. reinhardtii	*Chlamydomonas reinhardtii*
Da	Dalton
DTT	Dithiothereitol
DNA	Deoxyribonucleic acid
EME	Electromembrane extraction
ESI	Electrospray ionization
E-SPE	Electric field assisted solid phase extraction
FASP	Filter-aided sample prep
FT-ICR	Fourier transform ion cyclotron resonance
FWHM	Full width at half maximum
GELFrEE	Gel-eluted liquid fraction entrapment electrophoresis
GRAVY	Grand average of hydropathy
HSM	High salt medium
HPLC	High performance liquid chromatography
IAA	Iodoacetamide
IEF	Isoelectric focusing
LC	Liquid chromatography
LC-MS	Liquid chromatography mass spectrometry
LC-MS/MS	Liquid chromatography tandem mass spectrometry
LC-UV	Liquid chromatography ultraviolet
m/z	Mass to charge ratio
MALDI	Matrix-assisted laser desorption/ionization
MBAS	Methylene blue active substances
MS	Mass spectrometry/ mass spectrometer
MS/MS	Tandem mass spectrometry
MW	Molecular weight
MWCO	Molecular weight cut off
NP	Nernst-Planck
pI	Isoelectric point
PSM	Peptide spectral match/peptide spectral count
PTFE	Polytetrafluoroethylene
PTM	Post-translational modification
QqTOF	Quadrupole-time-of-flight
RNA	Ribonucleic acid
RP	Reverse phase

RPLC	Reversed phase liquid chromatography
S. cerevisiae	*Saccharomyces cerevisiae*
SDS	Sodium dodecyl sulfate
SDS-PAGE	Sodium dodecyl sulfate polyacrylamide gel electrophoresis
SLM	Supported liquid membrane
TDP	Top-down proteomics
TFA	Trifluoroacetic acid
TIC	Total ion chromatogram
TME	Transmembrane electrophoresis
TPCK	N-tosyl-L-phenylalanine chloromethyl ketone
Tris	Tris(hydroxymethyl)aminomethane
UV	Ultraviolet
$\times g$	Times acceleration of gravity

Acknowledgments

I would first like to thank my supervisor Dr. Alan Doucette for all the wonderful learning opportunities he has provided me over these last few years. His enthusiasm for research, teaching, and entrepreneurial pursuits is contagious and inspirational. I thank him for providing me with unending helpful criticism, extensive training, and life advice throughout the years. I would also like to thank my committee members Dr. Heather Andreas and Dr. Dev Pinto for helpful guidance and feedback, and for reviewing my thesis. In addition, I would like to thank Dr. Roderick Chisholm, Dr. Peter Wentzell, and Xiao Feng for their advice and assistance with my research throughout the years. I would also like to extend a special thank you to Mike Boutilier for his help with construction and design of some of the parts used in this thesis.

I would also like to acknowledge funding sources: Dr. Jean Cooley fellowship in analytical chemistry, and the Natural Sciences and Engineering Research Council.

Thank you to my wonderful lab mates and friends within the department Subin Raj, Jess Nickerson, Steve Driscoll, Phil Jakubec, Kirsten Jones, Zach Caterini, Renée Abbott, and Mallory Davis. Thank you for all the coffee, laughs, good memories, and emotional support; my time at Dalhousie would not be the same without you.

Finally, I would like to thank my friends and family in Ontario and Nova Scotia. I would have never been able to accomplish this without your constant encouragement and support. I would especially like to thank my parents Rick and Shelley and my brother Matthew, for all the love, encouragement, and understanding you've given me while I pursue this path. I would be nowhere without you.

Chapter 1: Introduction

1.1 Proteomics

Proteins are large macromolecules consisting of long folded chains of amino acids. They are often referred to as the "building blocks of life" and are fundamental to the biological reactions necessary for life (*e.g.* reproduction, movement, respiration, response to stimuli). Proteomics, in analogy with genomics, is the large-scale study of all proteins. Specifically, it comprises the analysis and characterization of the entire set of proteins produced by an organism at a given time, commonly known as the proteome. Proteins have been studied since the early 18th century when they were discovered as a biological molecule which coagulated upon addition of heat or acid. The first protein to be sequenced, insulin, by Frederick Sanger in the 1950s, confirmed that proteins were comprised of long polymers of amino acids[1,2]. Within a decade, protein structures had been resolved for hemoglobin and myoglobin proteins[3,4]. Protein research has since flourished into an important, relevant, and increasingly complex field. Functional proteins such as enzymes, ion channels, or receptors are frequently used as drug targets, and are the dominant focus of nutritional, immunological, cancer, biomarker, and proteopathic research fields. The true significance of proteins became known following the completion of the human genome project, when it was found that humans possess far fewer genes than originally estimated. The project discovered approximately 20-25 thousand protein-encoding genes[5], which is slightly fewer than a common roundworm[6]. The evidence indicated genes alone were not responsible for instilling humans with their biological complexity. It became clear that proteins are the functional units of a cell and their expression represents actual conditions within the cell at a given time. Although single-protein analysis can be enlightening, the

complexity of metabolic and other biosynthetic pathways requires a more holistic view. Studying networks of protein interactions and expression patterns under varying environmental conditions and disease states provides a more informative picture on the development and processes of life. The term proteome was coined in 1995 by Marc Wilkins[7], and since then the techniques for studying a proteome have developed quite rapidly. Nevertheless, analysis of any organism at the protein-level presents new and significant analytical challenges which must be overcome.

1.1.1 Goals and Challenges of Proteomic Studies

A proteome can contain a vast array of information on a variety of functionally and chemically distinct proteins over a large concentration and temporal range. In addition, variations in heterogeneity, post-translational modifications (PTMs), and splicing events gives rise to approximately 10^5-10^6 unique protein forms, also known as proteoforms. The term proteoform denotes all the different molecular forms in which the protein product of a single gene can be found[8]. Although seemingly trivial, analyzing which proteoforms are present at a given time in a sample is essential to gaining an overall understanding of the system, because different proteoforms can display massive differences in functionality. For example, phosphorylation can control the activity of a protein, alter its physical structure or cellular localization, induce protein-protein interactions, or even mark it for degradation. Multiple forms of PTMs exist, including acetylation, methylation, glycosylation, hydroxylation, and ubiquitination, each having their own specific purposes and outcomes. In addition, gene splicing adds to the variety of protein forms. When these types of events are altered or prevented, this can give rise to a multitude of cell functionality problems and ultimately disease/death.

Evidently, the complexity of a proteome cannot be understated, and it is inherently more difficult to work with than a genome. Most cellular proteins are expressed transiently, with an average half-life ranging from ~1.5 hours to 1-2 days[9], at which point they are degraded to prevent accumulation of toxic damage. Less abundant protein species are difficult to analyze without removal of highly abundant proteins (*e.g.* albumin, collagen, histones, ribosomal proteins, depending on the sample) which mask their detection. However, removal of highly abundant proteins risks sample loss *via* co-removal, loss of protein complexes, and a misrepresentation of expression ratios. Clearly, there is still a long and complicated pipeline between sample collection and obtaining results in modern proteomics research. This is one of the main hindrances to wide-spread implementation of mass spectrometry (MS) analysis in clinical settings, teaching laboratories, and other fields of research.

Despite the difficulties, proteomic research has significant impacts on a wide range of fields including medicine, biochemistry, chemistry, biology, pharmacology, atmospheric science, environmental science, and food science. For example, protein phosphorylation has tremendous impacts on the promotion of tumorigenesis because of its roles in the regulation of cell proliferation pathways, cell cycle progression, and autophagy[10]. Proteomic data has also been used in the drug discovery process in the identification of disease biomarkers and possible drug targets, elucidating their mechanisms of action, and evaluation of efficacy and toxicity[11]. Quantitative proteomic studies revealed the phosphorylation of cardiac troponin I as a biomarker for congestive heart failure[12]. In addition, studying changes in the abundance/PTMs of proteins in the cardiac proteome during hypertensive stress revealed new drug targets for the treatment of cardiac disease[12].

Alternatively, proteomics is used to provide insights on the response of various microorganisms to temperature, chemical, and environmental stressors indicative of climate change. Work in this area has provided the basis for improvement of wastewater treatment, bioremediation, genetically modified plants/crops, and environmental monitoring[13]. One of the most important goals of proteomics studies is improvement of sensitivity, specificity, and analytical methods for pre- and post-analysis. Advances in technology and methodology are still required to increase throughput, reproducibility, and sensitivity/selectivity of proteomic studies.

1.1.2 Methods for Proteomic Analysis

The field of proteomics encompasses many techniques for large scale identification and quantification of proteins, including 2-dimensional gel electrophoresis (2-DE), immunoassays, and MS-based methods. Although Wilkins and colleagues (1995)[7] are credited for the origin of the term proteomics, the idea of analyzing the complete set of proteins being produced by a cell came nearly 25 years before with the invention of 2-DE[14]. Through a combination of isoelectric focusing (IEF) and sodium dodecyl sulfate polyacrylamide gel electrophoresis (SDS-PAGE) two independent forms of separation were combined to resolve a sample of serum proteins. The basis of 2-DE encompasses separation of proteins according to their isoelectric points (pI) by IEF, and afterwards further separation by their mass (SDS-PAGE). This technique, after a few small changes by O'Farrell in 1975[15], is still widely used today because of its simplicity, affordability, high resolving power, and cooperativity with other techniques like electroblotting, immunoassays, Edman sequencing, and MS analysis. The resulting gels provide both qualitative and quantitative data, and have been shown to resolve up to 10,000 proteins at

once[16]. Some modern applications of 2-DE include use as an alternative detection method for protein modifications, identification of different protein isoforms, and analysis of pI and molecular weight (MW) outliers[17]. Following 2-DE, a variety of techniques is available for protein identification such as, N-terminal/C-terminal sequencing, or antibody recognition *via* immunoblotting assays. However, problems involving separation of minimally expressed proteins, hydrophobic proteins, and highly acidic/basic proteins limit the applicability of 2-DE to cooperative and abundant proteins of the proteome. In addition, the low reproducibility, and limited dynamic range leaves room for other techniques.

The major breakthrough in high-throughput protein identification technology came with the development of methods for protein analysis *via* MS. Until the 1970s, peptide and protein analysis by MS was not practicable, due to the low volatility and large MW of each protein, along with the lack of "protein-friendly" soft ionization techniques.

1.1.3 Mass Spectrometry

MS is an analytical technique used to measure the masses of different species in a sample. More accurately, MS ionizes chemical species and sorts them based on their mass-to-charge ratio (*m/z*). MS instruments have provided the largest contributions to the development of the field of proteomics due to the speed, sensitivity, and high-throughput capabilities. The scientific foundation and initial instrumentation for MS was developed in the early 20th century, but modern MS instruments are much more sophisticated with a variety of working configurations. Nonetheless, most MS contain at least 3 basic components: the ion source, the mass analyzer, and the detector. Each module has advantages and disadvantages associated with proteome analysis.

1.1.3.1 The Ion Source

The ion source functions to vaporize samples into the gas phase and ionize the analytes. Ionization and vaporization initially posed a critical challenge to the application of MS to protein samples. Difficulties in production of gas phase ions without causing sample degradation largely prevented the MS analysis of peptides, proteins, and any large polar/organic molecules.

Early ionization techniques such as electron and chemical ionization were too destructive for protein samples, being limited to small, thermally stable, volatile molecules. The ability to "softly" ionize molecules arrived with laser desorption techniques like secondary ion mass spectrometry and fast-atom bombardment[18]. These techniques proved to be highly sensitive and amenable to higher MW protein and peptide analysis (>1000 Da) but created significant background noise in the low mass regions of the spectrum due to a large portion of the energy from the laser being absorbed into the matrix.

Matrix-assisted laser desorption ionization (MALDI), is a soft ionization technique developed in the late 1980s, the more well-known version being described by Hillenkamp and collegues[19]. MALDI is amenable to the analysis of proteins or large organic molecules, and generally produces singly charged species making spectra analysis simple. Tanaka and colleagues applied a different version of MALDI to the analysis of large proteins (>25 kDa)[20]. Later Caprioli and colleagues adapted MALDI to chemically desorb and analyze compounds in a spatial arrangement to create a now popular technique known as MALDI imaging[21].

The most popular soft ionization method for proteins and peptides is currently electrospray ionization (ESI), and is the main technique employed in the experiments in this thesis. First introduced by Dole and colleagues in 1968[22]. ESI was refined in 1989 by Fenn and colleagues for use with large biopolymers, oligonucleotides, and proteins with masses up to 130 kDa[23]. ESI involves ionization by nebulizing a solution containing the analyte out of a fine needle tip and applying a potential difference of 1.5-5 kV between the sample tip and the MS entrance[18]. The applied voltage induces charge separation, forming sample droplets with a net positive or negative charge depending on the polarity of the needle. Each droplet emerges from the needle off of what is called a "Taylor cone", formed by the solution leaving the needle tip when exposed to an electric field (see Figure 1.1).

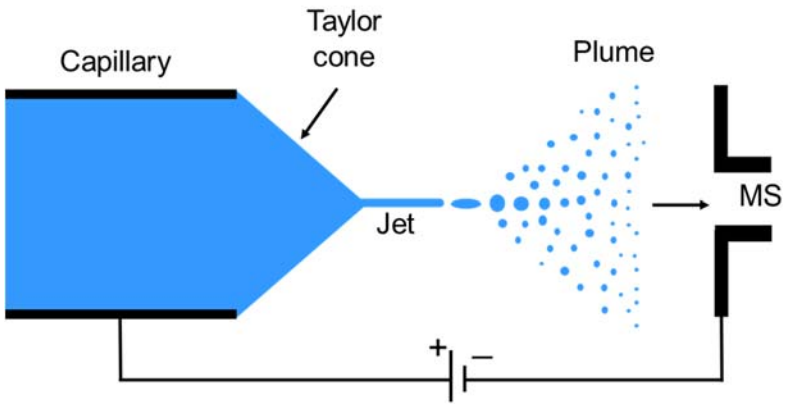

Figure 1.1 Schematic of the electrospray ionization mechanism. Application of a high voltage, promotes the formation of the Taylor cone which emits a jet of liquid droplets towards the mass spectrometer.

As the effects from the electric field become more prominent, and the effects from regular surface tension get smaller, the combination of these forces forms the characteristic cone shape. Once a threshold voltage is reached, the tip of the cone breaks and forms what is known as a "cone-jet", emitting a jet of liquid droplets towards the MS. The droplets are then partially desolvated *via* passage through a heated capillary or with a counter current

of nitrogen gas. As the large droplets evaporate, the repulsive Coulombic forces between the ions inside eventually overcomes the surface tension of the droplet, and the droplet bursts to form smaller droplets. Eventually, solvent-free ions are produced and can enter the MS. The final stages of this mechanism are under debate and a few different models have been presented[24]. This ionization technique results in the formation of multiply charged protein ions, which display a characteristic "charge envelope" on the produced spectra. Charge envelopes contain multiple peaks on a mass spectrum corresponding to the same molecule but with different amounts of charge. They can make the resulting spectrum quite complex and difficult to interpret. The appearance of a given charge envelope can be influenced by many experimental factors such as pH, flow rate of drying gas, and temperature. As a liquid phase technique, ESI allows a direct interface between MS and separation techniques like high performance liquid chromatography (HPLC). However, ESI has a low tolerance to contaminants resulting in reduced sensitivity. Shortly after the popularization of ESI, Wilm and Mann in 1996 demonstrated nano-electrospray (nanospray) techniques with lower flow rates (~20 nL/min), and smaller tip emitters (1-2 μm) to give improvements in ionization efficiency and reduced sample consumption[25].

1.1.3.2 Mass Analysis

The next stage is the mass analyzer, which separates the newly formed ions based on their *m/z* value through the application of magnetic and/or electric fields. There are many different types of mass analyzers available, the nature of which can determine the *m/z*, resolution, and range of ions that can be analyzed. Resolution can be thought of as how well an MS instrument can distinguish two ions of slightly different *m/z* values at a given mass range. Resolution is calculated with the following equation:

$$R = \frac{M}{\Delta M} \tag{1.1}$$

where M is the observed *m/z* value of the peak, and ΔM is the smallest difference for two ions that can be separated. It is especially important when determining the charge state of an ion. A singly charged ion would display an isotope cluster with mass differences of 1.0 Da, while a doubly charged ion would have 0.5 Da mass differences, and so on (see Figure 1.2).

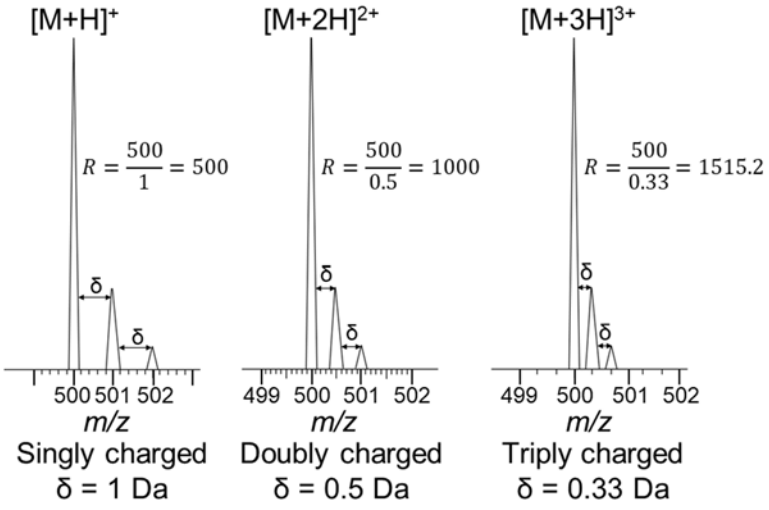

Figure 1.2 ESI-MS spectra for a singly charged, doubly charged, and triply charged ion of 500 *m/z*. The number of charges affects the apparent mass and the observed *m/z* differences between the peaks. The resolution is also calculated for each set of peaks using Equation 1.1.

The range of a mass analyzer dictates the range of *m/z* values that can be analyzed, and many different aspects can limit this. For typical proteomics experiments, doubly/triply charged peptides are analyzed up to 2000 *m/z*. There are a number of other important parameters to be considered when choosing a mass analyzer like sensitivity, energy of fragmentation, and the data acquisition speed. The sensitivity refers to how efficiently ions are transmitted from the source to the detector, and the proportion of ions from the source that are used for analysis.

One of the simplest mass analyzers used in this thesis, is a time-of-flight (TOF), which measures the *m/z* of ions based on the time they take to move from the ion source to the detector. The velocity of each ion is related to its *m/z*, and ions with a small *m/z* will move faster than ions with a large *m/z*. TOF analyzers are favoured for their essentially unlimited *m/z* range and high resolution (typically 10,000), however, there are still limitations in terms of vaporization of large molecules. In addition, TOF analyzers boast rapid data acquisition (hundreds of spectra per second), and high sensitivity (high ion efficiency, *i.e.* all ions make it to the detector). Another mass analyzer employed in this thesis is the Orbitrap, which "traps" ions using electric fields that move them at characteristic frequencies depending on their *m/z*. The ions are detected based on their image current and Fourier transform is used to create a spectrum. These types of mass analyzers show fantastic sensitivity, and very high resolution (>50,000). Several other types of mass analyzers exist, including quadrupoles, ion traps, and Fourier transform ion cyclotron resonance (FT-ICR) instruments[26,27]. In addition, hyphenated systems which combine multiple mass analyzers (*e.g.* quadrupole + quadrupole + TOF = QqTOF system) are capable of performing tandem MS (MS/MS) experiments.

1.1.3.3 Tandem MS

Tandem MS instruments are capable of performing multiple MS experiments. Specifically, an ion of select *m/z* can be isolated in the "first" mass analysis, then fragmented, and the resulting pieces analyzed in a second mass analysis. Tandem MS instruments (see Figure 1.3), are useful for structural analysis and sequencing studies.

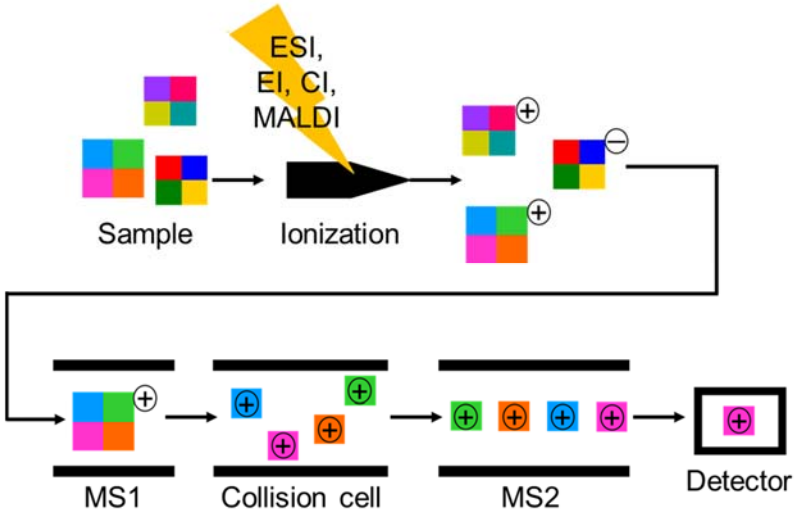

Figure 1.3 Schematic overview of a "tandem-in-space" mass spectrometer, which includes an ion source, an initial mass analyzer (MS1) which selects a precursor ion, a collision cell for fragmentation of the precursor ion, a second mass analyzer (MS2) to sort the fragment ions, and a detector.

There are a number of different fragmentation methods used in MS/MS, each resulting in different types of fragmentation, which can provide different information about the structure and composition of the original molecule. Collision-induced dissociation (CID) is used exclusively in the work described in this thesis. CID or sometimes referred to as collisionally-activated dissociation is by far the most common fragmentation method for MS/MS of proteins. For CID, a selected precursor ion is pushed into a high-pressure dissociation chamber and collided with neutral gaseous atoms or molecules (usually He or N_2). The collisions between the precursor ion and the gas converts some of the kinetic energy of the precursor ion into internal energy, which drives fragmentation reactions within the ion. The fragment ions, once formed, are analyzed with a second mass analyzer (tandem-in-space) or a second mass analysis scan (tandem-in-time). Certain bonds or structural features within a protein are more susceptible to fragmentation than others, and this can drive fragmentation in a rather predictable manner. The predictability in

fragmentation can be rather useful in peptide and protein analysis (discussed in Section 1.1.4.1). Other fragmentation methods have been reviewed discussing the advantages and appropriate uses for each[28].

1.1.4 MS-based Proteomics Workflows

There are two main approaches for MS-analysis of proteins, bottom-up proteomics (BUP), or top-down proteomics (TDP). More recently, a third approach has gained popularity called middle-up/down proteomics[29,30].

1.1.4.1 Bottom-up Proteomics

Bottom-up is the most commonly used process, it entails the MS identification and characterization of peptide fragments to identify proteins. Prior to MS analysis, the proteins of interest are purified to reduce sample complexity, and proteolytically digested by an enzyme (*e.g.* trypsin or pepsin), by chemical methods (*e.g.* CNBr, NTCB), or by electrochemical oxidation[31]. The resulting peptides are separated by one or more dimensions of LC coupled to MS analysis. Alternatively, the pre-purification step prior to MS can be skipped, and the crude protein extract is simply digested and injected into the MS (known as shotgun proteomics). Peptides entering the MS are ionized and separated based on their different *m/z* values. Ionized peptides are selected, fragmented, and detected by a second mass analysis. The MS/MS spectra for the fragments are compared to a library of theoretical peptide fragment spectra for identification. The theoretical library is constructed based on an organism's published genome or proteome. First, the genome is translated into protein sequences, if necessary, using computer programming, then theoretically cleaved at the appropriate proteolytic enzyme sites. Finally, the fragmentation

patterns of the theoretical peptides are predicted and compiled to create a library of possible spectra, this library is referred to as a peptide spectral library. The identification process here is generally considered faster than other methods because of the limited search space. However, spectra which aren't included in the library won't be identified and data collected on different mass spectrometers can vary considerably in fragment spectra appearance. Other limitations to the BUP technique include the loss of labile PTMs or sequence variant information after digestion, limited sequence coverage (typically only 50-90%), poor digestion of small MW proteins, and uncertainty in the origin of redundant peptides[18,32].

1.1.4.2 Top-down Proteomics

The alternative method to BUP, top-down, was first proposed by Kelleher and colleagues in 1999[33]. TDP studies attempt to eliminate many of the disadvantages of BUP studies simply by introducing the undigested (intact) protein into the MS, allowing both the intact and fragment ion masses to be measured (by MS/MS). Top-down MS involves detection of a much higher mass range than BUP, and as such requires much higher resolving power[18]. Sufficient mass resolution for both the intact protein and the fragment product is essential for the assignment of charge states and protein identification. As such, TDP is limited to "higher-end" instruments with superior resolving power like FT-ICR or Orbitrap. This approach routinely achieves 100% sequence coverage and has the capacity for full characterization and quantitation of unique proteoforms, sequence variants, and degradation products. TDP has become extremely useful for single small proteins (often difficult to detect *via* BUP) or simple protein mixtures. However, as the sample size and complexity increase, the technical difficulty in protein identification also increases. The proteome coverage, sensitivity, and throughput all suffer when TDP is scaled up to an entire

proteome. Much of the front-end sample processing techniques utilized in BUP workflows are less effective with intact proteins. Additionally, maintaining solubility of intact proteins is much more difficult than peptides and generally requires a solubilizing agent. As such, advances in sample preparation methods, MS instrumentation, and data processing tools are still needed to bring TDP studies to the level of success and popularity of BUP studies.

1.1.5 Sodium Dodecyl Sulfate in a Proteomics Workflow

Sodium dodecyl sulfate (SDS) is an anionic surfactant and solubilizing agent, widely recognized as one of the most popular and valuable reagents in protein analysis. SDS is an amphiphilic molecule (*i.e.* both hydrophilic and hydrophobic) containing a long hydrocarbon tail and a polar head group (see Figure 1.4).

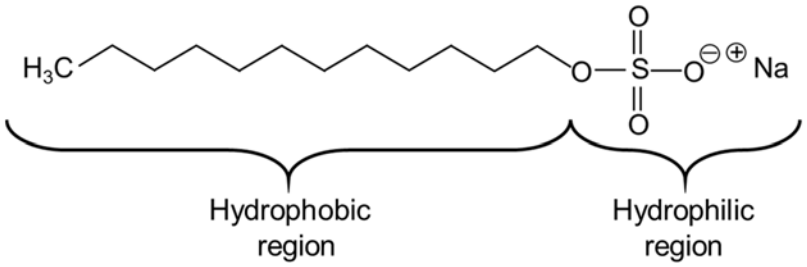

Figure 1.4 The structure of the anionic surfactant sodium dodecyl sulfate with hydrophobic and hydrophilic regions of the molecule labelled.

SDS binds to proteins very readily through both ionic and hydrophobic interactions, and disrupts the non-covalent bonds within the protein, effectively unfolding any tertiary structure or native conformation. By far the most common use for SDS in proteomics is mass-based separation through SDS-PAGE. First proposed in 1970 by Laemmli[34], SDS-PAGE is a powerful and robust electrophoretic separation and quantitation technique for complex mixtures of proteins. It is still highly favoured for its reliability, sensitivity, and applicability to almost any type of protein sample. The ability of SDS to unfold proteins is

essential for SDS-PAGE because proper separation is reliant on all proteins having a similar shape/charge. SDS also confers a net negative charge onto the proteins *via* its sulfate head group, granting the proteins predictable mobility in an electric field (*i.e.* all proteins migrate towards the anode). Under the conditions for SDS-PAGE, SDS binds to most proteins in an approximate ratio of 1.4 g SDS/g protein or ~1 SDS molecule:2 amino acids[35]. However, SDS-protein binding ratios can be influenced by a number of factors including amino acid sequence, buffer components, capacity, and temperature[36,37], which will be discussed further in Section 1.1.5.1. The binding of SDS to protein gives each protein a net negative charge which is roughly proportional to its mass, thus each protein will have a unique charge-to-mass ratio. Separation is achieved based on the electrophoretic mobility of the SDS-bound protein through a polyacrylamide gel matrix of defined pore size. Larger proteins migrate slower than smaller proteins. SDS-PAGE and 2-DE are still widely used today as cheap but effective proteomic screening and separation tools prior to bottom-up MS-analysis[38–44].

SDS is also used in another commercially available mass-based protein fractionation technique known as gel-eluted liquid fraction entrapment electrophoresis (GELFrEE), developed previously in this lab[45]. This technique is analogous to SDS-PAGE in that protein-SDS complexes migrate through a polyacrylamide gel matrix of defined pore size based on their MW. However, the proteins are allowed to migrate through the entire gel matrix and are collected as discrete aqueous fractions. This type of fractionation is advantageous because samples are recovered as aqueous intact fractions, which are suitable for both BUP and TDP studies.

Aside from protein separation technologies, SDS plays critical roles in the extraction and solubilization of proteins, especially hydrophobic/membrane proteins. Due to its amphipathic nature, SDS can coordinate at the boundary between hydrophobic and hydrophilic regions and interact favourably with both sides. The hydrophobic moiety of SDS binds to the hydrophobic regions of a protein, while the polar head group interacts with the aqueous buffer. This results in a reduction in surface tension, and an increase in miscibility. In terms of cell lysis, SDS helps to break up the phospholipid bilayer of the cell membrane, releasing all of the cellular contents. Membrane proteins and other largely hydrophobic proteins are notoriously challenging to work with, and as a result, they are often underrepresented in proteomic studies[46,47]. Yet these types of proteins make up a significant part of any proteome because they play major roles in cell-to-cell signalling, transport, cell adhesion, immune response, and are often targets for many modern pharmaceuticals[48–50]. For instance, there are ~1000 membrane proteins in the yeast proteome[51], and ~6700 in the human proteome[49], analysis of which would be almost impossible without surfactants like SDS.

1.1.5.1 SDS-protein Interactions

SDS clearly plays critical roles in many protein workflows, and because of this, there is a wealth of literature on the interactions between SDS and proteins. The amphipathic nature of SDS means it strongly interacts with proteins and with other SDS molecules through multiple different ionic, electrostatic, and hydrophobic mechanisms. Pure SDS solutions exist as monomers until a specific concentration is reached, called the critical micelle concentration (CMC). In pure water, the CMC is ~0.2% (2000 ppm, 7-8 mM); at or above this concentration SDS monomers aggregate to form ellipsoid-shaped

micelle structures (see Figure 1.5)[52]. The CMC will vary based on the properties of the surrounding environment like temperature, ionic strength, and pH[53].

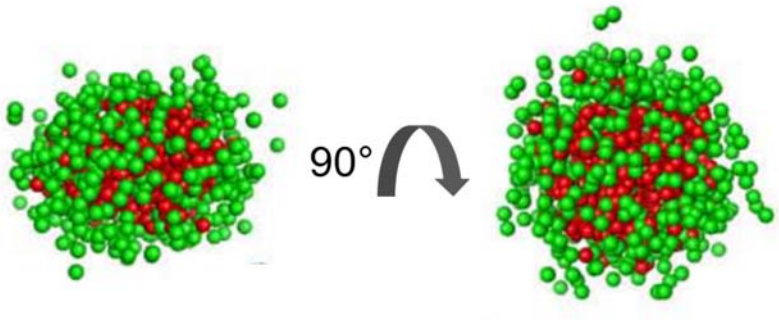

Figure 1.5 Pure elliptical-shaped SDS micelle structures produced from small angle X-ray scattering and an indirect Fourier transform method. The hydrocarbon tails of the SDS are shown as red spheres orienting towards the inside of the micelle, while the hydrophilic head groups are shown as green spheres on the outside of the micelle. Figure reprinted with permission from Andersen *et al*., 2009[52].

Upon micelle formation, the hydrophilic sulfate head groups come together to create an outer shell which remains in contact with the surrounding solvent. Meanwhile, the hydrophobic tails orient inwards to the center of the micelle, reducing their interaction with water which provides structural stabilization.

The literature reports SDS-protein binding ratios ranging from 0.4 – 2.2 g SDS/g protein[35,37], attributing variations to protein type, number of disulfide bonds, amino acid content, pH, temperature, and ionic strength[37,54]. These differences also affect the speed with which SDS and protein reach binding equilibrium, with times ranging from 1 hour to a few days[36]. Additionally, the tertiary structure of a protein can affect the level and ease of SDS binding. β-sheets unfold very slowly and resist the binding and denaturing activities of SDS[55]. In contrast, α-helices facilitate the binding of SDS by promoting the formation of helical structures which stabilize and facilitate micelle formation[36,56,57].

In general most ionic surfactants go through four main stages when binding to proteins (see Figure 1.6)[58].

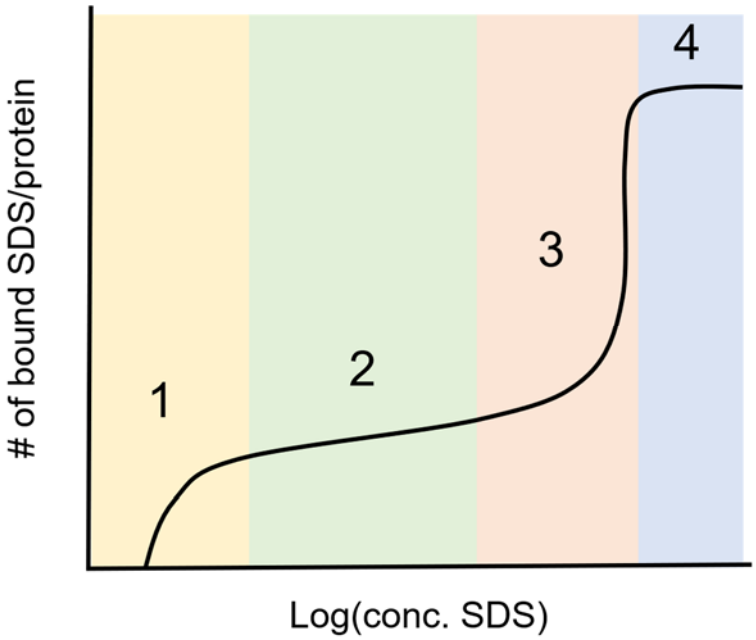

Figure 1.6 Cartoon schematic of the binding isotherm for SDS and protein. The number of bound SDS molecules per protein is plotted as a function of the logarithm of the concentration of free SDS. The four stages of binding are labelled on the curve: (1) specific binding, (2) non-cooperative binding, (3) cooperative binding, and (4) saturation. Figure modified from Jones, 1975[58].

First is specific binding, which is mainly characterized by specific electrostatic interactions between the hydrophilic head groups on SDS and the charged amino acids on the outer region of the protein[58]. This stage of binding involves a small number of SDS molecules and can be manipulated based on the pH of the solution. Decreasing the pH (where protein becomes more positively charged) will promote onset of stage 2 at lower concentrations of SDS and increasing the pH will have the opposite effect. The second stage is general non-cooperative binding of a much larger number of SDS molecules through hydrophobic interactions, characterized by a plateau region in the binding isotherm curve[58]. Third is cooperative binding, which means the binding affinity increases as more SDS binds. This

stage involves a large number of binding sites and is characterized by a steep rise in the binding isotherm. Micellar structures will begin to interact with the protein, initiating major protein unfolding events, quickly revealing new hydrophobic binding sites[59]. The last region is the saturation point, characterized by a second plateau region in the binding isotherm[58].

A number of different models exist for the structure of protein-SDS complexes, but the model most supported by the literature is the "beads-on-a-string" or "necklace model". The model was initially proposed by Tanford in 1980[60] and later confirmed by a number of other studies involving small-angle neutron scattering, fluorescence, and nuclear magnetic resonance[52,53,61,62]. The model correlates well with the stages of binding described above. The name comes from the idea that a single unfolded polypeptide chain acts as the "string" and wraps around multiple SDS micelles acting as "beads" (see Figure 1.7).

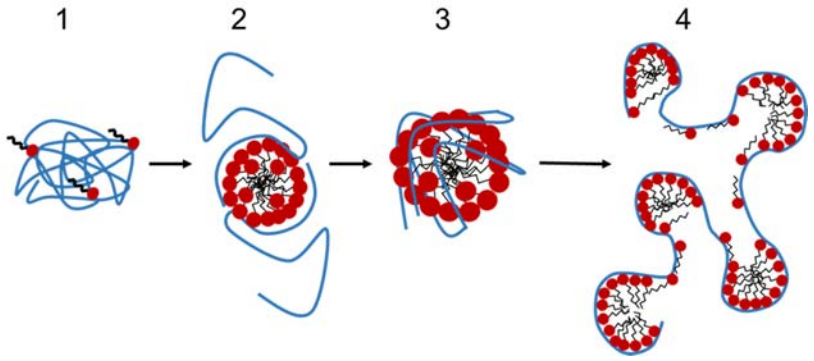

Figure 1.7 Schematic cartoon representation of the different stages of protein-SDS binding. The blue represents a polypeptide chain, and the red and black represent the head group and tail of SDS. In stage 1, no significant changes to protein tertiary structure are observed. Between 1 and 3 SDS molecules bind to specific sites on the protein sequence, *via* the hydrophilic head group. In stage 2, denaturation begins to occur and SDS micelles begin to form (~16-20 molecules in size). It is at this stage a single micelle often binds two separate polypeptide chains. In stage 3, a massive uptake of SDS molecules increases the micelle to ~40 SDS molecules. The complex returns to 1 polypeptide chain:1 micelle, and the polypeptide chain winds around the micelle in a "shell-like" structure. In stage 4, the micelles contain 60+ molecules and the protein is saturated with large micellar structures. This stage constitutes a single polypeptide chain wrapping around multiple

SDS micelles giving a "beads-on-a-string" appearance. Figure modified from Andersen *et al.*, 2009[52].

1.1.5.2 Problems with SDS

It is well known within the proteomics community that high concentrations of SDS can be severely detrimental to certain downstream analytical processes (such as LC and ESI-MS)[63]. Above a certain threshold, commonly quoted as 0.01% (100 ppm)[64], downstream sample analysis becomes extremely difficult. During reversed phase (RP) LC, SDS can increase the hydrophobicity of a protein promoting tight binding to the stationary phase. This results in peak-broadening which lowers signal intensities, and increases elution times[64,65].

Due to the fact that SDS is readily ionizable, ESI-MS analysis is severely hindered in the presence of this anionic surfactant. Recall the mechanism of ESI (Section 1.1.3.1), high concentrations of SDS in the sample alter the surface tension of the droplets which prevents proper nebulization, ionization, and desolvation prior to entering the MS[64,66]. Although 100 ppm is quoted as the "threshold limit" concentration of SDS in a sample matrix, strong reduction in MS signal intensity may still be observed at this level (up to 90% reduction), as well as the presence of multiple SDS adducts[64]. Above 1000 ppm SDS, some proteins will have no MS signals, suggesting a complete lack of ionization[67]. In addition to the production of adducts, charged SDS monomers are present within the spectrum up to very high *m/z* values[66,67].

Additional problems with SDS are seen in BUP studies where a digestion step is required prior to analysis. The digestion abilities of trypsin are significantly lowered in concentrations of SDS exceeding 0.08%[68]. At this threshold, the trypsin enzyme has lost

most of its tertiary structure and no longer has the ability to digest proteins[68]. Other studies have reported threshold limits slightly higher at 0.1%[69,70].

Finally, SDS interferes with several popular assays which are mainstays of a biochemist's tool box. For example, the common protein assays Bradford and Lowry, used for the global quantification of protein content in a sample are incompatible with SDS[71,72]. SDS is also incompatible with cell or enzymatic-based assays because it is highly cytotoxic and inactivates enzymes at working concentrations. In addition, SDS can also inhibit protein-dye binding for SDS-PAGE gel staining (Coommassie Brilliant Blue and silver) and other dye-binding assay interactions (*e.g.* Pyrogallol Red)[73,74].

1.1.5.3 SDS Removal Methods

While SDS is considered an extremely useful tool in proteomics workflows, with many different applications, its several incompatibilities mean it must be removed prior to other downstream processes (*i.e.* digestion, LC-MS detection). Several SDS alternatives, like organic solvents[75,76], non-ionic surfactants[77], and acid-cleavable surfactants[78], have been explored but often suffer from poorer solubilization, other downstream incompatibilities, and higher costs[79–81]. As such, several different SDS removal strategies have been developed, though showing varying levels of efficiency[80]. Some of the most popular and effective SDS removal strategies include in-gel digestion[82], solvent precipitation, and filter-based techniques[83].

In-gel digestion is effective at removing both free- and protein-bound SDS with >99.9% depletion observed[80]. However, limitations include inability to extract intact

proteins, inefficient digestion (*i.e.* missed cleavages and undigested deeply entrenched proteins), and reduced yields for large or highly hydrophobic peptides[31,84,85].

Protein precipitation (with acetone[64,86,87] or chloroform-methanol-water[88,89]) has been shown to remove both free and protein-bound SDS to levels acceptable for LC-MS analysis[64,80]. However, the reproducibility (especially at low µg quantities) varies significantly from lab-to-lab as precise pipetting technique is required during the wash steps[64,90]. To alleviate the need for a precise hand and boost reliability/reproducibility, Crowell and colleagues developed a two-stage centrifugal cartridge which removes the need for precise pipetting during precipitation[90]. An alternative strategy to protein precipitation is contaminant precipitation (usually with KCl), but this method is less effective at removing protein-bound SDS[91].

Use of an ultrafiltration membrane to filter out SDS was popularized by Wiśniewski and colleagues in 2009 when they demonstrated SDS removal to below 10 ppm SDS with molecular weight cut off (MWCO) regenerated cellulose filters[83]. Their method, termed filter aided sample preparation (FASP), constitutes several 8 M urea sample washes followed by digestion to recover the peptides from the filter[83]. The FASP protocol is one of the most cited papers in the field of proteomics, but has a well-documented history of ≥50% sample loss, with differences in yield based on "trivialities" like brand of filter and which digestion enzymes are employed[80,92–94]. Moreover, the protocol is quite lengthy, and contains numerous steps (including a seemingly mandatory digestion step), which makes it a somewhat unattractive protein clean-up method.

There are also a variety of column-based SDS removal strategies with much lower levels of success[95–99]. Strong cation exchange is generally the most popular/effective, and

can deplete >99.9% SDS from a sample, however, significant yield losses still occur (~30-40% loss)[80]. Other column-based methods show problems depleting protein-bound SDS and substantial sample loss from unrecovered or poorly retained peptides[80,100,101].

The methods summarized here do not constitute an exhaustive list. There are several other methods which are not discussed but have previously been shown to lack the capability to deplete protein-bound SDS or give large sample losses[80]. There are several comparison reviews available in the literature for further information on available methods and their relative effectiveness in terms of clean-up and sample yield[44,80,102].

1.1.5.4 Transmembrane Electrophoresis for SDS Removal

Although there are many available SDS depletion technologies, the limitations and disadvantages discussed above clearly outline the need for a reliable method capable of depleting protein-bound SDS without significant compromises to sample yield. Recently Kachuk and colleagues from the Doucette group introduced a new SDS removal approach termed transmembrane electrophoresis (TME)[65]. TME can be universally applied to BUP and TDP workflows because intact proteins are recovered in solution when depletion is complete. This electrophoretic-based method combines MWCO dialysis membranes with an applied electric potential to pull SDS away from the sample. The assembled TME device can be seen pictured in Figure 2.6 in Chapter 2, and a schematic of the basic principles can be seen below in Figure 1.8.

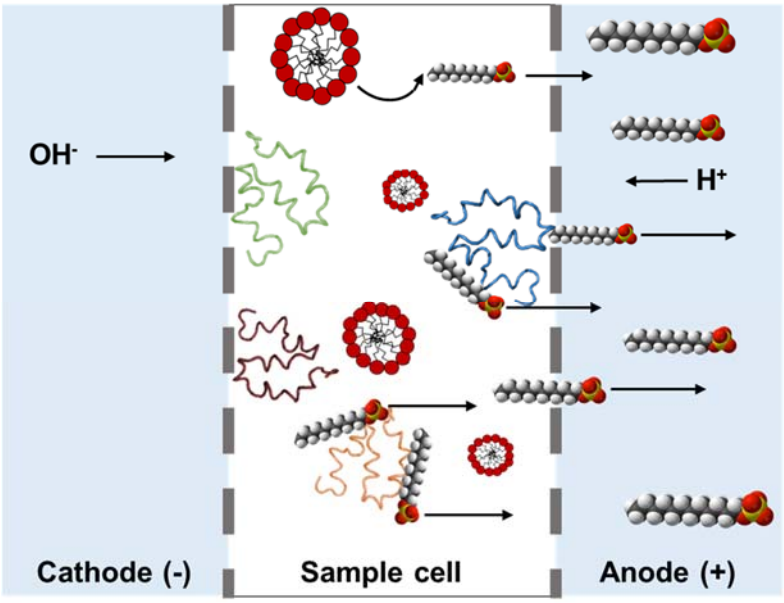

Figure 1.8 A schematic diagram of the basic principles of transmembrane electrophoresis. Anionic SDS is electrophoretically driven through the MWCO membrane towards the anode. Both free and protein-bound SDS migrate out of the sample cell. The proteins are too large to cross the membrane and remain inside the sample cell. They localize towards the cathode and anode sides of the sample chamber depending on net charge. As the concentration of SDS inside the sample chamber lowers to below the CMC, SDS micelles will break up into monomers and migrate out of the sample cell. Figure modified from Kachuk *et al*., 2016[65].

TME is not a completely new technology, one of the first examples of an electric field utilized to remove SDS was in 1975 by Tuszynski and Warren[103]. In this study, a version of electrodialysis (see Section 1.3.1.1) was used for the removal of SDS (both free and protein-bound) from samples of bovine serum albumin (BSA) and cytochrome c. Depletion occurred over 11 hours at 20 mA constant current and presented significantly improved purity over conventional dialysis. Their method has been employed with varying levels of sample recovery owing to differences in membrane pore size, buffer constituents, and electric field strength[99,104].

Although similarities exist between TME and Tuszynski and Warren's method, TME is a multiplexed system which has been previously shown to reliably deplete SDS to

<10 ppm while maintaining sample yields ≥90% within one hour of operation[65]. TME has also been shown to successfully deplete SDS from both simple protein solutions (*e.g.* BSA), as well as more complex proteomic samples (*Escherichia coli*)[65]. Furthermore, SDS depletion of membrane protein-enriched samples was demonstrated through utilization of an 80% (v/v) cold (-20°C) formic acid wash[65,88].

A more recent example of electric field-based SDS depletion is Wang and colleagues (2017) electro-ultrafiltration device for LC-MS of proteome extracts[105]. The device consists of two centrifugal ultrafiltration tubes fused together by the top and electrodes placed on either end. The sample is added to the middle portion confining it between the two ultrafiltration membranes and separated from the SDS *via* electromigration. This approach is similar to TME as it utilizes a size-exclusion-based uncharged membrane to confine the proteins within the sample cell, while the SDS migrates out through the pores of the membrane. Although the study claims to be successful, the work lacked any quantitation of residual SDS, nor sample recovery, and low numbers of peptides and proteins identified leaves much to be desired. It is difficult to assess whether this SDS-depletion method had merit.

Although TME is superior to these methods, Kachuk's version required a substantial amount of human input during depletion in the form of multiple voltage pause/mix events. Manual pausing and mixing is laborious, repetitive, likely contributes to sample loss, and their application is non-uniform across depletion experiments (*i.e.* certain experiments require more or less pausing/mixing events). Furthermore, attempts to decrease the one hour run time by increasing the applied potential resulted in increased sample temperatures (+60°C), which decreased sample yield (<50%). These previous

results highlight the necessity for sample temperature control during TME. Cooling the TME device (-20°C) and electrolyte buffer solutions (4°C), and periodic manual pausing/mixing are the current strategies in use for temperature control. These strategies are certainly not ideal because they necessitate human intervention and display upper limits to their capacity for cooling. The development of elegant and automated temperature control methods could help decrease the sample depletion time by allowing for operation at higher potentials. There are a number of factors that can affect the sample cell temperature, depletion rates, and sample recovery, such as physical design of TME, membrane characteristics, and electrophoretic phenomena. An exploration of these variables constitutes the primary focus of this thesis. A better understanding of the principles governing electrophoretic movement of SDS inside TME is required before true improvements can be made to sample run time and depletion rates/recovery.

1.2 Electrophoretic Theory

1.2.1 Principles of Electrophoresis

When an electric potential is generated between two electrodes by a power supply, electrons will move between the two electrodes from anode (+) to cathode (-). As electrons migrate to the cathode they induce a reduction reaction with water forming hydrogen gas and hydroxide ions. Meanwhile at the anode, water molecules are oxidized to release oxygen gas and protons. The protons produced combine with water to form hydronium ions. In addition, any charged particles present within the electrolyte cell will migrate in the generated electric field, anions toward the anode and cations toward the cathode (see Figure 1.9).

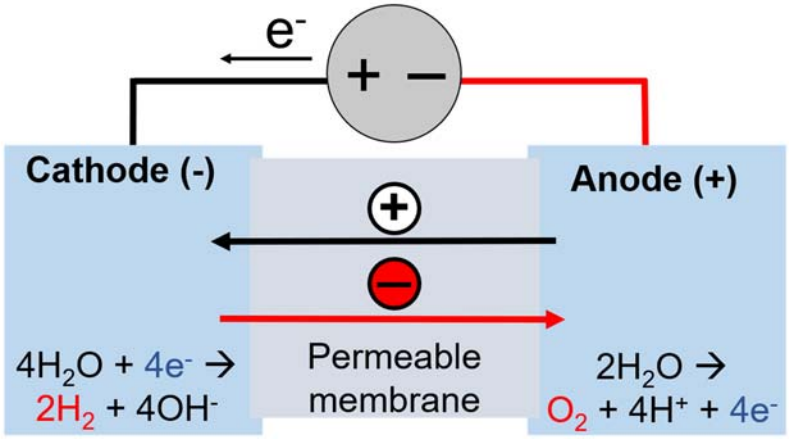

Figure 1.9 The basic set up of an electrophoretic cell. Two electrodes, the anode and the cathode, are immersed in buffer chambers. The buffer chambers are connected through a permeable membrane to allow charged particles to migrate from one side to the other. A power supply generates an electrical potential difference between the two electrodes, which causes electrons to flow from the anode to the cathode. At applied potentials >1.23 V, electrons at the cathode react with water to form hydrogen gas and hydroxide ions, while water at the anode provides electrons by decomposing into oxygen gas and protons. The generation of an electric potential allows other positive ions to move towards the cathode and negative ions to move towards the anode. Figure modified from Hegyi *et al.*, 2013[106].

The set-up for an electrophoretic cell is different from a conventional Galvanic cell and should not be confused. A Galvanic cell creates electrical energy from spontaneous reduction reactions at the positively charged cathode, while oxidation occurs at the negatively charged anode. In an electrophoretic cell, the reactions are non-spontaneous and an externally provided electrical energy is required. Oxidation still occurs at the anode but the anode is positively charged, and reduction occurs at the cathode which is negatively charged. In both configurations electrons will flow from anode to cathode.

Electrophoresis, in its most general sense, is a method of separation based on differences in the migration rate of ions in an electric field. The speed of a charged particle's migration is dictated by its size, the number of charges it carries, the viscosity of the medium, and the magnitude of the electric field. Attempting to formulate an exact theory

for the motion of different ions in an electric field has been of scientific interest for over 100 years[107]. Some of the general principles can be understood with fairly basic mathematical relations and assumptions. To begin, Coulomb's law (Equation 1.2) describes the force exerted on a charged particle in an electric field, F_e ($\frac{J}{cm}$), as a product of the particles charge, and the magnitude of the electric field (note the similarity to Newton's second law of motion $F = ma$):

$$F_e = q \times E = zeE \tag{1.2}$$

where q $(Coulomb)$ can be represented as the product of the charge number, z, and the elementary charge, e $(Coulomb)$, and E is the electric field ($\frac{V}{cm}$). This force is opposed by frictional forces working against the motion of the charged particle, known as the drag force, F_{drag}. Stoke's law (Equation 1.3) gives an expression which describes F_{drag} ($\frac{kg \cdot m}{s^2}$) as a product of the velocity of the particle, v ($\frac{m}{s}$), and the frictional coefficient, f ($\frac{kg}{s}$):

$$F_{drag} = f \times v = 6\pi\eta r \times v \tag{1.3}$$

The frictional coefficient, f, reflects the size and shape of the molecule, and the viscosity of the medium. It can be alternatively expressed as $6\pi\eta r$, where η is the dynamic viscosity ($\frac{kg}{m \cdot s}$) of the medium, and r is the ionic radius (m). During electrophoresis, a charged particle reaches its final velocity (or drift velocity), v_{drift} ($\frac{m}{s}$), when F_e is equal to F_{drag}:

$$v_{drift} = \frac{zeE}{6\pi\eta r} \tag{1.4}$$

This means each different charged particle in a given medium will move at a different velocity based on its size and charge. Furthermore, each particle has a characteristic velocity for a given specific electric potential and medium.

1.2.1.1 Electrophoretic Mobility

The movement of charged particles in an electric field can be alternatively expressed by the parameter electrophoretic mobility, $\left(\frac{m^2}{Vs}\right)$, which is proportional to the charge of the particle and inversely proportional to the frictional coefficient:

$$\mu \propto \frac{ze}{f} \propto \frac{ze}{6\pi\eta r} \tag{1.5}$$

Electrophoretic mobility defines the migration of a charged particle through a stationary medium under the influence of an electric field. The mobility can be expressed in terms of a molecule's drift velocity from Equations 1.2 and 1.4 as seen below:

$$v_{drift} = \mu F \tag{1.6}$$

where F is any applied force (*e.g.* electrical, $\frac{V}{m}$) acting on the molecule, and the mobility acts as a proportionality constant.

1.2.1.2 Joule Heating

Another very important parameter to discuss in the context of electrophoretic motion is Joule heating. Joule heating, also known as Ohmic or resistive heating, is the production of heat as an electric current is passed through a conductor. The heating is a result of the resistance of the conductor (*i.e.* the solution) to the flow of current and is described by Equation 1.7 below:

$$H = I^2Rt \tag{1.7}$$

where H is the Joule heat generated (J), I is the applied current (A), R is the resistance (Ω), and t is the time (sec). The equation can be alternatively expressed to reflect the relationship to the strength of the electric field and the molar conductivity of the electrolyte by Equation 1.8 below:

$$H = E^2 \Lambda_m c \quad 1.8$$

where H is the Joule heat generated $\left(\frac{\Omega}{cm^3}\right)$, Λ_m is the molar conductivity of the electrolyte $\left(\frac{cm^2}{mol \cdot W}\right)$, and c is the concentration of electrolyte $\left(\frac{mol}{L}\right)$. At a molecular level, when an electric field is applied it provides kinetic energy to charged particles. As charged particles begin to move they collide with other particles in solution, which scatters the particles and converts some of the energy from the electric field into random motion or thermal energy (heat). All electrophoretic procedures suffer to some degree from Joule heating effects. As such, the effects of Joule heating have been thoroughly studied for popular separation procedures that occur at high voltages such as capillary electrophoresis (CE)[108–110]. However, there is minimal literature for other types of electrophoretic processes as it is often considered negligible because the applied voltage is much lower (*e.g.* SDS-PAGE). High degrees of Joule heating are often associated with a general decrease in performance. Excessive Joule heating during CE causes peak broadening[111]. Additionally, Joule heating can cause unwanted temperature gradients which can affect the properties of the liquid medium such as viscosity, density, dielectric constant, thermal conductivity, and pH[112]. Changing these properties will change the electrophoretic mobility of an ion, which changes its motion and how it separates. Moreover, gas bubble formation, decomposition of sample, membrane breakdown, and even device breakdown (especially with microfluidic chip systems) are all side effects of high levels of Joule heating. A few studies have attempted to mathematically model the production of Joule heating and how it effects the flow of ions in an electric field[112–114]. These studies suggest certain strategies to minimize the effects of Joule heating (other than chilling) such as utilizing a different buffer

solution (*i.e.* one where the zeta potential and temperature are less correlated), rectangular channels rather than circular[115], or increasing surface area:volume ratio by changing the dimensions of the system. The dimensions of a system can be a very important factor in mitigating Joule heating. CE is operated at extremely high voltages (>20-30 kV) but experiences little Joule heating because the high surface area:volume ratio dissipates heat very effectively. TME must operate at a field strength high enough to overcome the binding energy between SDS and protein (~35.5 kJ/mol)[116], and as such experiences relevant levels of Joule heating which must be alleviated. In contrast, some studies suggest Joule heating can be used to power other types of processes, taking advantage of it rather than trying to minimize it. Procedures such as IEF[117], temperature gradient focusing[118], and polymerase chain reaction[119] have all been shown to use Joule heating to control separation and bioreaction.

1.2.2 Theory of Mass Transport

Mass transport, as the name suggests, is the net movement of mass from one location to another, for example the evaporation of water from a puddle back into the atmosphere. Most electrophoretic processes involve some form of mass transport (*e.g.* protein separation through a fixed medium). TME is concerned with the transport of SDS ions through a membrane. An understanding of the theories governing mass transport is important for understanding the movement of SDS in TME. The following equations used to describe mass transport are parallel to the theories describing transport of momentum and heat[120,121].

1.2.2.1 Mass Transfer Across Interfaces

Mass transfer is generally represented as a flux, which is a flow rate per unit area having the dimensions $\frac{[quantity]}{[time]\cdot[area]}$. The area is the surface or substance the mass is passing through, for example a semi-permeable membrane. Flux of a species i is normally given the symbol $\boldsymbol{N}_i$ or $\boldsymbol{J}_i$ and defined as a combination of fundamental chemical potentials (*e.g.* solubility, pressure, concentration, electric forces). A basic equation for flux based on a concentration potential can be seen below:

$$\boldsymbol{J}_i = k\Delta c \tag{1.9}$$

where k is the overall mass transfer coefficient, and Δc is the concentration difference across the interface. There are typically three basic mechanisms which govern mass transport in electrophoretic devices: diffusion, electromigration, and convection. Each contribution has an additive effect but must be considered individually to properly understand mass transport phenomena seen in different systems.

1.2.2.2 Diffusion

Molecular diffusion is the net movement of molecules from an area of high concentration to an area of lower concentration and only occurs when there is a non-uniform distribution of molecules. Diffusion is mainly controlled by random motion and collisions between the molecules diffusing and the background molecules. Diffusion can occur without direct bulk motion (*e.g.* from a pressure or temperature gradient). The driving force for diffusion comes from the gradient in concentration of the diffusing molecules. The process of diffusion is mathematically represented by Fick's first law, which states the

diffusive flux (the amount of substance that will flow through a unit area during a unit time interval), $\boldsymbol{J}_d$, has a magnitude that is proportional to the concentration gradient:

$$\boldsymbol{J}_d = -D\frac{dc}{dx} \tag{1.10}$$

where D is the diffusion coefficient (also called diffusivity,$\frac{m^2}{s}$), c is the concentration (mol), and x is the position. The negative symbol indicates motion from a high concentration to a low concentration. The diffusion coefficient is proportional to the electrophoretic mobility (μ) of the diffusing particle as seen in the Einstein relation in Equation 1.11 below:

$$D = \mu k_B T \tag{1.11}$$

where k_B is the Boltzmann constant ($\frac{J}{K}$), and T is the absolute temperature (K). This is the most general form of the equation, and various special forms have been derived for specific situations such as diffusion of charged particles (electrical mobility equation) and diffusion through liquids (Stokes-Einstein equation), and the Einstein relation for semiconductors, to name a few. As a baseline, in dilute aqueous solutions, most ions have a D value ranging between 0.6×10^{-9} to $2.0 \times 10^{-9}\ \frac{m^2}{s}$, and 1.0×10^{-11} to $1.0 \times 10^{-10}\ \frac{m^2}{s}$ for biological molecules[120,121].

1.2.2.3 Electromigration

Perhaps the strongest and most dominating force for any electrophoresis-based experiment is electromigration, sometimes referred to as just migration. It is the movement of charged particles in response to the applied electric field. The velocity of each ion depends on the strength of the applied electric field, $\frac{d\phi}{dx}$, it's mobility, μ, and the charge

number, z. The force experienced by each ion in an electric field is given by Equation 1.2 and when combined with the velocity of the ion given by Equation 1.6 the following expression for the drift velocity of an ion is produced:

$$v_{drift} = \mu zeE \tag{1.12}$$

The resulting flux due to migration, $\boldsymbol{J}_m$, is simply the product of the velocity and the ion concentration, $c\ (mol)$:

$$\boldsymbol{J}_m = \mu zeE \times c \tag{1.13}$$

This can be expressed in terms of a diffusion coefficient by substituting into Equation 1.11 to arrive at the following expression:

$$\boldsymbol{J}_m = D\frac{ze}{k_B T}cE \tag{1.14}$$

1.2.2.4 Convection

The final contribution, convection, refers to the mass transfer due to bulk movement of molecules within a fluid. There are two forms of convection, natural and forced. Natural convection is present in all solutions, and stems from minor thermal or density differences within the solution that act to randomly mix the solution. The effects of natural convection can be completely negligible if temperature, and density remain relatively constant or if forced convection is introduced. Forced convection is the deliberate introduction of convection by an external force (*e.g.* pumps, fans, stirring). The equation describing flux due to convection is relatively simple:

$$\boldsymbol{J}_c = v_s c \tag{1.15}$$

where v_s is the velocity of the solvent ($\frac{m}{s}$, not to be confused with v_{drift}, the velocity of the ion). It should be noted this is a common simplification of the general equation for

convective flux, which would normally include terms for both convection (advection) and diffusion. The equation above only includes the advective flux portion of convective flux.

1.2.2.5 The Nernst-Planck Equation

It is known that there is a relationship between flux and current density given by the following expression:

$$Current\ density = zF\boldsymbol{J} \tag{1.16}$$

Since this relationship exists, the comparison to an electric circuit is intuitive. In an electric circuit the total resistance in series is equal to the sum of the individual resistances and calculated as follows:

$$R_{total} = R_1 + R_2 + R_3 \ldots \tag{1.17}$$

The same can be done in combining the three contributions to mass transport into one equation:

$$\boldsymbol{J}_{total} = \boldsymbol{J}_d + \boldsymbol{J}_m + \boldsymbol{J}_c \tag{1.18}$$

The above equation is used to describe the movement of charged particles in an electric field across a membrane. When each of the flux components is subbed into Equation 1.18, one will arrive at what is known as the Nernst-Planck (NP) equation:

$$\boldsymbol{J}_{total} = -D\frac{dc}{dx} + D\frac{ze}{k_B T}cE + v_s c \tag{1.19}$$

Versions of this equation in combination with the theories governing mass transport across a membrane have been used to successfully describe various electrophoretic membrane processes[35,107,122–126]. A less computationally expensive model comes from combining the

NP equation with Poisson's equation to arrive at the Poisson-Nernst-Planck equation. The NP equation describes the drift velocity of ions in a potential gradient *via* Ohm's law and diffusion theory (Fick's law), while the Poisson equation relates charge density and electric potential. Although easier to solve, the Poisson-Nernst-Planck equation is criticized for over simplifying the representations of the ions in the system leading to incorrect predictions of ion concentrations in narrow pores[127]. The Poisson-Nernst-Planck theory represents ions as point charges in a dielectric background (the solvent), which limits its applicability to very dilute and microscopic systems. Furthermore the theory does not take into account the size of the ions and ionic correlations[128]. Nonetheless, the Poisson-Nernst-Planck equation has been successfully used to model electrochemical systems with no current flow, or with ionic currents, such as those present in ion channels inside biological membranes[129]. It has also been extensively used in the modelling of semiconductor devices and ion selective electrodes[130].

1.2.2.6 The Diffusion Coefficient

There are multiple types of diffusive movement depending on the properties of the system and its components. The diffusivity coefficient (D) is present in two different components (diffusion and electromigration) in the NP equation and can be calculated based on what type of diffusive movement is occurring, each type is summarized in Figure 1.10 below.

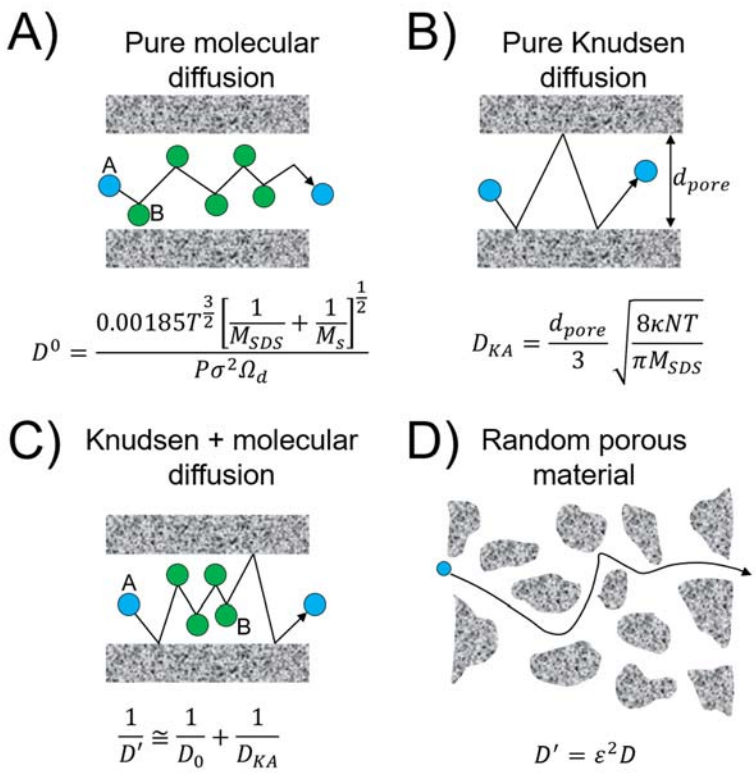

Figure 1.10 The different types of porous diffusion. A) Pure molecular diffusion, B) pure Knudsen diffusion, C) a combination of Knudsen and molecular diffusion, and D) diffusion through a random porous material. The shaded gray areas represent non-porous solids. Equations for the diffusivity coefficient for each type of diffusion is displayed underneath. Figure modified from Welty *et al.*, 2000[131].

Pure molecular diffusion (Figure 1.10 A) occurs when there are at least two components in the system, and the pore size is sufficiently larger than the mean free path of the diffusing molecule. The mean free path is defined as the average distance traveled by a moving particle between collisions. When these conditions are met, the diffusing species is more likely to encounter another component in the system than a pore wall. Knudsen diffusion (Figure 1.10 B) occurs when the pore diameter is smaller than the mean free path of the diffusing molecule. Knudsen diffusion generally only applies to gases as the mean free path length in liquids is extremely small[131]. Knudsen diffusion and molecular diffusion can sometimes occur together (Figure 1.10 C) and compete with one another in a "parallel"

manner, as reflected by the equation reminiscent of the classic resistance in parallel equation $\left(\frac{1}{R_{tot}} = \frac{1}{R_1} + \frac{1}{R_2} + \cdots\right)$. The three types of diffusion discussed thus far are based on cylindrical straight pores, whereas most porous materials are random and molecules will follow a more tortuous path through the material *via* random porous diffusion (Figure 1.10 D)[131].

Since the regenerated cellulose MWCO membrane in TME is considered a random porous material, the effective diffusion, D' can be calculated *via* this relation:

$$D' = \varepsilon^2 D \tag{1.20}$$

where ε is the volume void fraction of the membrane, which is given by:

$$\varepsilon = \frac{volume\ occupied\ by\ pores\ within\ porous\ membrane}{total\ volume\ of\ porous\ membrane\ (membrane + pores)} \tag{1.21}$$

Since the TME sample chamber is immersed in liquid buffer, it is assumed no Knudsen diffusion takes place. Therefore, the molecular diffusion through the MWCO is assumed to take on the "hindered solute diffusion in solvent-filled pores" model[121]. This model represents diffusivity through a pore using the formula below:

$$D = D^0 F_1(\varphi) F_2(\varphi) \tag{1.22}$$

where D^0 is diffusivity of SDS *via* pure molecular diffusion, $F_1(\varphi)$ is the stearic partition coefficient, and $F_2(\varphi)$ is the hydrodynamic hindrance factor, both are correction factors which are functions of the reduced pore diameter, φ. The reduced pore diameter, φ, is represented below:

$$\varphi = \frac{d_s}{d_{pore}} = \frac{solute\ molecular\ diameter}{pore\ diameter} \tag{1.23}$$

where if φ>1, the solute is too large to enter the pore (known as solute exclusion; the underlying process of conventional dialysis). Finally, D^0, is calculated *via* the pure molecular diffusion model seen in Figure 1.10 A:

$$D^0 = \frac{0.00185T^{\frac{3}{2}}\left[\frac{1}{M_{SDS}} + \frac{1}{M_s}\right]^{\frac{1}{2}}}{P\sigma^2\Omega_d} \quad 1.24$$

where M_{SDS} is the molecular weight of SDS $\left(\frac{g}{mol}\right)$, M_s is the molecular weight of the solvent $\left(\frac{g}{mol}\right)$, P is the pressure (atm), σ is the collision diameter (pm), and Ω_d is the collision integral (a dimensionless function of the temperature and of the intermolecular potential field for the collision between two molecules of interest). The collision diameter is evaluated by:

$$\sigma = \pi(r_1 + r_2)^2 \quad 1.25$$

where r_1 and r_2 are the kinetic radii of the two particles colliding.

1.2.2.7 Mechanisms of Flux Decrease Across a Membrane

Any membrane-based process is influenced by some level of flux decline. Flux decline is simply a decreased driving force for the separation process and an increase in resistance against transport across a membrane. As pictured in Figure 1.11, the main causes of flux decline are concentration polarization (reversible and directly occurring) and various fouling phenomena (irreversible and long-term) such as adsorption, pore-blocking, and deposition of solutes.

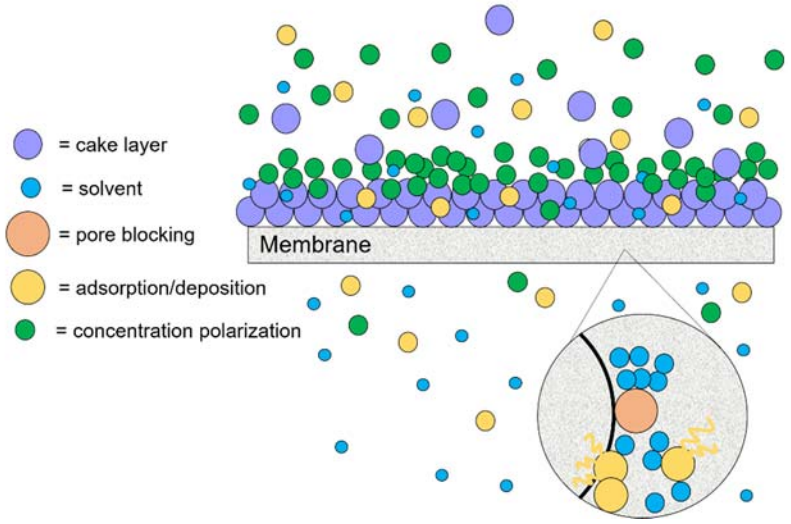

Figure 1.11 Illustration of the factors contributing to the decline of flux across a membrane. The portion within the circle is a zoomed in pore of the membrane. The purple circles represent molecules which are impermeable to the membrane and form a "cake layer" on the membrane surface. The green circles represent molecules which are slow-permeating and exhibiting the concentration polarization phenomenon. The orange circle represents a molecule which is too large to pass completely through the pores of the membrane and as a result is stuck inside, blocking the pore. The yellow circles represent permeating molecules which have a higher tendency to adsorb/deposit onto the membrane. The blue circles represent solvent molecules which are completely permeable.

Concentration polarization is a phenomenon inherent to all membrane processes. It is characterized by the presence of concentration gradients at the membrane-solvent interface. This gradient is due to the fact that there are non-permeating or slowly permeating components in the solution trying to pass through the membrane. As a result, a build up of solute against the membrane occurs, rich in non- or slow-permeating solutes and depleted of permeable solutes. The concentration of this solute decreases moving away from the membrane until it reaches equilibrium with the bulk solution at a distance δ (see Figure 1.12). The distance, δ, is known as the boundary layer thickness, and relates the diffusion coefficient to the mass transfer coefficient.

$$k = \frac{D}{\delta} \qquad 1.26$$

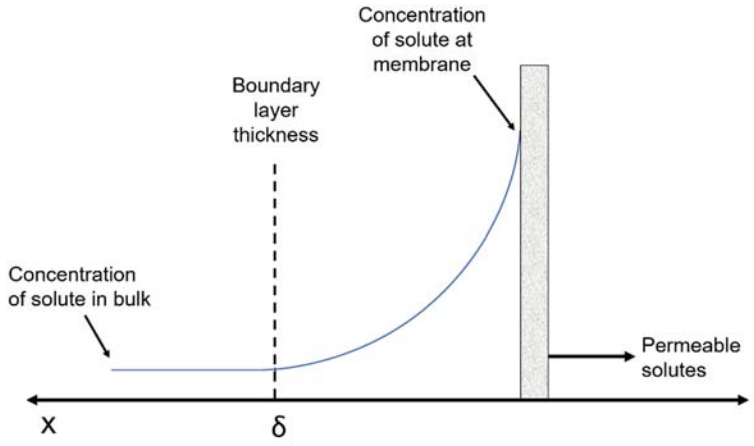

Figure 1.12 A schematic diagram of the concentration polarization phenomenon. As a solution is fed through the membrane from left to right, slow or non-permeating solutes build up at the membrane-solvent interface. As a result, a concentration gradient is formed, depicted by the blue curve. The concentration increases as the membrane is approached (from left to right). The concentration decreases moving away from the membrane until equilibrium is reached with the bulk solution. The area where the concentration of solute begins to increase away from equilibrium up to the membrane is considered the boundary layer and is also the point at which the concentration gradient reaches equilibrium, represented by δ. Figure reprinted with permission from Etzel, 2008[132].

The phenomenon of concentration polarization is a function of the hydrodynamic conditions of the membrane system and independent of the physical properties of the membrane being used[133,134]. More specifically, the success of ultrafiltration (the membranes used in TME) and electrodialysis processes are greatly influenced by concentration polarization. Concentration polarization can be reduced *via* the promotion of turbulence (usually through increased flow rates, stirring, or back flushing) resulting in a decrease in the thickness of the boundary layer[120,131,134,135].

Fouling phenomena are distinct from concentration polarization, and also play a large role in the observed flux decline during membrane processes. They are slightly more complicated processes often considered a function of concentration polarization by driving material deposition and hence fouling. Protein adsorption/deposition simply refers to

protein irreversibly and directly interacting with the membrane surface (sometimes referred to as a protein monolayer). Proteins carry a net surface charge and if this charge is opposite to the surface charge of the membrane, there will be high levels of adsorption *via* electrostatic interactions. Membranes carrying no net charge can promote adsorption in the form of hydrophobic interactions. It is suggested in the literature, BSA adsorption onto ultrafiltration membranes occurs in two stages, electrostatic formation of a protein monolayer, followed by intermolecular hydrophobic interactions[133,136–140]. Additionally, initial adsorption of a properly folded protein onto a membrane causes significant tertiary structure disruption, revealing hydrophobic regions of the protein further promoting adsorption[134,141]. Membrane processes which continue for long periods of time are vulnerable to the formation of a "cake layer" (see Figure 1.11). In short, the most retained species forms a dynamic membrane (also called filter cake layer, surface layer, or gel layer) on the surface of the filtration membrane essentially creating a new membrane surface where the working pore size is dictated by the particles themselves instead of the pores of the membrane. This has been documented to happen in the form of lattice-like sheets (BSA, β-lactoglobulin) or large granules (γ globulin)[142]. Additionally, small solutes can deposit within the pores of this new protein membrane surface, further slowing flux. Many different factors contribute to the formation of a cake layer on the membrane surface, and it usually occurs late in the filtration process[143]. The ionic environment, components of the solution being filtered, length of filtration, volume, and applied pressure all contribute to whether a cake layer will form, which means certain membrane processes don't get the chance to observe its formation. It has been suggested that flux decline occurs in 3 stages (see Figure 1.13).

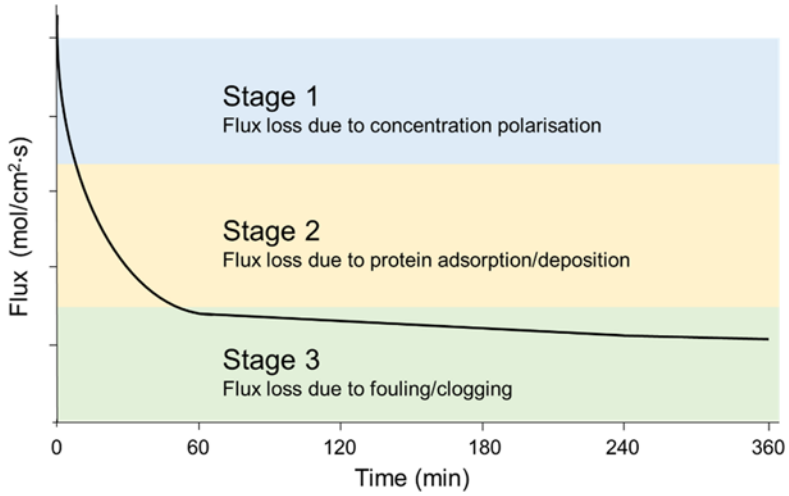

Figure 1.13 The three stages of flux decline. The first stage, occurring within minutes, is a rapid drop due to concentration polarization. The second stage, occurring for up to an hour, is another rapid drop due to protein deposition/adsorption onto the membrane. At the third stage, flux reaches a pseudo steady state where any further decline is due to fouling and clogging of the membrane. Figure modified from Marshall *et al*., 1993[134].

The first stage, concentration polarization, occurs within minutes of the filtration process beginning, and causes a rapid decline in flux. Some studies on protein membrane filtration theorize the initial stages of flux decline occur within seconds of the filtration process beginning[133,134,144]. The second stage, protein deposition, will continue to rapidly decrease flux as a protein monolayer builds. Finally, in the third phase, as flux loss steadies there is small loss due to further deposition or fouling. The decline of flux observed in membrane processes resembles an exponential decay plot, and many theories which model flux decline utilize exponential decay functions[135,145,146,139]. The plots of SDS depletion over time for TME also very closely resemble exponential decay plots and can be modelled as such (further discussed in Chapter 3). The observed decline in the rate of SDS depletion over time is likely amenable to the mechanisms of flux decay outlined above, which are inherent to all membrane processes.

There are a number of parameters discussed in this section which are important for understanding and optimizing TME operation. The origins and implications of Joule heating are discussed, which is an important limiting factor in electric field strength during TME. Furthermore, understanding the components responsible for the motion of SDS (*i.e.* diffusion, electromigration, and convection) will help to maximize overall flux through the membrane. A more detailed understanding of the diffusivity and how it is affected by membrane pore size and thickness, and levels of Joule heating are also relevant to the movement of SDS. Finally, understanding the mechanisms of flux decrease which are common to membrane processes such as proteins concentrating near the membrane, and protein-membrane interactions is important for achieving and maintaining ideal TME operation.

1.3 Electric Field as a Tool in Sample Pre-treatment

Protein sample pre-treatment is often considered the rate-limiting step and commonly associated with high degrees of error and sample loss. As a result, the use of auxiliary driving energies such as heat, microwaves[147], ultrasound[148], UV light[149], and more recently, electric fields[150–154] has been explored to speed up the process, increase efficiency, and enhance detectability. SDS-PAGE, IEF, 2-DE, and CE are widely used analytical separation techniques which utilize an electric field. However, outside of separations, the concept of using an electric field as an auxiliary driving force has been largely unexplored for sample pre-treatment. The development of liquid-liquid electroextractions (LLEE) by Stichlmair and colleagues in 1992[155], followed by electric field enhanced microextraction through supported liquid membranes (SLM) by Pedersen-Bjergaard and Rasmussen (2006)[156] helped popularize the concept.

Considering solvent extraction, the distribution of an ion (or partitioning) between two phases can be defined by Equation 1.27:

$$K_D = \frac{c_i^o}{c_i^a} \tag{1.27}$$

where c_i^o is the concentration of species i in the organic phase, and c_i^a is the concentration of species i in the aqueous phase. When an electric field is added, it can alter the distribution of a species between the two phases and the new K_D can then be expressed *via* Equation 1.28, which is a combination of Equation 1.27 and the Nernst equation[157]:

$$\ln(K_D) = \frac{zF}{RT}(E^0 - E) \tag{1.28}$$

where E is the equilibrium ion transfer potential (Galvani potential difference between the phases), E^0 is the standard potential difference of the transfer (V), R is the universal gas constant $\left(\frac{J}{K \cdot mol}\right)$, and F is Faraday's constant $\left(\frac{Coulomb}{mol}\right)$. Thus, variation in the applied voltage can change the selectivity, rate of transfer, and overall efficiency of the process. The application of an electric field is therefore an attractive and easily implemented technique for enhanced sample preparation.

The use of an electric field in sample preparation can be divided into a few categories: separation techniques, membrane-based approaches, membrane-free approaches, and electrochemical approaches. Separation approaches have been previously mentioned, are well known in the proteomics community, and have been covered in many extensive reviews[44,158–160]. Electrochemical methods are obscure, under studied, and not directly relevant to TME nor this thesis however, some literature information is available on its uses[161–164]. This section will provide an overview of the most popular/successful

electric field-based sample preparation techniques, along with their advantages and challenges in the context of TME.

1.3.1 Membrane-based Approaches

Membrane-based sample treatment (with and without the use of an electric field) has a long history of being employed in a wide array of industrial processes[165]. More recently, electro-membrane techniques have been widely employed as an analytical purification strategy for complex sample matrices[166,167]. There are generally two accepted modes of membrane filtration, dead-end and cross-flow. When the solution being filtered flows perpendicular to the membrane surface, it is considered dead-end filtration (see Figure 1.14 A). Alternatively, when the solution being filtered flows parallel to the membrane surface it is known as cross-flow filtration (see Figure 1.14 B). It should be noted, these filtration methods differ from TME in that the solution being filtered has velocity, while in TME, the sample is stationary. Even so, the methods share similarities in terms of mathematical models and membrane features/function. Furthermore, popular strategies to reduce flux decline and Joule heating in these procedures can be extended for use in TME. The most popular techniques employing a membrane and an electric field include: electrodialysis, electrofiltration, and electromembrane extraction (EME).

1.3.1.1 Electrodialysis

TME can be considered a form of classic electrodialysis. The concepts of electrodialysis are not new, and were developed at the beginning of the 20th century[168,169]. Although there is some disagreement over when the first electrodialysis experiments were conducted[169,170], these early electrodialysis experiments are far removed from the version

evoked by the same term today. The current definition of electrodialysis is a membrane-based separation process during which ions are driven through multiple alternating ion exchange membranes under the influence of an electric field. In contrast, classic electrodialysis was conducted with uncharged and non-selective membranes[171], with the first multicell electrodialyzer being developed in 1939[170]. The theory of electrodialysis dates back to 1911[170], far before the first ion-exchange membranes (as used in modern electrodialysis) were created and commercially produced[172]. In 1926, a basic 3-chamber electrodialysis cell was developed and used to separate ions from colloidal soil mixtures[171]. Shortly after in 1927, Wolfgang Pauli developed an electrodialysis cell and used it to study serum proteins[169]. Later in 1938, Joseph and Stadie demonstrated the electrodialysis of blood serum for the determination of total base and chloride content[173]. These types of devices were used in protein purification, precipitation, and material transport/separation throughout the 1920's-40's[169,174–176]. Classic electrodialysis is considered a pioneering technique in sample preparation with an electric field. In traditional dialysis (movement of ions through a membrane without an electric field), the only driving force on the ions is the concentration gradient, meaning the ions would diffuse (very slowly) until equilibrium is reached over the course of hours. The application of an electric field significantly enhances the mass transfer across the membrane making the entire process much faster, preventing any back diffusion, and improving selectivity. The velocity of the ions can be increased by increasing the voltage however, Joule heating must be considered as a limitation at higher voltages. Classical electrodialysis (with an uncharged membrane) has been used for the treatment of many samples ranging from wastewater[177], drinking water[178], soil[179,180], various food matrices[181], and cell cultures[182]. It has also been shown to provide concentration factors ranging from 10-fold[183] to 50-fold[182] in under 1 hour, and effectively

extract low MW peptides with recoveries as high as 85%, making it an interesting potential tool in biomarker discovery[184]. However, there are some disadvantages to electrodialysis, such as the change in pH resulting in sample instability/loss, and thermal degradation of analytes and/or membranes due to Joule heating at high voltages[185].

Modern electrodialysis (*i.e.* with ion-exchange membranes) utilizes membranes which have pore sizes far too small for work with proteins/peptides, and is used mainly for water desalination, and production of chlorine.

1.3.1.2 Electrofiltration

Electrofiltration combines dead-end membrane filtration with an electric field and is often used for the separation and/or concentration of DNA, RNA, polypeptides, polysaccharides, and other biopolymers[186,187]. Generally, filtration membranes are categorized into different groups based on their pore sizes (see Table 1.1), each with a different intended use. With that, there are also a multitude of configurations for electrofiltration such as flat sheet membranes (dead-end or crossflow), tubular membranes, and SLMs, all of which are pictured in Figure 1.14.

Table 1.1 Pore sizes for different types of filtration membranes.

Membrane Type	Pore Size
Conventional filtration	≥ 10 μm
Microfiltration	0.1-10 μm
Ultrafiltration	0.001-0.1 μm (1-1000 kDa)
Nanofiltration	1-100 nm
Reverse osmosis	<1 nm

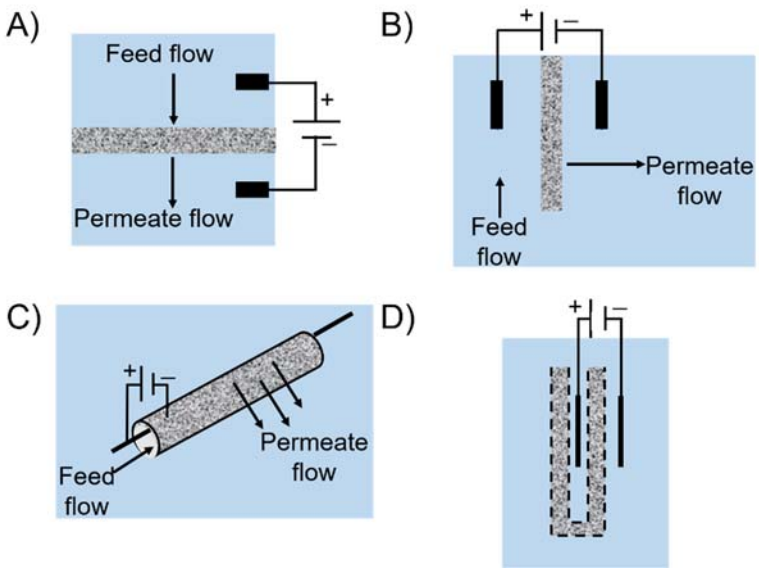

Figure 1.14 Different types of membrane configurations for electrofiltration. A) Dead-end, B) cross-flow, C) tubular membranes, and D) filtration with a supported liquid membrane (SLM).

The mass transfer across a membrane can be significantly decreased due to phenomena like concentration polarization, and fouling (see Section 1.2.2.7), however, the use of an electric field has opened new opportunities for preventing or decreasing these phenomena. There are generally two types of electrofiltration, (1) those where the electric field is used to form a solid cake layer, and (2) those where the electric field is used to prevent formation of a cake layer[188]. The first application is generally used for filtration of solids from a liquid medium for industrial applications (*e.g.* dewatering of mineral slurries), while the second is used in cross-flow filtration devices. Cross flow filtration is a favoured approach when utilizing ultra- and nanofiltration membranes. Here, the electric field can help delay and reduce the formation of a cake layer by decreasing the net force pushing a particle into the membrane surface. It is important to note the electric field must be perpendicular to the membrane surface. Many studies have shown the improvement of filtration procedures by the application of an electric field[189–191]. Improvements to

electrofiltration have been suggested by combining cross-flow electrofiltration with applied pressures of up to 4 bar[189,190]. In addition, pulsed electric fields, rather than continuous, have been shown to reduce cake layer formation without sacrificing filtration efficiency and consuming less power[191]. Due to electrofiltration being applicable to biological macromolecules its use has gained popularity in the pharmaceutical, cosmetic, and nutrition industries for the separation and isolation of naturally produced products[187,192].

1.3.1.3 Electromembrane Extraction

One of the most popular membrane-based techniques for extraction is EME, it is a recently developed technique which utilizes a specialized membrane called an SLM inside a porous hollow fibre (see Figure 1.14 D). The analytes of interest electro-kinetically migrate as promoted by an electric field applied across the SLM into an acceptor phase. EME has become very popular in recent years and has been used for the extraction of various biologicals (plasma, urine, breast milk, and saliva), pharmaceuticals (acidic and basic drugs), and environmental samples (wastewater, ocean and river samples, snow, *etc*.)[151,193–199]. Typically, EME provides sample yields ranging from 55-80% in recovery volumes between 0.3 – 3 mL on the time scale of minutes[195]. The type of solvent used for the SLM is very important as it effects the flux of analyte through the membrane, the diffusion coefficient, and overall selectivity towards an analyte[125,150]. Other parameters that affect the overall success of the extraction include agitation, temperature, extraction time, and strength of applied electric potential. Although EME provides fast and efficient extraction, the limited knowledge of SLM analyte interactions/compatibilities, and the small sample loading capacity are still limiting factors.

1.3.2 Membrane-free Approaches

There are also a wide variety of electric-field driven sample preparation techniques that do not utilize a membrane, for example electric field assisted solid phase extraction (E-SPE)[200,201] and LLEE[202]. In these approaches, a phase boundary acts as a "selective membrane" for separation of sample and contaminants. The ability of an analyte to cross the barrier depends on the polarity, physiochemical properties, chemical content (*i.e.* amino acid content), and mobility of the analyte[203]. E-SPE combines the effects of chromatographic separation with electrophoretic migration to provide a faster and more efficient extraction process[204]. E-SPE has been utilized for the successful extraction of antimicrobials and amines from milk[185,205], quinolones and sulfonamides from egg[206], ionic dyes[207], various ionic species from environmental water samples[157], and successfully interfaced to CE or LC-MS[185,208–210]. Each of these studies reported a significant increase in extraction efficiency as compared to conventional SPE. LLEE generally consists of a biphasic system containing immiscible solvents where analytes partition based on their polarity, however, with the added auxiliary energy of an electric field. There are many examples of LLEE being utilized for extraction of biological fluids and subsequently coupled to methods like CE, HPLC, and LC-MS[154,198,211]. Additionally, LLEE with low-volume (nL-μL) droplets has also been proposed to enhance the degree of contact between the two phases, providing higher mass transfer rates over conventional LLEE[212].

Utilization of electric fields as a driver for sample preparation/purification is an emerging trend in analytical chemistry. Integrating an electric field with more traditional/older sample preparation processes is easily achieved, helps to accelerate the process, adds an additional dimension of selectivity, and is considered a "green" alternative

to harsh/toxic solvents. Recently, electric fields have been applied to both membrane-based and membrane-free approaches, as well as driving new electrochemical-based approaches. These techniques are being regularly employed for the clean-up and separation of complex sample mixtures like blood, environmental, and food samples prior to downstream analysis[185,213,214].

1.4 Research Objectives

The utility of MS towards complex proteomic analysis is unmatched, and as MS instrumentation continues to advance, front-end sample processing techniques continue to be developed as well. SDS is undoubtedly the most favored additive for protein sample extraction, solubilization, separation and/or fractionation, however, its detriments to downstream analysis (LC-MS) are well understood[63]. As such, the development of SDS removal methods has become a very relevant and active research area. There are many methods available for the removal of SDS (see Section 1.1.5.3), each with their own advantages and drawbacks. Many methods fail to deplete free and protein-bound SDS, and those that do often sacrifice significant portions of the sample. Recently, Kachuk and colleagues (2016) presented a novel electrophoretic, membrane-based SDS removal method called TME (see Section 1.1.5.4). The technique is robust and reproducible, successfully depleting SDS from simple and complex protein samples to levels acceptable for LC-MS analysis while maintaining >90% protein yield[65]. In addition, TME successfully depletes SDS from protein samples enriched with hydrophobic membrane proteins for LC-MS analysis. Although the originally developed TME was successful, it required 1 hour of operation time, and rigorous sample mixing throughout the depletion process. The requirement for sample mixing lengthened the time required for depletion, necessitated

manual intervention, and contributed to error/sample loss; all very unfavourable features for a newly emerging sample clean-up method. It was clear further improvements to the sample run time and automation aspects were still required. In addition, little was understood about the electrophoretic properties of TME, and how Joule heating effects depletion success. A more thorough understanding of these concepts would provide insight on how to further optimize both the rate of depletion as well as maintenance of sample integrity.

Chapter 3 presents an exploration into the electrophoretic properties of TME and the different variables affecting the success of each depletion experiment on a model protein BSA. In addition, a simple mathematical approximation for SDS depletion over time is presented to help appropriately compare TME experiments that were run under different parameters. The mechanisms of protein aggregation during and after TME were evaluated, as well as variables including thickness of membrane, implications of SDS back diffusion, depletion rates at higher currents, membrane pore size, and alternate modes of operation (constant voltage or power). The overarching implications of Joule heating during TME are discussed throughout.

In Chapter 4, operation of TME at higher currents is investigated in the context of constant stirring. Constant stirring is presented as a potential method for excess heat dissipation, and a method to increase SDS mass transfer. Optimization of depletion rates and sample yields with the addition of a stir bar is presented. The implications of a stir bar are observed experimentally and correlated to mathematical expressions representing the motion of ions in electric fields and mass transfer across membrane interfaces. Impacts on method automation are also discussed.

Finally, Chapter 5 presents experiments on more complex proteomic samples using TME with a stir bar at higher operating currents. Furthermore, SDS depletion of protein samples by TME (simple and complex mixtures) is compared to the two favoured membrane-based methods of SDS removal in BUP and TDP workflows (acetone precipitation and FASP). In this study, acetone precipitation is successfully demonstrated using an "in-house" designed and constructed two-stage spin cartridge containing a 0.2 μm filter. Parameters including residual SDS, sample yield, quantity of proteins/peptides identified, number of peptide spectral matches (PSM), MW, and hydrophobicity of proteins identified are compared for all three methods. To conclude, Chapter 6 provides a summary of the results obtained and their implications, followed by recommendations for future research.

Chapter 2: Materials and Methods

2.1 TME Instrument Design and Assembly Guide

The TME device was constructed in house, based on a design previously described by the Doucette group[65]. The device comprises multiple pieces, pictured and labelled in unassembled format in Figure 2.1. The membrane that retains protein in the TME sample cell is Spectra/Por® RC 0.5-1 kDa MWCO dialysis tubing (Fisher Scientific, Ottawa, CA); the dry version of this membrane is shown in Figure 2.1 (labelled 1). A similar pre-wetted version was also used. Alternate sizes of MWCO membrane (3 kDa and 12-14 kDa) were utilized in select studies, as indicated. The anode and cathode buffer chambers were machined from polyoxymethylene (common name Delrin®) and are seen in Figure 2.1 labelled 2 and 3 respectively. A more detailed photo of these chambers can be found in Figure 2.2. Multiple gaskets were required for TME to maintain a water-tight seal around the assembled device. Outer silicone gaskets (labelled 4 in Figure 2.1) were placed on the outside of the buffer chambers to seal additional holes in the buffer chambers (non-essential byproducts of the machining process). Custom made silicone inner gaskets were cast using a Sylgard 184 silicone elastomer kit (Dow Corning), pictured in Figure 2.1, labelled 5. The elastomer base and curing agent were combined in a 10:1 ratio, mixed to ensure uniformity, and poured onto a glass plate (thickness ~0.8 mm) and allowed to solidify at room temperature for 48 hours. Once cured, gaskets were cut to shape (~10 cm × 7.5 cm). Each gasket had 4 holes cut into it (using a scalpel for square cuts or a circular punch) to align with the 4 holes in the sample cartridge. A version of the sample cartridge is pictured as number 6 in Figure 2.1. More detailed images and descriptions of the two versions of sample cartridge used in this thesis can be found in Figures 2.4 and 2.5. Wrenches (7 in

Figure 2.1) were used to tighten nuts affixed to threaded rods, guiding aluminum plates (8 in Figure 2.1) around the entire apparatus to hold all pieces together.

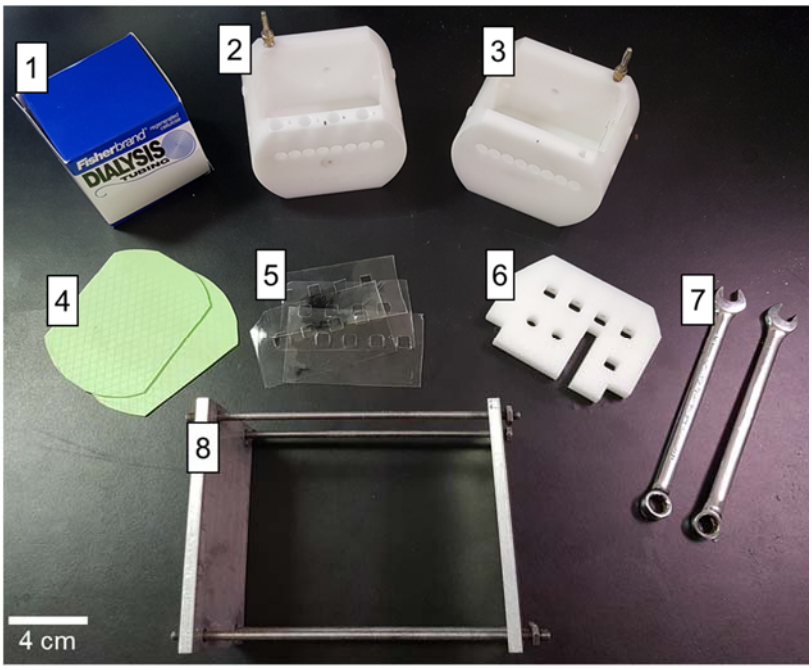

Figure 2.1 Photos of the pieces required to assemble the TME. 1 = dry roll of dialysis MWCO tubing, 2,3 = anode and cathode buffer chambers, 4 = outer gaskets, 5 = inner gaskets, 6 = sample cartridge, 7 = wrenches, 8 = aluminum brackets connected with rods and nuts.

The anode and cathode buffer chambers (~10 cm × 7 cm × 7.5 cm) are pictured in greater detail in Figure 2.2 below. Each chamber contained 0.127 mm diameter platinum wire (Sigma Aldrich) which was attached to electrical leads. The leads were used to connect the TME apparatus to a PowerPac^{TM} Basic Power Supply (Bio-Rad, Mississauga, CA). The anode chamber also contained 4 ventilation holes, which helped prevent the build up of gas bubbles against the membrane while TME was running. The gas bubbles prevent proper flow of current and reduce/prevent SDS depletion.

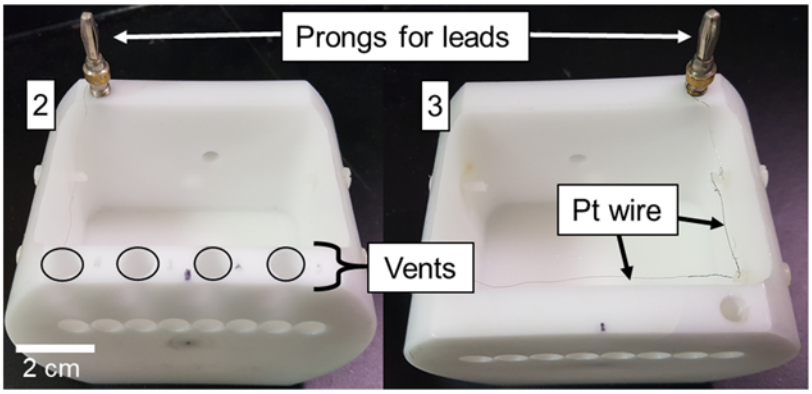

Figure 2.2 Anode (2) and cathode (3) buffer chambers with important pieces labelled. Platinum wire is present inside both chambers and is wound across the front of each chamber and down to the back where it is wrapped around the metal prongs. The prongs are where the leads from the power source are connected. The anode (2) chamber has an added feature of 4 vents to help prevent gas bubble build up along the membrane during TME.

Photos of the TME assembly process can be seen in Figure 2.3 below. Each piece is stacked layer-by-layer on the benchtop in the following order: outer gasket, anode buffer chamber, inner gasket, pre-soaked dialysis membrane, inner gasket, sample cartridge, inner gasket, pre-soaked dialysis membrane, inner gasket, cathode buffer chamber, outer gasket, as per Figure 2.3 A and B. Care must be taken to ensure each layer is laid precisely to line up the holes on each piece. Once all pieces are layered, they are picked up by the middle (see dotted box in Figure 2.3 B) and placed inside the metal brackets as seen in Figure 2.3 C and D. The nuts on the edges of the metal brackets are tightened using wrenches to seal the pieces together. Care must be taken to ensure metal brackets are tight enough to prevent buffer leakage but not over tightened which would induce bowing of the pieces and ripping of the dialysis membrane. Once metal brackets are appropriately tightened, proper alignment of all layers was confirmed by visual inspection.

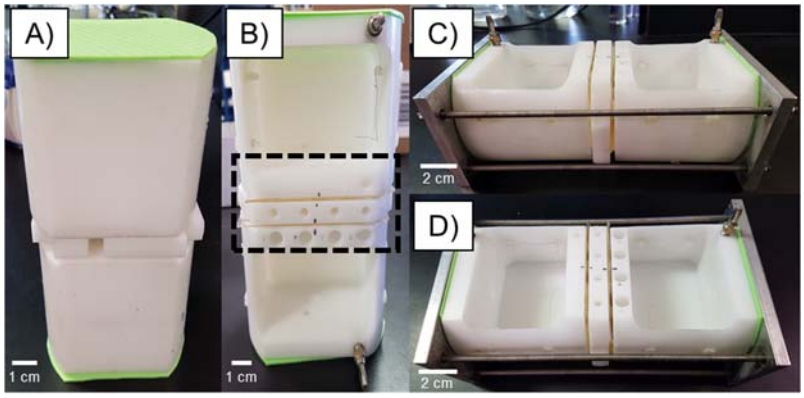

Figure 2.3 A) and B) depict assembly of TME by stacking each layer on the bench-top in the following order: outer gasket, anode buffer chamber, inner gasket, pre-soaked dialysis membrane, inner gasket, sample cartridge, inner gasket, pre-soaked dialysis membrane, inner gasket, cathode buffer chamber, outer gasket. Once the layers are stacked, they can be lifted and inserted into the metal brackets as seen in C) and D). The dotted box in B) indicates the optimal location for lifting the layers for insertion into the metal brackets. Lifting from this point ensures all layers remain aligned. The platinum wire should not be touched during lifting, as it is thin and delicate.

A detailed photo of the original TME sample cartridge is seen in Figure 2.4. The cartridge was machined from a 1 cm thick Teflon sheet, with 4 sample wells (diam. = 1 cm). The top of the sample cartridge contained 4 access holes which allowed for sample loading and removal once the TME apparatus was assembled. Each sample well had an approximate volume of 785 μL, and the approximate dimensions of the piece were 7.5 cm × 10 cm.

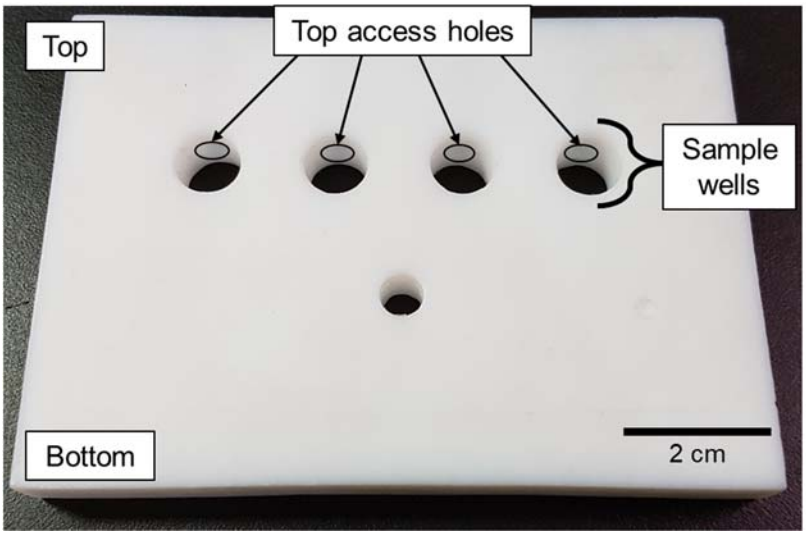

Figure 2.4 The original version of the TME sample cartridge machined from a 1 cm thick Teflon sheet with 4 sample channels (diam. = 1 cm). The piece is approximately 7.5 cm in height and 10 cm in length. The access holes present in the top of the cartridge, which penetrate through to each sample well can be seen labelled and circled in black. Note – the added hole at the center of the Teflon sheet is a byproduct of machining but is not essential to operation of the TME device.

A new sample cell cartridge with square-cut channels (1 × 1 cm, total volume = ~ 1 mL) was machined from Teflon to accommodate a small stir bar. In addition, an incision was created underneath the sample well to accommodate a small motorized stirring device to agitate the stir bars. The new sample cartridge is shown in Figure 2.5. However, it should be noted, the motorized stir apparatus was later retired in place of a stronger stir plate, placed beneath the assembled TME device, which successfully agitates slightly larger stir bars (0.5 cm PTFE-encapsulated magnetic stir bar, Fisher) placed in the sample chambers of the TME device.

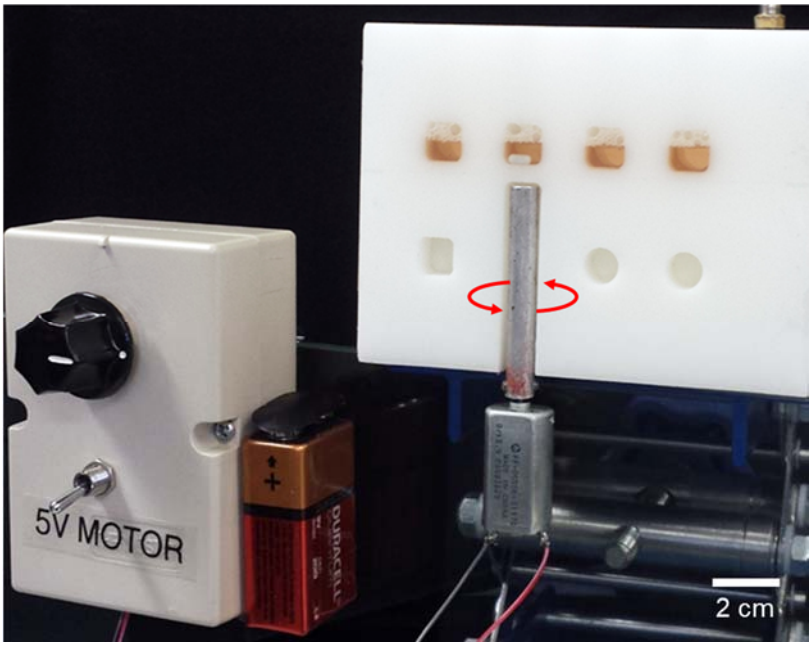

Figure 2.5 The new version of the TME sample cell cartridge with 4 square-cut channels (1 cm × 1 cm) machined from a 1 cm thick Teflon sheet, to accommodate a stir bar (as pictured in the second sample channel). The sample chambers contain ~400 μL of cytochrome c protein solution (orange). Also pictured, is the rectangular incision machined to just below the sample channel which accommodates a small motorized stirring apparatus.

The fully assembled TME apparatus can be seen in Figure 2.6, with a marker to establish approximate size. The TME can be seen plugged into the leads (red and black) from the power source. If TME was to be operated with a stir bar, the last step would be to place the apparatus onto a magnetic stir plate, centered on the sample cartridge.

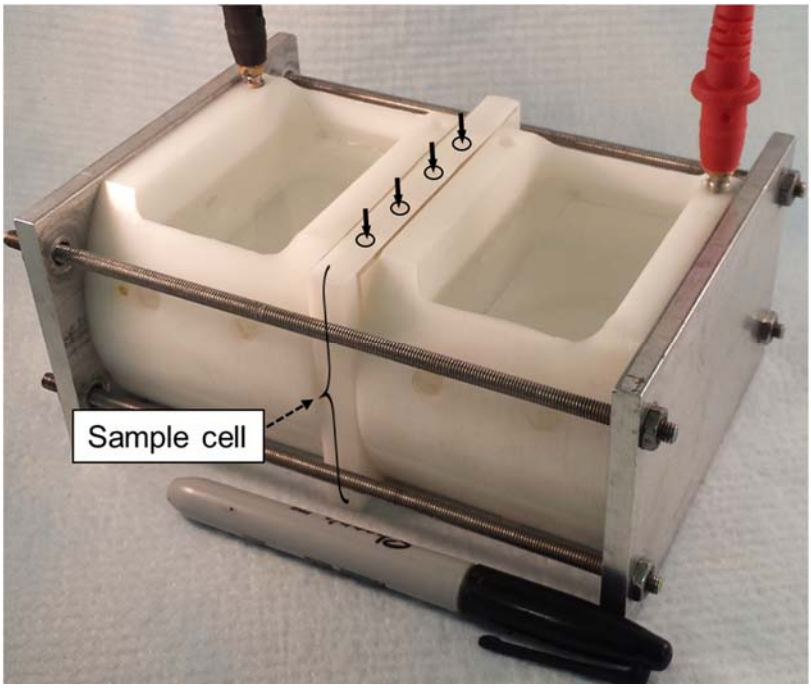

Figure 2.6 The assembled TME apparatus includes the sample cell cartridge (original version or new) with 4 chambers (as indicated with small black arrows), regenerated cellulose dialysis tubing on either side of the sample cell cartridge, and the two outer chambers containing (~160 mL) electrolyte buffer and platinum wire. All pieces are clamped together between two metal brackets tightened with 4 nuts on each side. A marker is shown for scale. Figure reprinted from previously published work[215].

2.2 Chemicals and Reagents

All protein standards, as well as N-p-tosyl-L-phenylalanine chloromethyl ketone (TPCK)-treated trypsin (T8802) were purchased from Sigma (Oakville, CA). Fleischmann's® traditional active dry yeast (*Saccharomyces cerevisiae*) was purchased from a local grocery store and stored at 4°C prior to extraction. Milli-Q water was purified to 18.2 MΩ-cm. HPLC grade solvents were from ThermoFisher Scientific (Ottawa, CA). Methylene blue (for active substances assay) was also from Fisher. Reagents for casting and staining SDS-PAGE gels, as well as urea, dithiothreitol (DTT), and iodoacetamide (IAA) were from Bio-Rad (Mississauga, CA). SDS and formic acid (98%) were from Fluka

(Mississauga, CA). All remaining chemicals were from Sigma and used without further purification.

2.3 Algal Cultures, Harvesting, and Storage

The microalgae *Chlamydomonas reinhardtii* (Canadian Phycological Culture Centre #532) were batch-cultured from a single colony at 23ºC in Sueoka's high salt medium (HSM)[216]. To make 1 L of HSM, 5 mL of Beijerinck's (salt) solution (100 g/L NH_4Cl, 4 g/L $MgSO_4 \cdot 7H_2O$, 2 g/L $CaCl_2 \cdot 2H_2O$), 5 mL of phosphate solution (288 g/L K_2HPO_4, 144 g/L KH_2PO_4), and 1 mL of Hutner's trace elements (ordered from chlamycollection.org) were combined with Milli-Q water up to 1 L. Media was autoclaved for 30 min at 121°C in a Market Forge Sterilmatic autoclave filled with water to the appropriate height. Media was cooled to room temperature before use or stored in the refrigerator at 4°C until needed.

Cultures began by plating and selecting a single colony off an HSM agar plate. Agar plates were prepared by combining HSM with 1.5% (w/v) agar, autoclaving for 30 min at 121°C in a Market Forge Sterilmatic autoclave, and poured into plastic petri dishes before the agar had set. Preparation of the HSM agar plates was performed in a Nuaire Biological Safety Cabinet Laminar flow hood (Class II Type A/B3, Model No. NU-425-600). Cultures were allowed to grow for 2-3 days on HSM agar plates, while being exposed to fluorescent white lights at 100 μmol/m^2/s (translating to a position of ~30 cm from the fluorescent lights) with a 12 hour on-off cycle. Once colonies started to appear, single colonies were plucked and transferred using sterile techniques into 3 mL liquid media. After 7 days growth with 12 hr. cycled light exposure on a continuous shaker (80 rpm, Kang Jian Orbital Shaker KJ-201BD), cultures were moved to 100 mL liquid media, and 7

days later moved to 1 L liquid media. Cultures were harvested in late exponential phase (~7 days after inoculation into 1 L) *via* centrifugation at 1750× *g* (3250 rpm, setting #6) using an International Equipment Co. Clinical Centrifuge (Model: CL, Serial No. 78430M-11), with an expected wet mass between 0.3-0.5 g per litre of culture. Pellets from 500 mL of liquid culture were flash frozen with liquid nitrogen and stored at -20°C until extraction (up to 2 weeks).

2.4 Protein and Proteome Sample Preparation

Protein samples (0.1 or 1.0 g/L) consisting of BSA, ubiquitin, or bovine hemoglobin (BHb) were dissolved in Milli-Q grade water with 5000 ppm SDS (0.5% w/v). A standard intact protein mixture consisted of 6 proteins (see Table 2.1) prepared in Milli-Q grade water or in 5000 ppm SDS to a final concentration of 0.05 g/L per protein.

Table 2.1 Identities and MW of 6 standard proteins used in the top-down studies.

Elution order	Protein	Species	Uniprot #	Molecular weight (Da)	GRAVY Score
(I)	Ubiquitin	*Bos taurus*	P0CG53	8564	-0.489
(II)	Cytochrome c	*Bos taurus*	P62894	11704	-0.866
(III)	Lysozyme	*Gallus gallus*	P00698	16239	-0.472
(IV)	Myoglobin	*Equus caballus*	P68082	17083	-0.396
(V)	Hemoglobin α	*Bos taurus*	P01966	15184	0.0142
(VI)	Carbonic anhydrase	*Bos taurus*	P00921	29114	-0.555
(VII)	Hemoglobin β	*Bos taurus*	P02070	15954	-0.00414

C. reinhardtii pellets (~0.3-0.5 g) or *S. cerevisiae* active dry cells (0.5 g) were resuspended in 5 mL 50 mM Tris-HCl (pH 8.0) with 1.0 % SDS. *C. reinhardtii* cells were lysed by three passes in a French press (16,000 psi). *S. cerevisiae* cells were lysed by grinding into a fine powder under liquid nitrogen using a mortar and pestle. Extracts were centrifuged at 16,200× *g* (13,000 rpm) for 10 min in a Fisher Scientific accuSpin

microcentrifuge (cat. no. 75003241, rotor no. 75003243) to establish clarified proteome extracts. The Pierce bicinchoninic acid (BCA) protein assay kit[217] (ThermoFisher Scientific, Ottawa, CA) was used to quantify initial protein concentration (ranging from ~5 – 8 g/L). The resulting proteome solutions were diluted with Milli-Q grade water and SDS depleted or subject to GELFrEE fractionation prior to SDS depletion.

2.5 Quantitation of Residual SDS and Sample Recovery

The methylene blue active substances assay (MBAS) was performed as described by Arand and colleagues[218]. To summarize, SDS-containing sample was combined in a 1:1 ratio with MBAS reagent (250 mg methylene blue, 50 g sodium sulfate, 10 mL sulfuric acid diluted to 1.0 L), and then combined with 4 parts chloroform. The combined reagents are mixed using a VWR Analog Vortex Mixer at max speed for 10 seconds (Pennsylvania, USA). The absorbance of the chloroform layer was measured at 651 nm in a 0.8 mL semi-micro optical grade glass cuvette with frosted sides and a path length of 1 cm. The limit of detection of the assay is reported as 0.5 ppm, while the limit of quantitation is 2 ppm[219]. The precision of the assay was determined to be satisfactory based on a % coefficient of variation <10%, and the accuracy of the assay was not evaluated in this thesis however previous literature determined accuracy of MBAS assay to be satisfactory[220]. Due to the limited linear region of the assay (2-15 ppm), samples taken from TME throughout the course of a run required varying amounts of dilution depending on how long the TME had been running. For example, early in the run when the concentration of SDS was more than 1000 ppm, only a few microliters needed to be removed from the sample cell. However, towards the end of the run, samples need far less dilution to be in the linear region, which means more volume was removed from the sample cell. Dilution factors and volumes

removed were specific to the conditions of the run, aiming to remove the minimal amount required to perform an SDS assay. Regardless of the volume removed, the amount was recorded and factored into final calculations involving sample recovery. The typical working volumes for this assay were 100 µL of SDS-containing sample, 100 µL of MBAS reagent, and 400 µL of chloroform however, the assay can be scaled down to 80 µL:80 µL:320 µL with enough final volume in the chloroform layer to measure with a UV-vis spectrometer. Additionally, the assay can be scaled as low at 20 µL:20 µL:80 µL, for visual inspection of the presence of SDS.

Intact protein recovery was quantified by a BCA protein assay kit[217]. To summarize, 15 µL of protein sample was combined with 300 µL BCA working reagent and incubated in 60°C water bath for 30 min. BCA working reagent was made fresh each time and created by combining 50 parts "reagent A" with 1 part "reagent B". Working reagent is sensitive to light and was covered with foil for protection. Following incubation, the sample's absorbance at 562 nm was measured against a calibration curve of buffer-matched BSA protein standards over a concentration range from 0.01 to 0.5 g/L. Buffer-matched standards contained an appropriate amount of SDS (depending on timing of sample, ranging between 5000 ppm to 0 ppm) and 25 mM Tris and 192 mM glycine to mimic the TME running buffer. All absorbances (for MBAS and BCA) were read using an Agilent 8453 UV-visible spectrophotometer (Mississauga, CA).

Trypsin-digested samples were quantified by universal high-recovery protein quantitation assay *via* LC-UV (*aka* temperature programmed liquid chromatography) described previously by Orton and Doucette in 2013[221]. To summarize, 98 µL of digested protein diluted with water (if necessary, linear region was 0.01 g/L – 0.1 g/L) were injected

into a self-packed 1 mm × 10 μm C18 column (5 μm octadecylsilyl beads, Waters, MA, USA) using an Agilent 1200 HPLC series instrument. After a 10 min hold, peptides were eluted as a single fraction through an instantaneous bump from 5% to 90% acetonitrile. After 15 min the acetonitrile was instantaneously bumped to 95%, and after 17.5 min the acetonitrile was instantaneously reduced back to 5% and remained there for the duration of the run (45 min). As the sample eluted, (t=10.5 min to t=12.5 min) peptides were quantified using UV absorbance recorded at 214 nm. A calibration curve consisting of trypsin-digested BSA was generated ranging from 0.02 g/L – 0.1 g/L for protein concentration calculations. This also served as a desalting step prior to LC-MS/MS, wherein the collected fraction was subject to complete solvent evaporation prior to analysis.

2.6 Basic TME Operation

Dialysis membrane (pre-wet or dry) was soaked for 20 min in Milli-Q grade water prior to assembling the TME apparatus. TME electrolyte buffer containing 25 mM Tris and 192 mM glycine (pH 8.3) was made in advance and chilled in a refrigerator (4°C). For temperature controlled studies, the TME sample cartridge and two buffer chamber pieces were stored in the freezer (-20°C). When no temperature control was employed, the TME pieces were at room temperature. Prior to assembling the TME, the sample cartridge and two buffer chambers must be removed from the freezer (if temperature controlled) and allowed to warm on the bench for ~5-10 min. This prevents the soaked dialysis membrane from freezing upon assembly. A detailed description of the pieces and assembly can be found in Section 2.1.

Once fully assembled, ice-cold electrolyte buffer was added to each buffer chamber until just covering the sample cartridge holes (~160 mL). SDS-containing protein (see

Section 2.4 for details on sample composition) is slowly and carefully deposited in 500 μL aliquots into each of the sample cells. At this point, the TME device is visually inspected to ensure no air bubbles are blocking the channels from the electrolyte buffer to the dialysis membrane. Air bubbles are cleared through the use of a Pasteur pipette. An electric field is applied using a PowerPac^{TM} Basic Power Supply noting that extreme caution must be taken while the device is in operation (see Section 2.22). The solution temperature within one of the TME sample cells was continuously monitored throughout the course of the runs using an Omega CN7500 series temperature/process controller with attached thermocouple. Voltage, power, and current data were recorded from the power supply readout. For TME runs conducted without stir bars (>30 mA), the TME power supply was periodically paused and unplugged to allow manual mixing of the sample cell contents with a pipette (repeatedly dispense contents 3 times). The frequency of these pause points was experiment-specific and is as described in each section. Briefly, ~30 second pausing events were chosen based on keeping the TME sample cell temperature below boiling. Each time the power supply was paused, the sample chambers were mixed *via* pipetting up and down 3 times.

For TME runs conducted with a stir bar (as specified), stir bars were placed in each of the TME sample wells prior to application of electric field. The entire apparatus was placed on top of a magnetic stir plate to agitate the stir bars within the sample cells. The stir plate was set to the slowest speed (250 rpm) unless otherwise stated.

TME runs were generally considered complete (in varying amounts of time, dependent on the strength of the applied electric field) when the residual SDS was < 100 ppm, wherein SDS-depleted samples were recovered to clean, pre-weighed vials. The

sample mass is recorded to determine the final volume, which increases (by ~100 uL) over the course of the run and so dilution factors must be considered. Any volume of sample removed over the course of the run (for MBAS or BCA assay) was also accounted for in the final volume calculation.

2.7 TME of Proteome Samples

A 3 kDa MWCO membrane was utilized in the TME apparatus for complex proteome mixtures, and a stir bar was always used unless otherwise stated. The TME device was positioned on top of a stir plate to agitate the magnetic stir bars inside the sample chamber. A constant current of 50 mA was applied. Runs were complete when concentration of SDS was ≤ 10 ppm, wherein SDS-depleted samples were recovered to clean, pre-weighed vials. The sample cells were optionally re-extracted with 400 µL of pre-warmed (65°C) 1% SDS where stated.

2.8 Alternate Modes of TME Operation

2.8.1 Constant Voltage

TME depletion experiments were performed at constant voltages of 300, 400, and 500 V with samples of BSA (see Section 2.4 for preparation). At 300 V and 400 V, TME was run for 30 min total, with manual pausing and mixing after every 5 min of run time and aliquots of sample removed every 10 min. At 500 V, TME was run for 15 min total, with manual pausing and mixing at t=5, 10, and 12 min. Aliquots of sample were removed at the pause points.

2.8.2 Constant Power

TME depletion experiments were performed at constant powers of 10, 15, and 20 W with samples of BSA (see Section 2.4 for preparation). At 10 W, TME was run for 40 min total run time, with manual pausing and mixing after every 10 min run time, and aliquots of sample removed at the pause points. At 15 W, TME was run for 20 min total, with manual pausing and mixing after every 5 min run time. An aliquot of sample was removed at t=15 min. At 20 W, TME was run for 20 min total, with manual pausing and mixing after every 2 min run time, and aliquots of sample removed at t=5, 10, and 15 min.

2.9 Cold Formic Acid Re-extraction of TME Sample Cells

Samples of BSA (see Section 2.4 for preparation) were TME depleted at 70 mA for 20 min. Protein samples were removed from the sample cell and transferred to a clean, pre-weighed vial. The sample cells were rinsed with 500 µL 80% cold (-20°C) formic acid. Sample chambers were either rinsed by repeated pipetting up and down 5 times, or the formic acid was allowed to mix with a stir bar inside the sample chamber for 3 min. The formic acid was then recovered to a clean vial.

2.10 Assessment of Different MWCO Membranes

Samples of BSA (see Section 2.4 for preparation) were TME depleted at 50 mA for 30 min using a 0.5-1 kDa or a 12-14 kDa MWCO membrane. For the 0.5-1 kDa MWCO run, pausing and mixing occurred at t=8, 10, 12, 26, and 20 min, while for the 12-14 kDa MWCO run, pausing and mixing occurred at t=8, 10, 12, 16, 20, and 24 min. For both experiments, sample aliquots were removed at t=10, 12, and 20 min.

Samples of ubiquitin (see Section 2.4 for preparation) were TME purified at 50 mA for 30 min using a 0.5-1 kDa or a 12-14 kDa MWCO membrane. For each membrane, pausing and mixing occurred after every 4 min run time.

Samples containing both ubiquitin and BSA (0.1 g/L each, see Section 2.4 for preparation) were TME purified at 50 mA for 30 min using a 12-14 kDa MWCO membrane. Pausing and mixing occurred after every 4 min run time. SDS depleted samples were loaded into a YM-30 Microcon centrifugal filter devices (Millipore Sigma) and spun at 16,200× g for 25 min to separate based on molecular weight. The BSA (retained on the membrane) was resolubilized off the membrane using 500 µL pre-warmed (65°C) 1% SDS with 30 min sonication. The ubiquitin was recovered as a 500 µL aliquot in the bottom of the filter cartridge.

2.11 SDS Back Diffusion into the Sample Cell

Samples of BSA (see Section 2.4 for preparation) were TME depleted at 50 mA for 30 min with a stir bar, resulting in a final SDS concentration below 10 ppm. The power supply was then disconnected and the stir plate turned off. A 100 µL sample from the outside anode buffer chamber was taken and levels of SDS quantified *via* MBAS assay. The protein samples were left inside the sample chambers, and the TME apparatus untouched. Aliquots from inside the sample chambers were taken periodically at t=2, 5, 10, 15, 20, 30, 60, 120, and 720 min and the SDS that had diffused back into the sample chamber from the anode buffer chamber was quantified *via* MBAS assay. Aliquot volumes varied depending on the time, samples taken between 0-5 min required no dilution (*i.e.* 80 µL were taken), but as the concentration of SDS increased in the sample cell over time, less

volume was taken as dilutions with Milli-Q water were required to remain within the linear region of the calibration curve (see Section 2.5).

2.12 Protein Localization Within the Sample Chamber During TME

Samples of BHb (see Section 2.4 for preparation) were TME depleted at 50 mA for 20 min without any mixing. Samples of 200 µL were taken by directing the pipette tip towards the cathode portion of the sample chamber and slowly drawing, while a second sample was taken towards the anode portion of the sample chamber. Samples were diluted 5 times and protein was quantified *via* BCA assay (see Section 2.5) and imaged using a conventional camera.

2.13 Assessment of Temperature-induced Protein Aggregation

Solutions of BSA (1.0 g/L) were prepared with 5000 ppm SDS, or without SDS to serve as a control. Another SDS-containing BSA sample was subject to TME depletion (30 mA without stirring or pausing, final SDS <100 ppm). The three solutions were analyzed using a JASCO J-810 spectropolarimeter to obtain circular dichroism spectra from 200-300 nm.

Following circular dichroism spectra acquisition, all three samples were gradually heated from 22°C to a final temperature of 85°C on a VWR standard heat block (Pennsylvania, USA). Samples were removed from the heat at various times points and centrifuged at 16,2000$\times g$ (13,000 rpm) for 5 min in a Fisher Scientific accuSpin microcentrifuge to pellet any precipitated protein. The BCA protein assay kit was used as described above (see Section 2.5) to quantify the soluble protein still present in the

supernatant. Samples were diluted as necessary prior to BCA assay with appropriate solvent (0.5% SDS, Milli-Q water, or TME buffer) to be within the linear region of the assay.

2.14 GELFrEE Fractionation and SDS-PAGE

GELFrEE fractionation of the extracted proteomes (*C. reinhardtii* or *S. cerevisiae*) was on a custom 8-channel GELFrEE system[45]. The 15% T polyacrylamide resolving gel was cast into 0.6 mm id tube gels. The resolving gel was ~1 cm in height (127 µL), while the stacking gel was ~3 cm in height (300 µL). Protein extract was combined with 5× sample buffer (0.25 M Tris-HCl, pH 6.8, 10% SDS, 50% glycerol, 5% β-mercaptoethanol, 62.5 mM EDTA, 0.05% bromophenol blue) in a 5:1 ratio and boiled in a heat block at 95°C for 5 min. The apparatus was propped up on a ~30° angle and samples were aliquoted into each GELFrEE channel, 100 µL per channel. Based on the initial extracted concentration, the volume of protein extract used was adjusted to give a total of 300 µg protein per GELFrEE channel. GELFrEE was run at 200 V using a PowerPac™ Basic Power Supply and fractions (100 µL/channel) were collected at varying time points as shown in Table 2.2. Fractions were pooled into 3 final samples consisting of small, medium, and large proteins, as per Table 2.2. A 20 µL portion of each GELFrEE fraction was loaded into a 10-well 15% T polyacrylamide gel, together with the original unfractionated sample, and resolved by SDS-PAGE at 200 V on a Bio-Rad mini-PROTEAN system (Mississauga, CA). The gel was silver stained by the method of Chevallet and colleagues (2006)[222] and imaged using a conventional camera.

Table 2.2 Time points in which GELFrEE fractions were collected and which fractions were combined into the final three samples small, medium, and large.

Pooled Fraction	Sample #	Time collected (min)
n/a	0	30
n/a	1	31
n/a	2	32
n/a	3	33
n/a	4	34
Small	5	36
Small	6	38
Small	7	40
Small	8	42
Medium	9	47
Medium	10	52
Medium	11	57
Medium	12	62
Large	13	72
Large	14	82
Large	15	92
Large	16	102

2.15 Filter-aided Sample Preparation

Filter-aided sample preparation (FASP) initially described by Wiśniewski and colleagues[83], was modified slightly for our purposes. FASP was done using 0.5 mL YM-30 or YM-10 Microcon centrifugal filter devices (Millipore Sigma). To reduce dilution, solid urea (110 mg, to make sample up to 8 M) was directly added to 150 µL of the SDS-containing (fractionated or unfractionated) proteome samples, along with 20 µL of 1.0 M Tris buffer and 6.5 µL of 200 mM DTT (final volume prior to initial spin was 230 µL). Samples were allowed to incubate with DTT for 10 min prior to first spin. After incubation, the cartridges were spun at 16,200 × g (13,000 rpm) for 20 min for YM-30 cartridges and 45 min for YM-10 cartridges in a Fisher Scientific accuSpin microcentrifuge. Following centrifugation, 200 µL UA buffer (8 M urea in 0.1 M Tris-HCl, pH 8.5) was added to each cartridge and spun again with the same speed and times. The flow through was discarded.

Next, 100 µL of IAA (0.05 M in UA buffer) was added to each cartridge, vortexed for ~30 seconds and incubated in the dark for 20 min. After incubation, cartridges were spun again, with the same speed and times. Finally, 100 µL of UB buffer (8 M urea in 0.1 M Tris-HCl, pH 8.0) was added to each cartridge and spun again with the same speed and times. This step was repeated two more times. Cartridges were transferred to fresh centrifuge tubes and trypsin was added directly to the cartridge at a 1:50 mass ratio along with 197 µL 0.05 M ammonium bicarbonate buffer, with overnight incubation at 37ºC. Peptides were recovered the following day by adding 50 µL 0.5 M NaCl and centrifuging with the same speed and times. Digestion was terminated by addition of 10% (v/v) 10% trifluoroacetic acid (TFA).

2.15.1 Filter-aided Sample Preparation for Intact Proteins

A modified "top down" FASP protocol was developed to deplete SDS from intact proteins. Following the six centrifugal spins in urea-containing buffers (as described in Section 2.15), 150 µL of LC-MS solvent (5% acetonitrile in Milli-Q grade water with 0.1% formic acid) was added to the filter. The cartridges were incubated at room temperature with sonication for 30 min, after which the spin cartridges were inverted and centrifuged for the same times and speeds described in Section 2.15 to recover resolubilized intact proteins. The cartridges were subject to the optional re-extraction with 150 µL of pre-warmed (65ºC) 1% SDS with sonication for 30 min, after which they were inverted and centrifuged for the same times and speeds described in Section 2.15.

2.16 Acetone Precipitation in a Custom Membrane Filter Cartridge

A custom centrifugal filter device, previously described by Crowell and colleagues (2015) was used to facilitate protein precipitation[90]. The device houses a 0.2 µm Teflon

membrane filter at the base of a 1 mL spin cartridge, which traps precipitated proteins. To 100 µL of SDS-containing protein, 400 µL of acetone was added and incubated in the cartridge overnight (-20°C), with the filter plugged to prevent solvent passage. The plug was then removed, and the cartridge was centrifuged (400× g, 2 rpm, 2 min) to flush the supernatant. The pellet was washed with 400 µL acetone (400× g, 2 rpm, 1 min). Intact proteins were recovered by sonicating the filter cartridge for 30 min in 100 µL LC-MS solvent (plug on), with brief centrifugation to recover the solution (plug off). An optional re-extraction with pre-warmed (65°C) 1% SDS was included. For bottom-up analysis, proteins were solubilized from the Teflon membrane of the filter cartridge with 20 µL 8 M urea (30 min, sonication). The sample was then diluted to 100 µL and digested in the cartridge (plug on) as described in Section 2.17.

2.17 Protein Digestion

For digestion, 10 µL of 1.0 M Tris buffer was added to 90 µL of SDS-depleted sample. Next, 5 µL of 200 mM DTT was added and the sample was incubated (30 min, 60ºC) prior to addition of 10 µL 400 mM IAA (30 min, room temperature, in dark). TPCK-treated trypsin was added in a mass ratio of 1:50, with overnight incubation in 37ºC water bath. The reaction was stopped with 10% (v/v) of 10% TFA.

2.18 LC-MS/MS of Digested Peptides

Following peptide desalting (Section 2.5), peptides were analyzed on an Orbitrap Velos Pro (ThermoFisher) coupled to a Dionex Ultimate 3000 LC nanosystem (Bannockburn, IL), operating in MS mode at a resolution of 30,000 FWHM, scanning in rapid mode for MS^2 (66,666 Da/s, at <0.6 Da FWHM). The column was a self-packed

monolithic C18 (0.1×150 mm, Torrance, CA), coupled to a 10 µm New Objective PicoTip non-coated emitter tip (Woburn, MA). A two hour linear ramp from water (0.1% formic acid) to 35% acetonitrile was employed. The Orbitrap was set to data dependent mode (MS followed by MS/MS of the top 10 peaks).

2.19 LC-MS of Intact Proteins

Ten microliters of the intact protein mixture was injected onto a 0.5×30 cm POROS R2 column (20 µm, Applied Biosystems), operating at 60 µL/min on an Agilent 1200 HPLC nanopump. The column was interfaced *via* ESI to a Bruker Compact QTOF (Billerica, MA) operating in positive mode at 4.5 kV. The LC gradient employed a 30 min linear ramp from 5 to 60 % acetonitrile (in Milli-Q grade water with 0.1% formic acid). The QTOF operated in MS-only mode, from *m/z* 350-2200. Nebulizer gas (N_2) was flowed at 6.0 L/min at 180°C. A spectral scan rate of 2×4.00 Hz was used.

2.20 Proteomic Data Analysis

Peptides were identified using the Proteome Discoverer software, searching the *C. reinhardtii* database (14339 entries, downloaded 1/09/2018), and allowing modifications of oxidized methionine or carbamidomethylation at cysteine. Mass tolerance was set to 20 ppm (MS mode) and 0.8 Da (MS/MS mode) with 2 missed cleavages at a peptide false positive rate of 5%, minimum 2 peptides per protein. Hydrophobicity GRAVY scores were obtained from www.bioinformatics.org/sms2/protein_gravy.html.

2.21 Statistical Analysis

All values are reported as a mean ± standard deviation from at least three replicates. Exponential curves and associated uncertainties were obtained through the LOGEST function in Microsoft Excel. Statistical analysis was done in GraphPad Prism version 7.02 using one-way ANOVA and t-test functions, results of which were deemed significant if $p<0.05$. All data was plotted using GraphPad Prism version 7.02.

2.22 Safety Considerations

TME operates under high voltage without approved safety mechanisms. Extreme caution should be exercised to avoid accidental shock. Prior to handling solutions within the TME apparatus, the power supply is always disconnected.

Chapter 3: Understanding the Effects of Joule Heating During TME[ǂ]

The overall goal for the studies presented in this chapter is to optimize different parameters associated with Joule heating during TME to maintain a low sample cell temperature and hence permit operation with stronger applied electric fields. Different TME operation modes (*i.e.* constant current, voltage, or power) are assessed in context of heat generation. Physical aspects of the TME such as the membrane thickness and pore size are explored. SDS depletion rates for TME operated at currents above 50 mA is also assessed. These studies begin by creating a consistent and reliable method to compare different TME experiments which had varying initial conditions, operation modes, or depletion times.

The decrease in flux across a membrane is broken up into 3 stages, and these stages can be appropriately modelled over time using an exponential decay function[135,139,145,146]. Similarly, the plots of SDS remaining in the sample cell over time closely resemble exponential decay plots, as seen in Figure 3.1.

ǂ Portions of this chapter have been published in: Unterlander, N.; Doucette, A. A.; Accelerated SDS depletion from proteins by transmembrane electrophoresis: Impacts of Joule heating. *Electrophoresis*. (2018). DOI: 10.1002/elps.201700410.

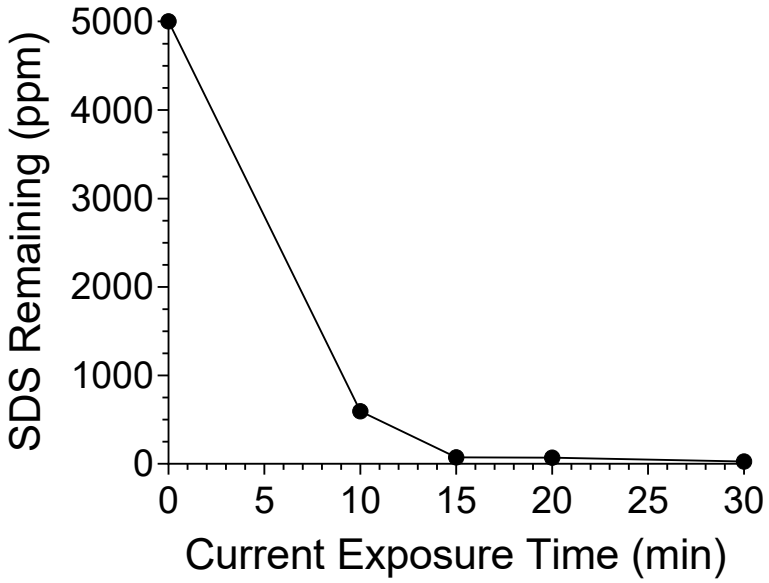

Figure 3.1 Representative SDS depletion over time curve for a typical TME experiment run at 50 mA constant current for 30 min.

It should be understood that flux of SDS, $\boldsymbol{J}_{SDS}$, is different than residual SDS (concentration of SDS remaining in sample cell), SDS_t, however, the two parameters are intimately related. To relate the two, a simplified version of the NP equation (Equation 1.19), in which the diffusion and convection terms are considered negligible, can be integrated to reveal the exponential decay function seen below[215]:

$$SDS_t = SDS_0 e^{-\lambda t} \tag{3.1}$$

where SDS_t represents the concentration of SDS at time t (ppm), SDS_0 represents the initial concentration of SDS (5000 ppm), λ represents the decay constant, and t represents the time (s). Here, λ is presented as a function of many parameters[215]:

$$\lambda = \frac{DzFE}{LRT} \tag{3.2}$$

where L is the length of the sample cell including the membranes (cm), and R is the gas constant $\left(\frac{J}{K \cdot mol}\right)$. Equation 3.1 is an approximation which assumes a constant temperature and voltage over time for simplicity. Although not constant, these factors remain relatively stable, but minor deviations from the exponential model are observed at high values of E.

The decay constant represents the negative slope of the logarithmic plots, and can be utilized to calculate the half-lives $\left(t_{\frac{1}{2}}\right)$ for each experiment using the following equation:

$$t_{\frac{1}{2}} = \frac{\ln(2)}{\lambda} \tag{3.3}$$

Equation 3.2 clearly depicts the relationship between applied electric field and the decay constant as being directly proportional. The electric field is proportional to the applied voltage (V) and inversely proportional to the distance (d, cm) between the electrodes:

$$E = \frac{V}{d} \tag{3.4}$$

The TME experiments presented in this work are mainly conducted at constant current (unless otherwise stated) however, it should be noted, the average voltage at each current value increases linearly in close approximation to Ohm's law, as seen in Figure 3.2.

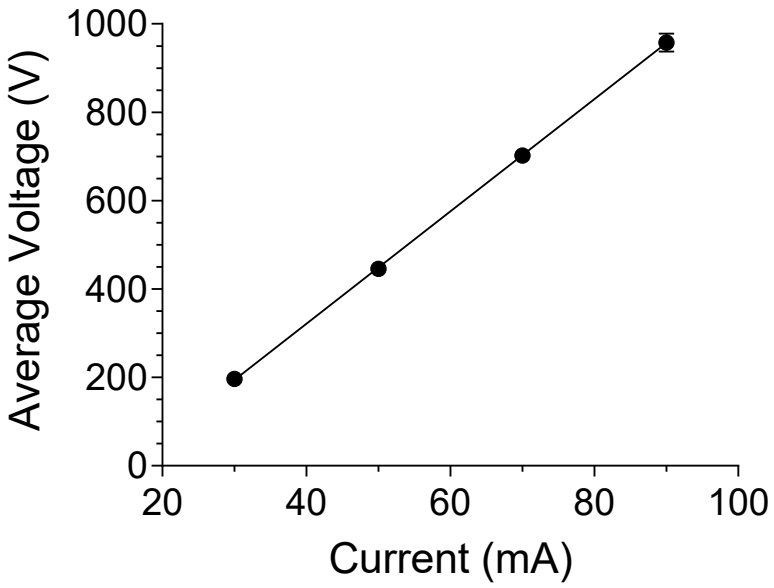

Figure 3.2 Ohm's law plot displaying the linear relationship between voltage and current in TME. Each TME experiment was run under identical conditions except for varying the current. Samples initially contained 0.1 g/L BSA in 5000 ppm SDS. The voltage plotted is the average observed over the time period 8 to 10 min. The error bars represent the standard deviation of 3 replicate measurements. The data are fit using a linear regression with the equation $y = 12.707x - 186.92$ and an $R^2 = 1.0$.

This relationship demonstrates how increasing the applied current can increase the rate of SDS depletion. Increasing the current provides a proportional increase in the applied voltage, and it is known from Equation 3.4, an increase in voltage will increase the strength of the electric field (E). Furthermore, the strength of the electric field is proportional to the flux of SDS as per Equation 1.19. Moreover, due to the variable nature of each TME experiment and the existing history of data, utilizing the exponential decay approximation allows for direct comparison between experiments despite variations in initial conditions. The SDS depletion data for TME presented in this work will be modeled using the equations discussed above.

It is understood that the application of an electric field during TME drives the production of Joule heating, which can be problematic when working with protein

solutions. Excessive heating causes proteins to aggregate and precipitate, and this effect is further emphasised when considering the progressive removal of solubilizing agent during TME. Based on Equation 1.8, the amount of Joule heating observed is proportional to the square of the strength of the electric field (E). This indicates in order to maintain a reasonable temperature for proteomic samples, there is a practical upper limit on the magnitude of the applied electric field. The limit of 40 mA maximum current previously imposed on the original TME work by Kachuk and colleagues in 2016 related to the decreased protein recovery observed at increasing TME sample tempertures[65]. The temperature in which BSA begins to aggregate and precipitate has been cited as 60°C[223]. In this regard, 60°C was considered the upper limit of temperature for the following experiments. As a result, frequent voltage pause events were used by Kachuk and colleagues to maintain a reasonable sample cell temperature. The pause events were a simple strategy employed in initial studies to maintain TME cell temperature when operating at higher currents and were only ~30 seconds in duration. The frequency of pause events was experiment-specific and is indicated as such. However, it should be noted that proteins are very chemically diverse and have been known to begin aggregating at lower (40 to 45°C)[224] and higher temperatures (65°C or more)[225,226]. A low sample cell temperature is important for maintaining sample integrity, and key to increasing the rate of SDS depletion by allowing for an increase in the applied current.

3.1 Varying Modes of TME Operation

The majority of TME experiments are/were performed at constant current however, most electrophoretic procedures operate using a constant voltage as the driving force for

migration (*i.e.* SDS-PAGE, GELFrEE, IEF). This is because there is a linear relationship between migration speed (velocity, v) and voltage:

$$v = \frac{qV}{df} \tag{3.5}$$

where d is the distance between the two electrodes (cm). For applications such as SDS-PAGE, the resistance increases over time, as the highly conductive ions like Cl^- are electrophoresed out of the gel. Therefore, in a hypothetical constant voltage experiment, the current will decrease over time as resistance increases (as per Ohm's law $V = IR$). This means, less heat will be generated as the experiment progresses (as per Equation 1.7, $H = I^2Rt$), which can be a desirable feature. However, a decrease in current means the rate of migration decreases and the experiment will take longer. When performing SDS-PAGE at constant current, the migration of sample proceeds at a uniform rate (giving predictable stop times), but as the resistance increases, the voltage and heat generated will also increase, which can be detrimental to the integrity and appearance of the gel.

In contrast, the resistance during TME is seen to decreases with time (like a Western blot transfer), as seen in Figure 3.3.

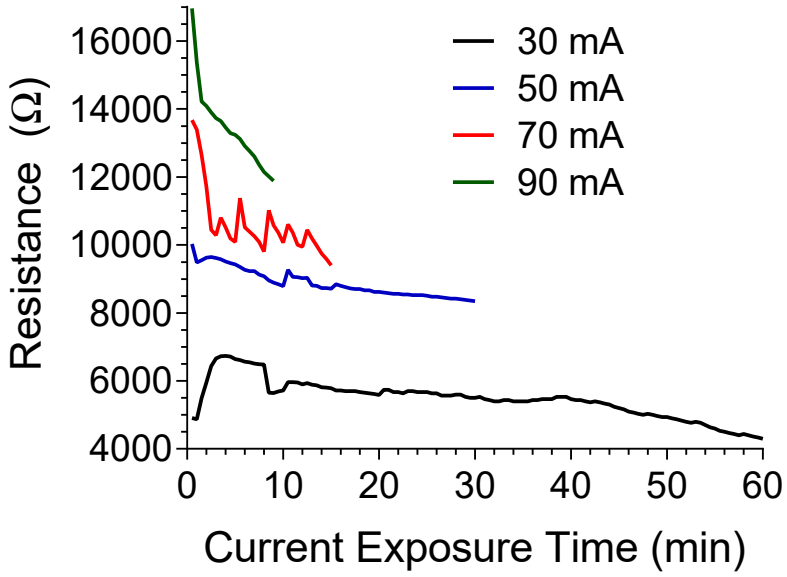

Figure 3.3 Plots of TME system resistance as a function of time during experiments run at constant currents of 30, 50, 70, and 90 mA.

This is possibly due to the ionic strength of the sample chamber changing over time. Specifically, the sample deposited into the TME device is prepared in water (with SDS) but without TME electrolyte buffer. As TME proceeds, the electrolyte buffer (25 mM Tris, 192 mM glycine, pH 8.3) is electrophoresed into the sample chamber, which increases the ionic conductivity and decreases the overall resistance. The lack of heat dissipation inside the sample chamber also causes a decrease in viscosity and an overall decrease in resistance. Furthermore, as the dialysis membrane warms it is possible the pore dimensions are being distorted and easing current passage. The voltage during a constant current TME experiment also decreases with time, which correlates with the observed resistance decreasing over time (as per Ohm's law $V = IR$). TME is a dynamic system and as the contents of the sample chamber change, the magnitude of the electric field at a set current will also change. However, it should be noted the effect of temperature on voltage is indirect and associated with other factors within the experiment such as contents of

electrolyte buffer and geometry of the system. Further experiments are required to clarify how temperature inside the sample cell impacts resistance and voltage during TME.

A decrease in both voltage and resistance should give an overall decrease in heat generated at constant current. Although the temperature of the sample cell increases with time, the magnitude of the increase becomes smaller over time, as less heat is generated overall. This means the temperature of the TME sample cell should increase more slowly over time, and possibly even reach a plateau. Alternatively, if TME is operated at constant voltage, as resistance decreases, the current must increase (recall: $V = IR$), which leads to an increase in the heat generated over time; an undesirable trait for preservation of soluble proteins. Furthermore, if TME is operated at a constant power, as resistance decreases, current will increase (but less than the increase observed with constant voltage, recall: $P = RI^2$), which suggests the generation of heat will remain approximately uniform. The trends in heat generation are clearly depicted in Figure 3.4 which plots the change in temperature of the sample cell over time for TME experiments run at constant current (A), constant voltage (B), and constant power (C).

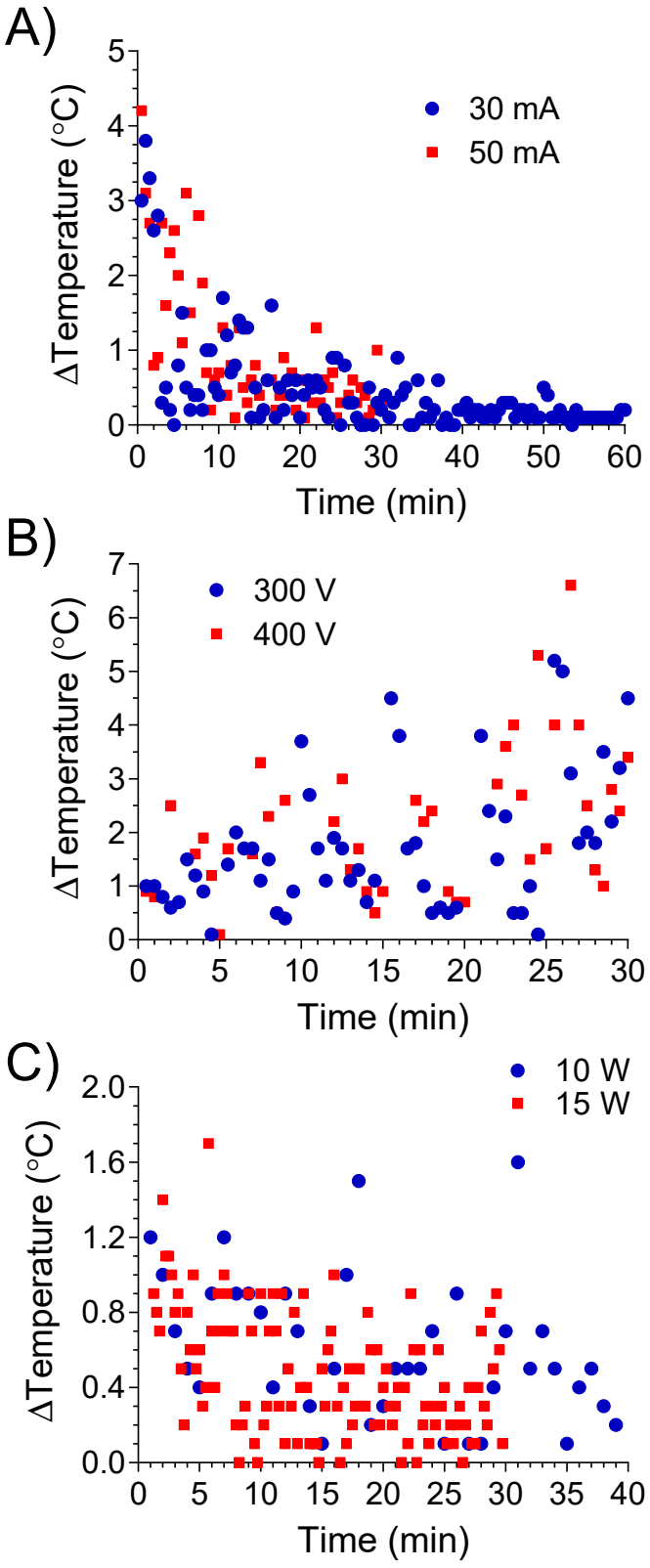

Figure 3.4 The change in temperature over time for TME experiments run at A) constant current, B) constant voltage, and C) constant power. TME samples initially contained 0.1 g/L BSA in 5000 ppm SDS.

The change in temperature for constant current shows a clear trend of decreasing in magnitude. This supports the concept that at constant current a decrease in the heat produced within the system should be observed. At constant voltage, the plot depicts an increase in the magnitude of the temperature difference over time. Also, as expected, TME at constant power shows no noteworthy trends, suggesting a uniform generation of heat over time.

The choice of constant current is even more appropriate when we consider how current is carried by each component in the TME system. The smaller molecules present in the system (buffer ions, SDS ions, sodium ions) contribute much more to the current than the macromolecules (proteins). This is corroborated by the mathematical expression, Equation 3.6, relating ionic conductivity, Λ_i, to an ion's mobility, μ, (which is a function of the size of the ion, recall Equation 1.5):

$$\Lambda_i = zF\mu \qquad 3.6$$

Since, TME is concerned with the migration of small SDS ions, maintaining a constant current (rate of migration) is an appropriate choice for fastest depletion. Meanwhile, constant voltage is more appropriate for procedures concerned with the predictable migration of the macromolecules, where a constant driving force will be applied to all components in the system.

These principles are based on available electrophoretic theories which mainly describe gel electrophoresis, and the simple relationships describing electrical circuits. To ensure, the TME agrees with these relationships, experiments were performed at constant voltage and constant power, and compared to previous results obtained at constant current.

3.1.1 Constant Voltage

TME depletion experiments on 0.1 g/L BSA initially at 5000 ppm SDS (0.5%) were run at 300, 400, and 500 V constant voltage. Figure 3.5 depicts the SDS depletion plotted as a function of time for each operating voltage. Each depletion curve is fit to an exponential decay function with equations and half-lives found in Table 3.1.

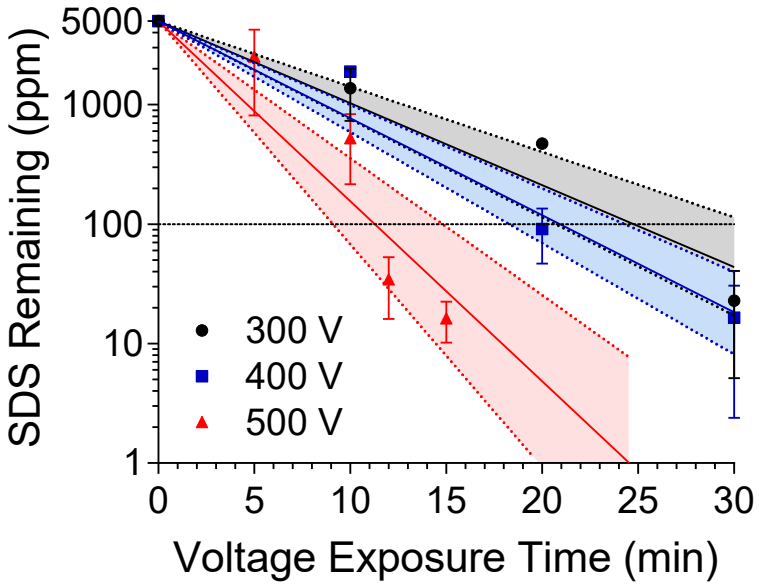

Figure 3.5 Residual SDS of 0.1 g/L BSA initially at 5000 ppm SDS, plotted as a function of TME run time at 300, 400, and 500 V constant voltage. The data are fit to exponential decay functions with the error of the fit displayed as the shaded regions within the dotted lines. Error bars represent the standard deviation from 3 replicate measurements.

Table 3.1 Equations for exponential decay fits of SDS depletion with TME at various operating voltages, and their corresponding half lives.

Voltage (V)	$t_{\frac{1}{2}}$ (min)	Equation
300	4.4 ± 0.8	$SDS_t = 5000e^{-0.158t}$
400	3.7 ± 1	$SDS_t = 5000e^{-0.187t}$
500	2.0 ± 1	$SDS_t = 5000e^{-0.347t}$

As expected, a similar trend of increasing voltage (electric field) gives increasing SDS depletion rates. At 300 V constant voltage, SDS is depleted to 23 ± 20 ppm within 30 min of run time. The half-life of SDS at 300 V was determined to be 4.4 ± 0.8 min, which is

the same half-life observed by Kachuk and colleagues in 2016 at 50 mA constant current[65]. At 400 V constant voltage, depletion to below 100 ppm SDS is achieved within 20 min (91 ± 44 ppm), and after 30 min the residual SDS is down to 17 ± 14 ppm. The half-life of SDS at 400 V was determined to be 3.7 ± 1 min. Furthermore, at 500 V constant voltage, 35 ± 20 ppm is achieved within 12 min of run time, and after 15 min the residual SDS is 16 ± 6 ppm. The half-life of SDS at 500 V was determined to be 2.0 ± 1 min. Although SDS is successfully depleted using constant voltage, the protein recovery is compromised at high voltages (Figure 3.6).

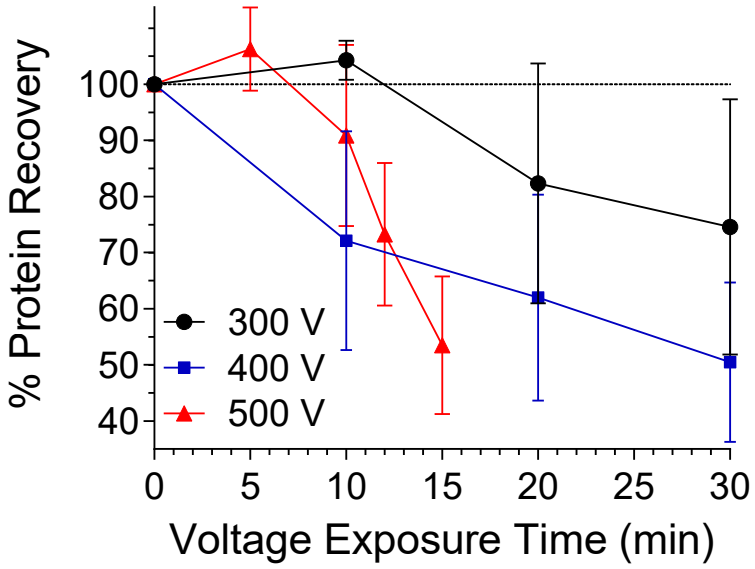

Figure 3.6 Protein recovery of 0.1 g/L BSA initially in 5000 ppm SDS plotted as a function of TME run time at 300, 400, and 500 V constant voltage. Error bars represent the standard deviation from 3 replicate measurements.

At 300 V constant voltage, the final recovery of BSA was 75 ± 23 % after 30 min of run time. At 400 V constant voltage, the final recovery dropped to 50 ± 14 % after 30 min of run time. Additionally, there are also marked losses in protein recovery observed at 500 V with a final recovery after 15 min of 54 ± 12 %. The pattern of protein loss observed in

Figure 3.5, can be better explained when the temperature of the TME sample well over time is considered (Figure 3.7).

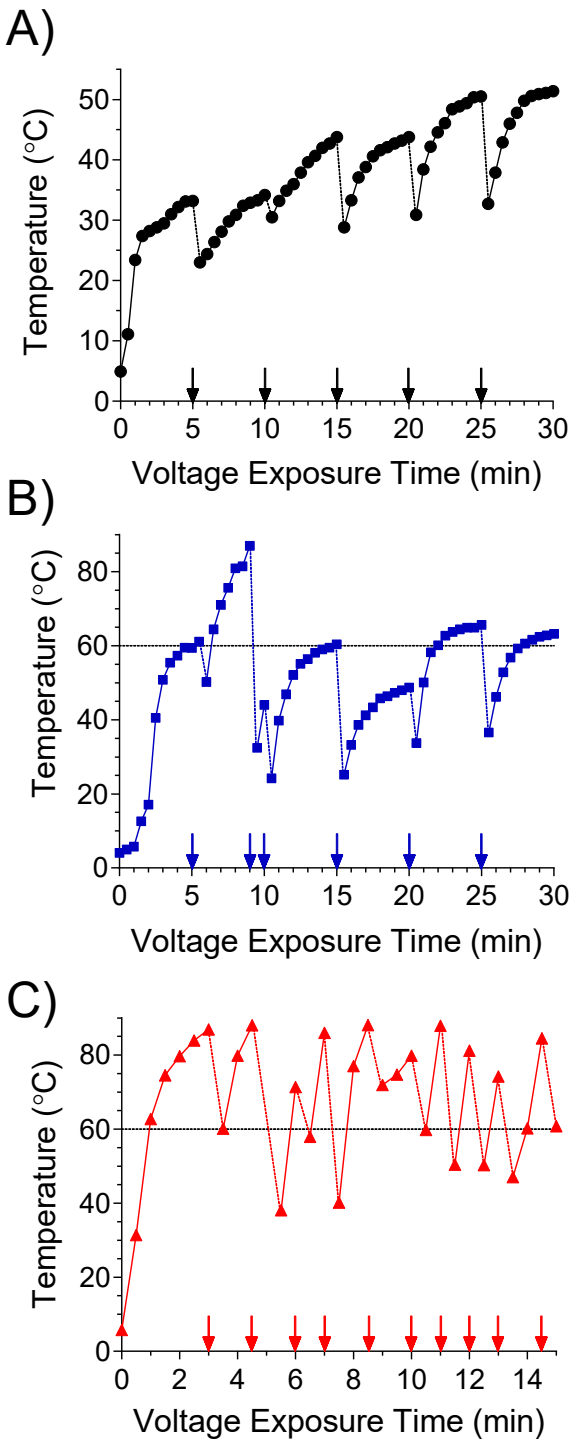

Figure 3.7 Temperature of the TME sample cell, recorded over the course of the runs at A) 300, B) 400, and C) 500 V constant voltage. The arrows on the x-axis correspond to

time points where the power supply was temporarily paused, explaining the rapid drop in temperture at these time points.

Each experiment required a number of voltage pause points to maintain a reasonable sample cell temperature. These pause points are denoted on the temperature plots by the arrows on the x-axis and is what gives the plots their non-uniform appearance. During the 300 V constant voltage experiment, seen in Figure 3.7 A, the TME sample cell temperature steadily ascended to 51.4°C despite incorporating pause/mix events every 5 min. When considering the 400 V run (Figure 3.7 B), the large loss in recovery in the first 10 min can easily be explained by the temperature reaching 87°C within 9 min of TME run time. At 500 V constant voltage, there is a steady decline in protein yield after the first 5 min, which is supported by the temperature plot in Figure 3.7 C. The temperature of the sample cell was difficult to maintain despite pause/mix events approximately every minute. Nearly the entire plot resides above 60°C, which is what contributed to the steady yield losses over a short period of time. A similar loss in protein recovery is seen at 500 V (compared to 400 V) though the run only required 15 min. Such significant losses can be attributed to the amount of time the sample cell was >60°C. A combination of high levels of Joule heating and time promoted the rapid losses observed between t=10 min and t=15 min for the 500 V run.

Returning to the discussion on electrophoretic theory, at constant voltage the current generated throughout the run confirms a general upwards trend (results not shown), however, it is worth noting that the maximum current reached by each experiment is relatively low compared to constant current experiments. For example, the maximum current reached at 400 V was only 26 mA, but as seen in Figure 3.7 B, the sample well gets much hotter than if the experiment were run at 26 mA constant current (see Supporting Info

ref. 65)[65]. While the SDS depletion half lives are an improvement upon those published by Kachuk and colleagues in 2016, the losses in protein are the highest among all the operation methods (see Supporting Info ref. 65)[65]. Protein recoveries ≤55 % are only observed during TME operated at constant voltage. Additionally, the recoveries observed in Figure 3.6 were not found to be significantly different from one another (t-test, $p>0.05$) suggesting poor recoveries are observed regardless of the magnitude of V. These results and observations, validate the hypothesis that constant voltage is unsuitable for TME, because there is an increase in heat generation over time.

3.1.2 Constant Power

TME depletion experiments on 0.1 g/L BSA initially at 5000 ppm SDS (0.5%) were run at 10, 15, and 20 W constant power. Figure 3.8 depicts the SDS depletion plotted as a function of time for each operating power and equations for exponential fits and half-lives found in Table 3.2.

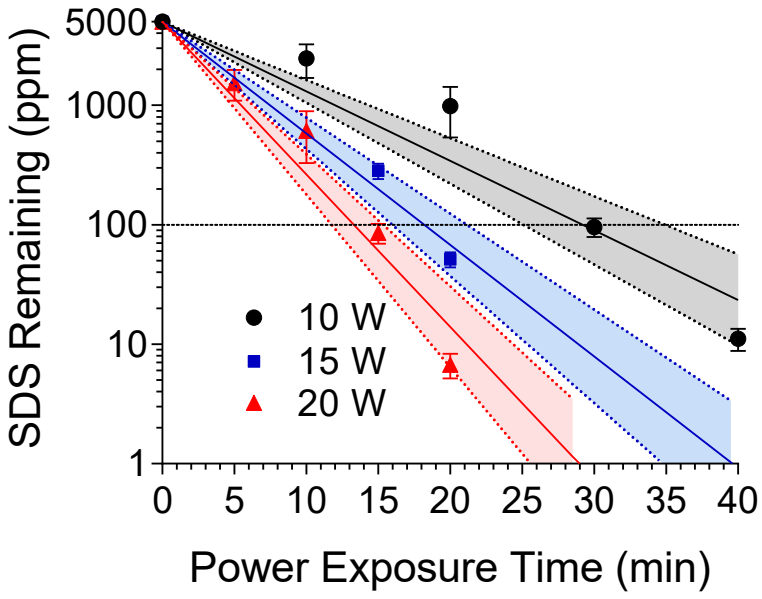

Figure 3.8 Residual SDS of 0.1 g/L BSA initially at 5000 ppm SDS, plotted as a function of TME run time at 10, 15, and 20 W. The data are fit to exponential decay functions with

the error of the fit displayed as the shaded regions within the dotted lines. Error bars represent the standard deviation from 3 replicate measurements.

Table 3.2 Equations for exponential decay fits of SDS depletion with TME at various operating powers, and their corresponding half lives.

Power (W)	$t_{\frac{1}{2}}$ (min)	Equation
10	5.2 ± 0.8	$SDS_t = 5000e^{-0.134t}$
15	3.2 ± 1	$SDS_t = 5000e^{-0.215t}$
20	2.4 ± 2	$SDS_t = 5000e^{-0.294t}$

As expected, increasing power gives increasing SDS depletion rates. At 10 W constant power, SDS is depleted to 96 ± 17 ppm within 30 min of run time, and 11 ± 2 ppm after 40 min of run time, with a half-life of 5.2 ± 0.8 min. At 15 W constant power, SDS was depleted to 51 ± 7 ppm in 20 min, with a half-life of 3.2 ± 1 min. Likewise, at 20 W constant power, SDS was depleted to 86 ± 20 ppm within 15 min, and 7 ± 2 ppm after 20 min, with a half-life of 2.4 ± 2 min. Unfortunately, the improvements on depletion time are of course offset by the loss in recovery depicted in Figure 3.9.

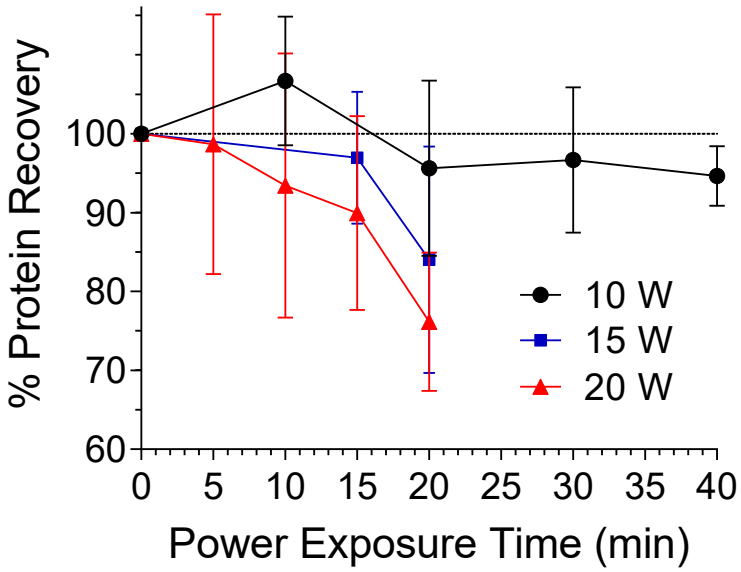

Figure 3.9 Protein recovery of 0.1 g/L BSA initially in 5000 ppm SDS plotted as a function of TME run time at 10, 15, and 20 W constant power. Error bars represent the standard deviation from 3 replicate measurements.

The protein recovery at 10 W remains relatively stable throughout the course of the experiment, with an end recovery of 95 ± 4 % after 40 min of run time. This yield corresponds to the minimal Joule heating observed throughout the 10 W run, as seen the temperature plot in Figure 3.10 A. The sample cell temperature remains below 38.3°C throughout the entire 10 W run, which agrees with the consistent high protein recovery. In contrast, the 15 W and 20 W experiments both have noticeable losses in protein yield after 20 min, ending with 84 ± 14 % and 76 ± 9 % respectively. The temperature at 15 W constant power (Figure 3.10 B) approached 50°C within 8 min of run time and reached ~60°C by the end of the run. Though losses are observed at 15 W, the final protein recovery is not significantly different (t-test, $p>0.05$) than the 10 W run, indicating maintenance of temperature below 60°C is important to sample recovery. When considering the steady drop in protein recovery for the 20 W experiment, the temperature plot (Figure 3.10 C) shows a dramatic increase up to 80.6°C, and a maintenance of temperature above 60°C for the duration of the experiment. Although frequent pause points were introduced every ~2 min, control of the TME sample cell temperature was difficult. The final protein recovery at 20 W was determined to be significantly different (t-test, $p<0.05$) than the 10 W run, which correlates with Figure 3.10 C depicting temperature >60°C.

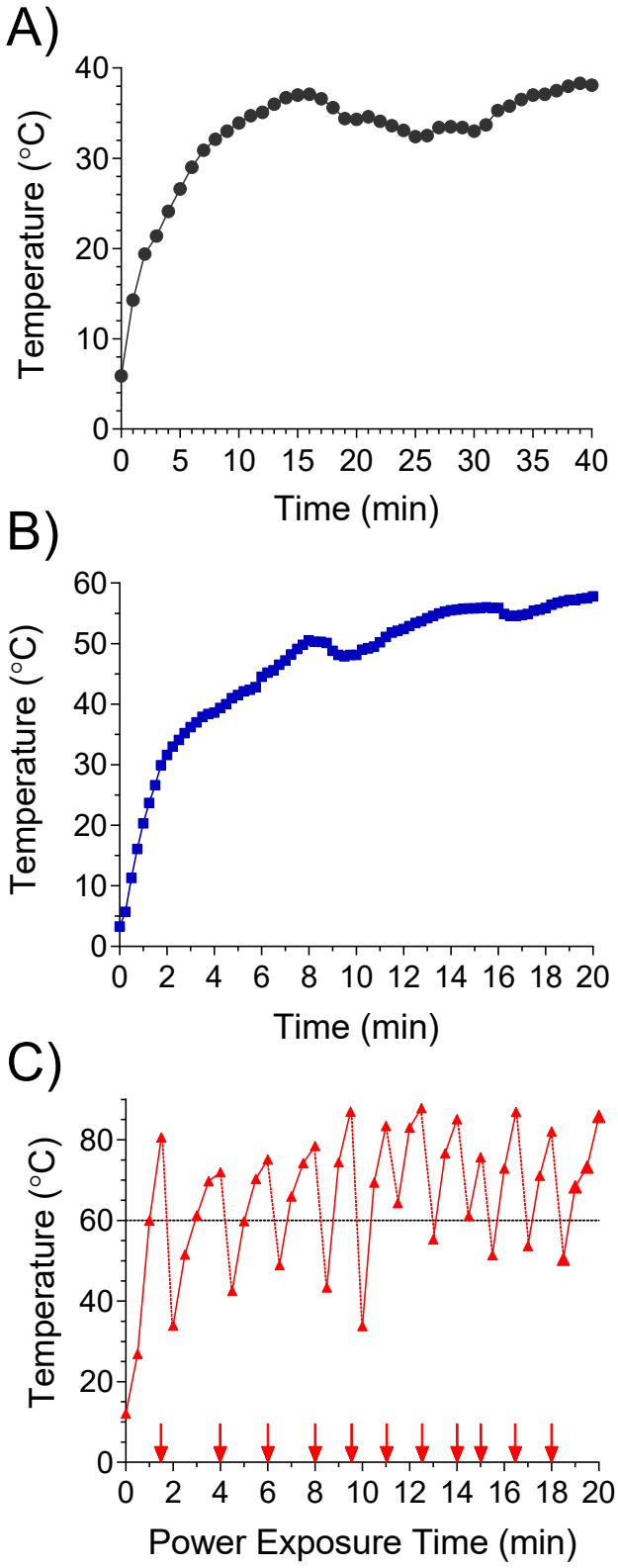

Figure 3.10 Temperature of the TME sample cell, recorded over the course of the runs at A) 10, B) 15, and C) 20 W constant power. The arrows on the x-axis in C correspond to time points where the power supply was temporarily paused.

As expected, constant power (like constant voltage) also worsened Joule heating within the sample cell. At constant power, the current increased over time however, not as much as with constant voltage (as per Joule-Lenz law: $P = I^2R$). For example, at 15 W, the maximum current achieved was 29 mA, but the temperature of the sample cell was higher than that observed for a typical 30 mA constant current run (see Supporting Info ref. 65)[65]. These results suggest maintaining a constant power (and a theoretically uniform generation of Joule heating) is not the optimal operation mode for best results with TME.

Each operation mode depletes SDS from the protein sample, and the rate of SDS depletion increases as the strength of applied voltage or power is increased. However, substantial losses in sample yield are observed for both operation methods. It has been shown heat generation during constant current experiments is the smallest (see Figure 3.4), and the experiments presented above demonstrate a decrease in sample yield compared to previous constant current data. For the remainder of experiments presented in this thesis, constant current was utilized to operate TME, mainly to minimize the generation of Joule heat.

3.2 Single Layer *vs* Double Layer MWCO Dialysis Membrane During TME

A point of high resistance is the dialysis membrane interface and modifying its parameters could provide changes in the resistance. The membrane employed during TME is from a roll of dialysis tubing. As originally disclosed by Kachuk and colleagues in 2016, the dialysis tubing was placed on either side of the sample chamber, partitioning the sample from the two electrolyte buffer chambers on either side[65]. This setup therefore places two layers of dialysis membrane on either side of the sample cell. Conventional dialysis employs a single layer of membrane tubing, so it is reasonable to assume that TME should

function with a single layer of the tubing. Assuming a constant resistance across the membrane, a single layer would decrease the overall thickness of the membrane, which in turn reduces the work done by the electric field to move a charged particle, as per the equation below:

$$W = qEd\cos\theta \qquad 3.7$$

where W is the work done by the electric field, and θ is the angle between the electric field and the path of the charged particle. Although this is a simplified explanation, the concepts of heat production and work are closely related[120,131], and it is appropriate to conclude they are correlated here. To provide evidence for this hypothesis, a simple experiment was conducted in parallel comparing SDS depletion rates at 50 mA, with a double layer and a single layer of membrane.

Figure 3.11 depicts the temperature of the sample cell measured in real-time with a single or double layer of dialysis membrane.

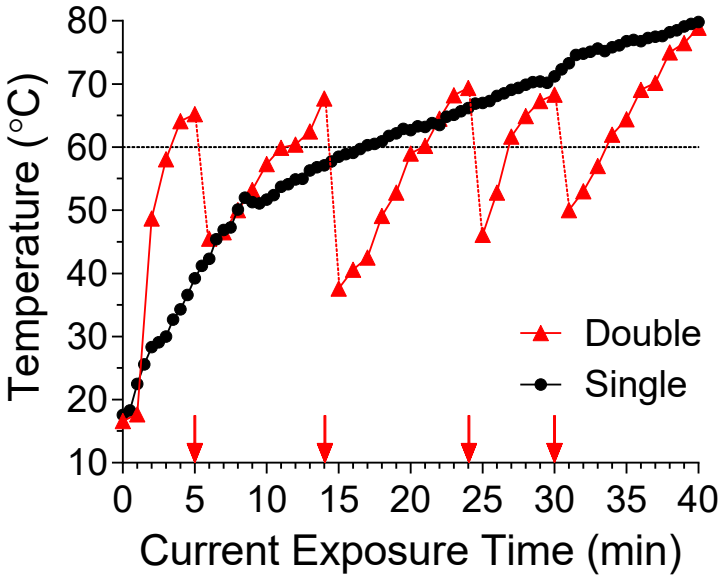

Figure 3.11 Temperature of the TME sample cell, run at 50 mA for 40 min with a single layer or double layer of dialysis membrane (0.5 – 1 kDa MWCO) covering each side of the sample cell cartridge. Initial sample contained 0.1 g/L BSA in 5000 ppm SDS. The

red arrows correspond to the time points where the power supply was temporarily paused (~30 seconds) during the double layer run to allow additional heat dissipation.

When using a single layer of dialysis membrane, a dramatic effect on temperature within the sample cell was observed. With a double layer of dialysis membrane, 65.2°C is reached within 5 min of run time, and regular voltage pausing events were performed throughout the run to maintain reasonable sample cell temperatures, though reaching a final temperature of 78.9°C (dangerously high in terms of both protein yield, and safety). In contrast, the single layer TME run doesn't reach 60°C until 17 min and displays a much slower increase in temperature, which resulted in fewer pause events required. This finding is corroborated by significant differences (t-test, $p<0.05$) in average resistance over time, 4.7 ± 0.3 kΩ for the single layer run, and 8.8 ± 0.2 kΩ for the double layer run (1.8 times). For context, the resistance across the system without membranes was determined to be ~4.3 kΩ, and with one membrane (2 layers) ~6.5 kΩ. The resistance is nearly halved when using a single layer of membrane. These values verify why lower temperatures are observed and suggests reducing resistance will permit the ability to operate at higher currents.

Reducing the thickness of the membrane has the potential to impact its retentive ability. A thinner membrane could result in more protein losses through the membrane during TME. However, as seen in Figure 3.12, the protein yield remains ≥90% and statistically similar between the two treatments (t-test, $p>0.05$).

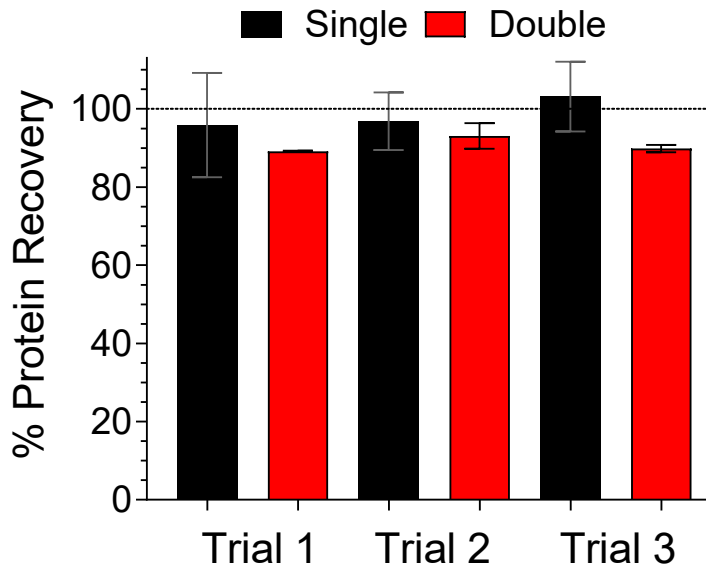

Figure 3.12 Protein recovery of samples containing 0.1 g/L BSA initially at 5000 ppm SDS after 40 min of TME run time using a single layer or a double layer of dialysis membrane (0.5 – 1 kDa MWCO). Error bars represent the standard deviation from 3 replicate measurements.

No significant changes in SDS depletion rates were observed over the course of 40 min when using a single layer of dialysis membrane (Figure 3.13).

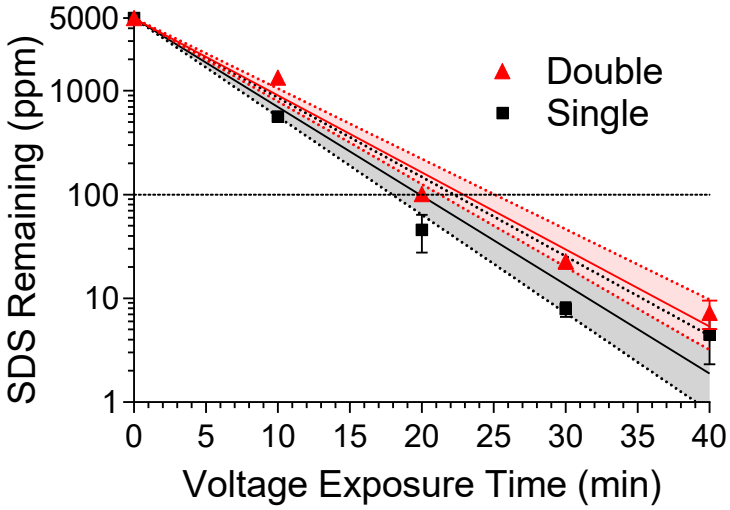

Figure 3.13 The residual SDS of a 0.1 g/L BSA solution initially containing 5000 ppm SDS, plotted as a function of TME run time with a single layer or a double layer of dialysis membrane (0.5 – 1 kDa MWCO). The data are fit to exponential decay functions with the error of the fit displayed as the shaded regions within the dotted lines. Error bars represent the standard deviation from 3 replicate measurements.

Table 3.3 Equations for exponential decay fits of SDS depletion with TME using a single or a double layer of dialysis membrane (0.5 – 1 kDa MWCO) and corresponding half-lives.

Treatment	$t_{\frac{1}{2}}$ (min)	Equation
Single	3.5 ± 2	$SDS_t = 5000e^{-0.197t}$
Double	4.0 ± 2	$SDS_t = 5000e^{-0.171t}$

Beginning with 5000 ppm SDS, both the single and double layer conditions reduced the level of SDS to below 100 ppm in under 20 min of TME run time (101 ± 2 ppm and 50 ± 20 ppm respectively). At 30 min, the residual SDS in the single layer run is lower than that of the double layer run by ~15 ppm, however, considering the starting value (5000 ppm) both samples could be considered equivalently "pure" at this point. After 40 min the levels of residual SDS are within error for both the single and double layer (5 ± 2 ppm and 7 ± 2 ppm respectively). Switching to a single layer of dialysis membrane did not significantly change the half-life (3.5 ± 2 min for the single layer *vs* 4.0 ± 2 min for the double layer). The marginal differences between SDS depletion rates can easily be explained when considering the basic equation describing flux through a porous membrane:

$$L_p = \frac{\varepsilon r^2}{8\eta\delta_m} \tag{3.8}$$

where ε is the volume void fraction of the membrane, δ_m is the membrane thickness, and r is the pore radius. This equation describes the hydraulic permeability of a membrane (*i.e.* ability for a material to transmit a fluid) as inversely proportional to the thickness of the membrane. Therefore, a reduction in the thickness should increase the ability for the membrane to transfer fluid and solutes within that fluid (such as SDS). This also supports the observed increase in resistance seen when the membrane is thicker.

Although minimal changes in SDS depletion rate were observed, the most important result is seen in the temperature and resistance data. It can be concluded that there is no decrease in TME depletion performance (in terms of SDS depletion rate and sample yield) when operating with a single layer of dialysis membrane. However, there are substantial changes to the temperature of the TME sample cell, which directly correlates to the overall resistance within the system being approximately halved.

3.3 Loss of Protein During TME

One of the main concerns when operating TME is the protein losses directly associated with Joule heating. It is assumed that heating promotes protein aggregation, adsorption onto the membrane, and perhaps even precipitation. SDS promotes solubilization but completely denatures a protein's tertiary structure, which exposes its hydrophobic regions. This exposure further promotes the tendency of proteins to aggregate as SDS is removed from the sample. To gain a clearer understanding of whether these truly are the methods of sample loss during TME, an experiment was conducted to evaluate the decrease in solubility of a protein sample after the SDS has been removed. Samples of BSA (0.1 g/L) prepared in water without SDS, or in 5000 ppm SDS, or following SDS depletion by TME (30 mA, final SDS <100 ppm) were gradually heated in a heat block to 85°C. Figure 3.14 displays the protein remaining in solution following heating for the specified times.

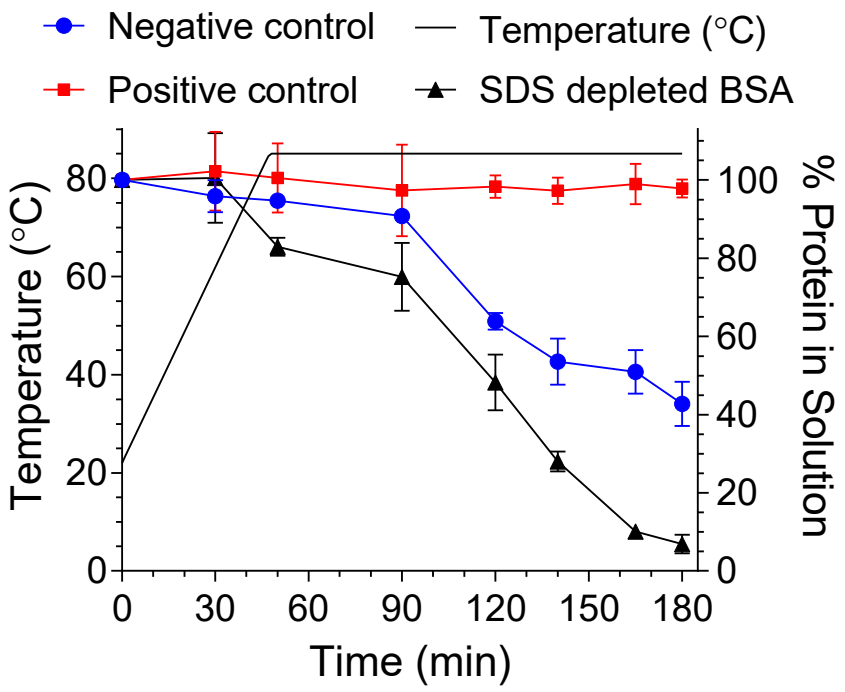

Figure 3.14 Samples of 0.1 g/L BSA prepared in water (negative control) or in 5000 ppm SDS (positive control), or following SDS depletion by TME (30 mA for 1 hour, final SDS <100 ppm) were gradually heated in a heat block to 85°C. The protein remaining in solution following heating is plotted on the right y-axis. The left y-axis is plotting the temperature of the heat block during the experiment. Error bars represent the standard deviation from 3 replicate measurements.

The negative control was the solution of BSA prepared in the absence of SDS, and the positive control was the solution of BSA in the presence of 5000 ppm SDS. As expected, the presence of a solubilizing agent allowed the SDS-containing protein to remain in solution throughout the heating process. The protein sample prepared in water is seen to precipitate out of solution as the sample is heated (Figure 3.14, blue curve). While, the SDS-depleted protein (Figure 3.14, black curve) begins to aggregate at a lower temperature, and to a greater extent over the course of 180 min. This indicates that the denatured but SDS-depleted protein sample is most susceptible to temperature-induced aggregation. In addition, this figure provides supporting evidence for the critical temperatures associated with TME protein loss. The SDS-depleted sample begins to precipitate after 30 min, which

corresponds to a temperature of ~60°C. However, BSA is a single protein and behaves differently than a complex mixture (such as a proteome) would in this environment. The MW, hydrophobicity, and amino acid content can all contribute to varying levels of heat stability above and below 60°C[227]. Overall, SDS-depleted denatured protein samples will aggregate and precipitate more readily upon heating, and at lower temperatures than native BSA. This study has confirmed the importance of maintaining sample cell temperatures below 60°C and illustrated the magnitude of impact Joule heating can have on the recovery of sample during TME.

3.4 Use of Cold Formic Acid to Rinse TME Sample Wells

Protein loss during TME due to Joule heating is a potential problem, most notably when operating at high currents. With only a single layer of membrane as a barrier, and much higher applied forces acting on the proteins, there is additional risk of sample loss out of the sample chamber. It is hypothesized the sample loss during TME pertains to proteins which are still inside the sample cell but have aggregated and adsorbed onto the membrane, which makes them difficult to recover. However, it is theoretically possible for some protein to have passed through the membrane. To provide a clearer picture of how sample is being lost, a re-extraction step is added to the clean-up procedure. Once TME has completed depletion, the sample is removed from the sample chamber and any remaining protein is resolubilized in appropriate solvent. It has been previously shown that rinsing the sample cell with 80% (v/v) cold formic acid[88] can recover some of the precipitated proteins, providing an increase in protein identification with MS[65]. TME experiments were run at 70 mA constant current for 20 min with initial recoveries between 72-83% (blue bars in Figure 3.15 A). As described, the sample chambers were rinsed with formic acid to recover any

remaining proteins missed when the initial sample was removed. The green bars in Figure 3.14 A depict the additional 12-20% protein recovery collected from the formic acid re-extraction, likely lost to aggregation/adsorption. This experiment was then repeated, but the formic acid step included a stir bar mixing the formic acid for ~5 min. As seen in Figure 3.15 B, the new final recoveries after rinsing with a stir bar all reach 100%.

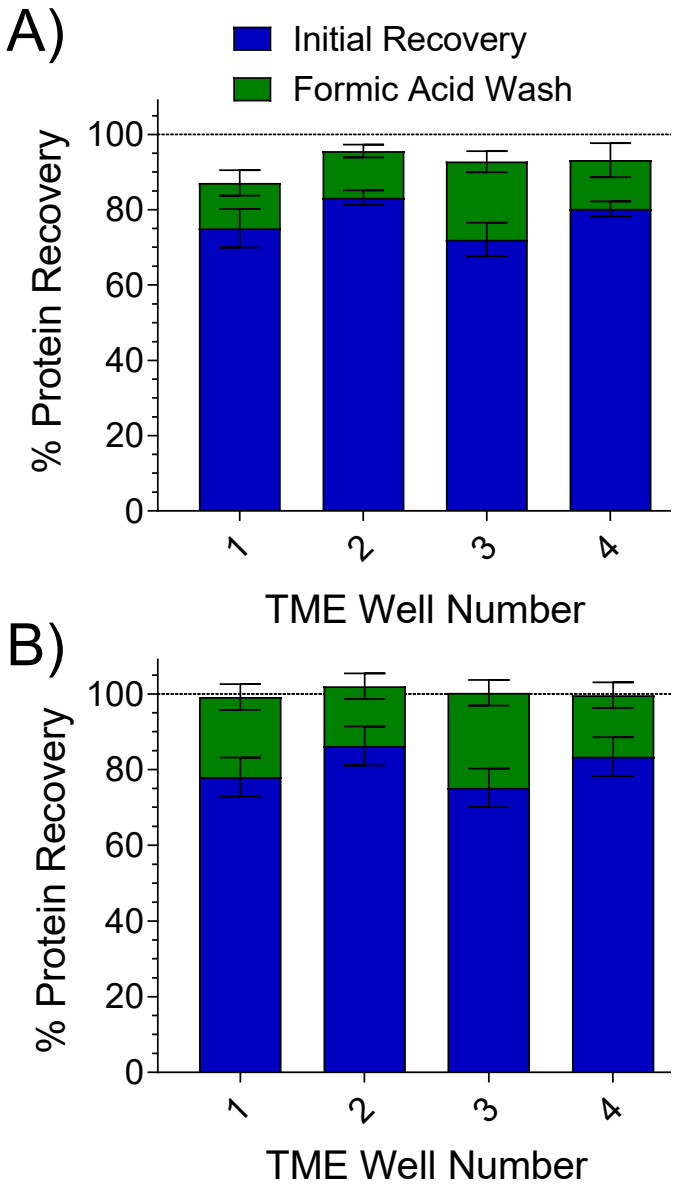

Figure 3.15 Initial protein recovery of samples containing 0.1 g/L BSA after SDS-depletion with TME at 70 mA for 20 min, and protein recovery after a rinse with 80% cold (-20°C) formic acid with a) no stirring, and b) with stirring for 5 min. Error bars represent the standard deviation from 3 replicate measurements.

It is clear from these figures, mixing inside the sample chamber is an important step in fully recovering all protein that may have come out of solution during the run. The requirement of mixing indicates some unfolded and aggregated proteins may have found their way into the pores of the membrane. Even though regenerated cellulose membranes are considered hydrophilic, and assumed to carry no net charge, there is still some interaction between the protein and the membrane. This theory is corroborated in the work done by Sheldon and colleagues in 1991, which states unfolded BSA can accumulate on the surface and within the bulk of regenerated cellulose MWCO membranes of pore sizes much smaller than BSA[228]. Additionally, it has been shown that an unfolded protein is more likely to deposit onto the membrane surface and have a larger negative impact on flux than a globular protein[141], which is likely because of its increased Stokes radius[229]. Although the cited results were collected without the influence of an electric field, it is a safe assumption that any drift velocity associated with the movement of protein in TME would further aid a protein's insertion into the membrane.

As SDS is depleted from the sample, it is known (from circular dichroism Spectra Figure 3.16) the protein remains in an unfolded, non-globular state, and is therefore much more likely to adsorb onto the membrane and lower overall flux and increase resistance. Mechanical perturbation in combination with a formic acid rinse is an effective strategy to recover proteins which have become deeply embedded or strongly adsorbed onto the membrane after depletion.

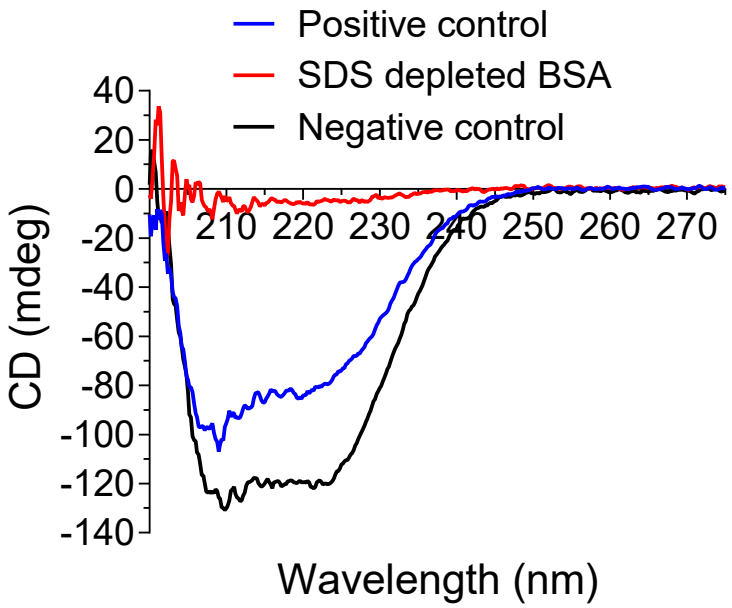

Figure 3.16 Circular dichroism spectra of a 0.1 g/L SDS depleted BSA sample, initially at 5000 ppm SDS (depleted using TME at 30 mA constant current for 1 hour), a 0.1 g/L sample of BSA in 5000 ppm SDS (positive control), and a 0.1 g/L sample of BSA in water (negative control).

3.5 SDS Back Diffusion with Removal of Electric Field

Conventional dialysis works on the principle of passive diffusion, and molecules move until equilibrium is established. Equilibrium occurs when the concentrations of said molecule (or solute) are the same on both sides of the membrane. It has been shown that conventional dialysis cannot completely purify a sample of the protein-bound SDS molecules, and only depletes the free in solution SDS. This is because the free energy of binding between SDS and protein cannot be overcome passively, no matter how long the dialysis procedure continues[116]. Because of this, dialysis was often used to determine binding ratios like SDS to protein (determined to be 1.4 g SDS/g protein)[35] or the binding of proteins to small molecule solutes or cofactors[230]. Additionally, previous experiments by Kachuk in 2016 show an assembled TME apparatus in the absence of an electric field (essentially conventional dialysis) only depletes 60% of the SDS after 1 hour[81]. The goal

of TME is to achieve purity levels appropriate for downstream MS analysis (≤100 ppm) in less than 1 hour, meaning conventional dialysis is not appropriate.

TME differs from conventional dialysis because it operates to the point where the concentration of SDS inside the sample chamber is much lower than that on the outside anode buffer chamber. As the concentration of SDS decreases in the sample chamber, the possibility of SDS back diffusing (in relevant quantities) into the sample chamber grows. At the end of a typical TME experiment (starting SDS conc. is 5000 ppm), the final concentration in the anode buffer chamber is ~65 ppm, while the final concentration in the sample chamber is below 10 ppm. This means, once the electric field is no longer applied, the SDS molecules have the potential to diffuse from the anode chamber back into the sample cell with a rate proportional to the concentration difference (as per Fick's law of diffusion, see Equation 1.10). As seen in Figure 3.17, once the electric field is removed, the increase in SDS in the sample chamber over time is rapid, increasing to 98 ppm within 10 min (plotted on right y-axis).

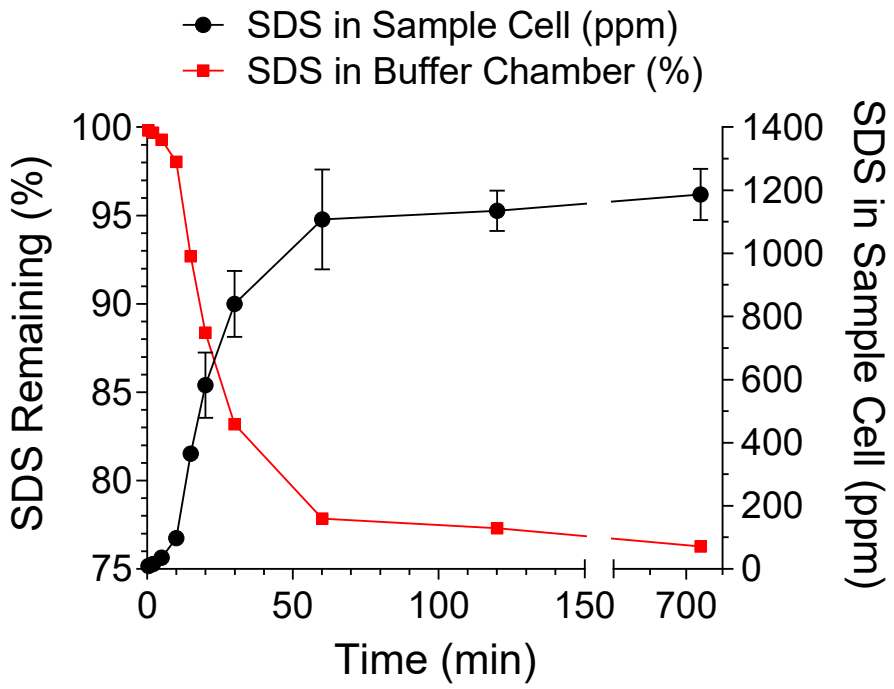

Figure 3.17 Quantification of the diffusion of SDS over time from the anode TME buffer chamber back into the sample cell after depletion is complete and the electric field is turned off. The red plot (squares) is quantifying the % SDS remaining in the anode chamber over time (left y axis), while the black plot (circles) is quantifying the increase in SDS (ppm) in the sample chamber over time (right y axis). Error bars represent the standard deviation from 3 replicate measurements.

Considering the sample was originally below 10 ppm after depletion, this is a significant level of back diffusion in a short period of time. During depletion, as the level of SDS in the sample chamber approaches lower limits, only a small amount of back diffusing is required to contaminate it. The red curve in Figure 3.17 (left y-axis) bears a close resemblance to a traditional dialysis curve in which the percent of solute remaining is plotted over time. It can be seen, the concentration of SDS in the sample chamber reaches a plateau around 1 hour at ~1100 ppm and remains statistically unchanged for the remaining 11 hours of the experiment, indicating the back diffusion of SDS has reached some form of equilibrium. This value is very high considering the concentration in the anode chamber after depletion was ~65 ppm. As mentioned, diffusion is based on concentration differences

of free solutes, and does not provide enough energy to facilitate the diffusion of protein-bound SDS. Therefore, as SDS diffuses back into the sample chamber, it re-binds to the protein and becomes unavailable for further diffusion, thus pushing the "equilibrium" further towards the sample chamber. SDS will diffuse back into the sample chamber until the protein binding sites are full and the concentration of free SDS is equal on both sides of the membrane. Based on a ratio of 1.4 mg SDS/mg protein and 0.05 mg protein in each well, ~0.07 mg of SDS will be completely bound within each well and will not contribute to the establishment of equilibrium. This indicates ~0.5 mg of SDS free in solution in each sample chamber (~2 mg total), in equilibrium with the buffer chamber (containing ~8 mg total). These numbers indicate a non-equilibrium state, but there may be other factors influencing the observed levels back diffusion, such as overall ionic strength of the sample chamber compared to the outer chambers. This experiment illustrates the need to remove the SDS depleted sample from the TME immediately upon completion, and the importance of this step increases as the level of sample purity increases. Additionally, this experiment further validates how ineffective conventional dialysis is at depleting protein-bound SDS.

3.6 SDS Depletion Rates at Higher Currents

It has previously been shown for TME that operating at higher current density will increase the rate of SDS depletion[65]. However, at higher currents excessive Joule heating encourages protein aggregation and membrane fouling[65]. It was for this reason, the TME

was limited to operation at 40 mA, to maximize protein recovery. Due to the low operation current, SDS depletion would require ~45-60 min to achieve the desired purity of ≤10 ppm.

The goal of the following work was to increase the depletion rates of TME to less than 1 hour of operation time. To do so, the operating current was increased up to a maximum of 90 mA, and SDS depletion rate was observed. For the purposes of this study, the effects of Joule heating on protein recovery were not discussed yet. In addition, the desired purity for these experiments was increased from 10 ppm to ≤100 ppm, to help reduce the effects of prolonged exposure to Joule heating. Assuming a 5000 ppm starting concentration of SDS, achieving ≤100 ppm corresponds to ≥98% depletion, which is still outperforming many alternative depletion methods. In addition, it should be stressed 100 ppm is considered acceptable for standard downstream MS analysis[64,80]. The threshold levels of 10 ppm and 100 ppm SDS were previously put forward by the Doucette group, and are both amenable to downstream analysis. Desired purity levels depend on sample type, LC-MS instrumentation, and what type of information is required (*i.e.* identification *vs* quantitation). Additionally, TME is one of the only available methods which provides "tunability" to the purity level of the sample, and this can be advantageous for maintenance of high sample yields. Figure 3.18 depicts SDS depletion with TME of a 0.1 g/L BSA solution (initially at 5000 ppm SDS) at 30, 50, 70, 80, and 90 mA constant current. Table 3.4 depicts the equations for the exponential fits seen in Figure 3.18 and corresponding half-lives, along with half-lives from the previous study by Kachuk and colleagues in 2016 for comparison[65].

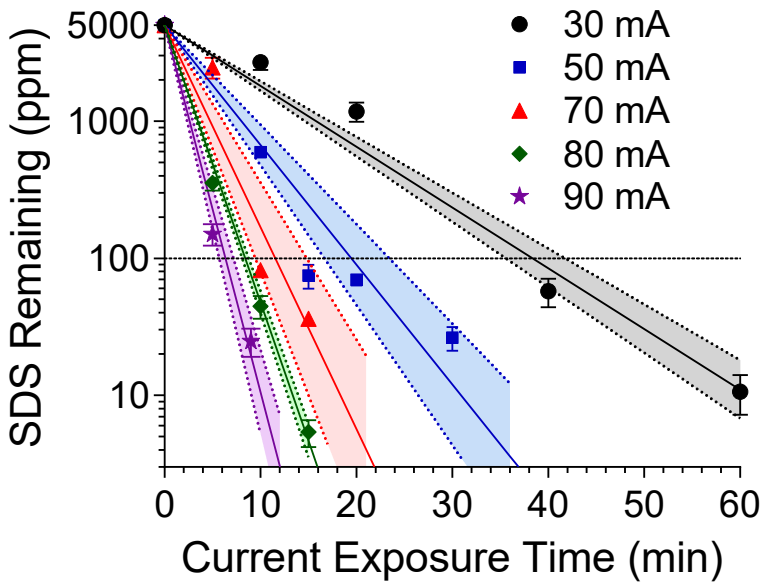

Figure 3.18 The residual SDS of a 0.1 g/L BSA solution containing 5000 ppm SDS, plotted as a function of TME run time at currents ranging from 30-90 mA. The data are fit to exponential decay functions with the error of the fit displayed as the shaded regions within the dotted lines. Error bars represent the standard deviation from 3 replicate measurements.

Table 3.4 Equations for exponential decay fits of SDS depletion with TME at various operating currents, and their corresponding half-lives.

Current (mA)	$t_{\frac{1}{2}}$ Present study (min.)	$t_{\frac{1}{2}}$ Kachuk *et al*, 2016[65] (min.)	Equation
0	n/a	77	n/a
20	n/a	12	n/a
30	6.8 ± 1	8.9	$SDS_t = 5000e^{-0.102t}$
40	n/a	5.9	n/a
50	3.4 ± 1	4.4	$SDS_t = 5000e^{-0.201t}$
70	2.0 ± 1	n/a	$SDS_t = 5000e^{-0.339t}$
80	1.5 ± 1	n/a	$SDS_t = 5000e^{-0.465t}$
90	1.1 ± 1	n/a	$SDS_t = 5000e^{-0.616t}$

When considering operation at 50 mA, SDS was reduced to 75 ± 15 ppm within 15 min of TME operation, which corresponds to 98.5% depletion. When the current is increased to 70 mA, 82 ± 8 ppm (98.4%) is achieved within 10 min of operation time. Similarly, increases to 80 mA and 90 mA required even shorter operation times (t≈8.5 min. and t≈6.4

min respectively) to achieve <100 ppm. It is difficult to directly compare the above results as each experiment was terminated at a different final concentration of SDS. However, based on the equations of the exponential fits, a plot depicting the time required to reach 100 ppm at each current is seen in Figure 3.19.

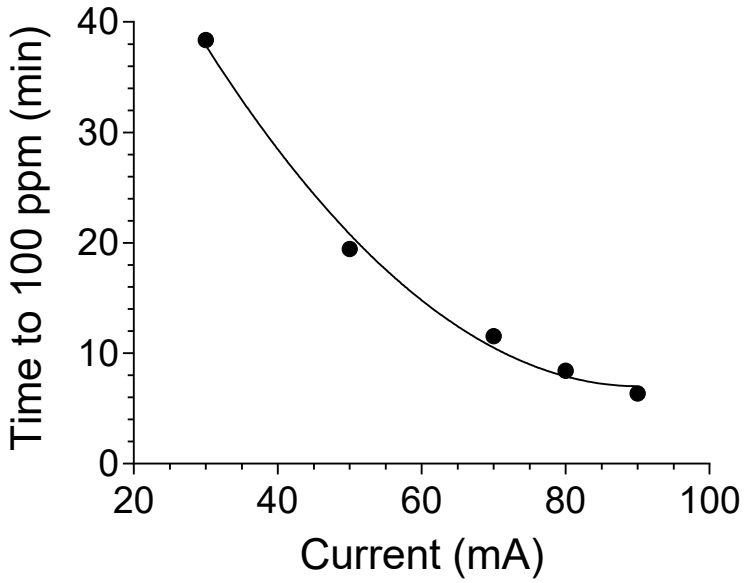

Figure 3.19 Plot depicting the time required by TME to reach 100 ppm for different operating currents. The curve is fit using a quadratic function with the equation $y = 0.00849x^2 - 1.53x + 76.3$ and an $R^2 = 0.995$.

This plot clearly shows a decrease in the time required as the applied current is increased, and interestingly, the trend is non-linear. A quadratic function is used to fit the data, with an equation of $y = 0.00849x^2 - 1.53x + 76.3$ and an $R^2 = 0.995$. The data validates an increase in current provides increase in depletion rates (increase in SDS flux). However, it is clear, further increases in current provide progressively smaller improvements to run time. It is unclear as to why this relationship exists, but it can be hypothesized excessive

levels of Joule heating experienced at high currents contributes to significant membrane fouling which ultimately slows depletion.

These values improve on the original 60 min operation time (see Table 3.4), but considerable amounts of Joule heating necessitated many pause/mixing events to avoid precipitation, membrane fouling, and potential boiling of the sample. This requirement made actual total run times ~10% longer than indicated on the x-axis.

From Table 3.4 the expected trend of reduction in the SDS half-life as current is increased can be seen. The relationship is expected to be proportional as per Equation 1.19, but a non-linear relationship is observed. When the decay constants are plotted as a function of current, the relationship trends towards a quadratic function (Figure 3.20).

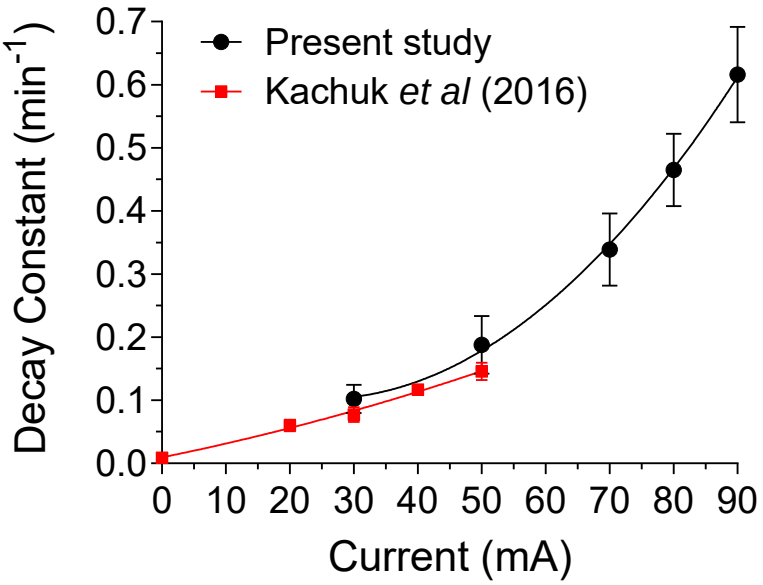

Figure 3.20 SDS depletion decay constants at varying currents from TME runs of the present study compared to SDS depletion decay constants of the previous study[65]. Each data set is fit to a non-linear second order polynomial curve with equations $y = 8.91 \times 10^{-5}x^2 - 0.00241x + 0.0868$ for the present study and $y = 1.37 \times 10^{-5}x^2 + 0.00205x + 0.00951$ for the previous study. Error bars represent the standard deviation from 3 replicate measurements.

This relationship is seen with the current study and with data from the previous TME studies[65]. There are a number of possible reasons the expected linear trend is not observed. To begin, at lower current densities diffusive transport may provide more of a contribution, which explains why the 2016 study curve appears "more linear" in nature compared to the current study[65]. For the current study, the contributions of convective flux could be considered. The high degree of Joule heating produced at higher currents bring appreciable levels of temperature fluctuation, which promotes increased convective transport. A similar trend of non-linearity is observed in the literature in Kasting's model of ion transport, which models diffusion and electro-migration[126]. Additionally, the trend of non-linearity is observed for similar electrophoretic membrane-based processes like EME[122], and electrodialysis[182,231]. In these studies the deviation from the expected trend is attributed to on-going changes in ionic content of the donor and acceptor solutions over time, as well as, large increases in Joule heating which lead to a decrease in solution viscosity, and hence an increase in ionic mobility[122,182,231].

3.7 Twelve Kilodalton *vs* One Kilodalton MWCO Dialysis Membrane

Previous changes to the parameters defining the membrane (*i.e.* thickness) resulted in significant changes in resistance within the system. Just as the thickness of the membrane affected the overall resistance of the system, the diameter of the pores in the membrane have an influence as well. A lower overall resistance will produce less Joule heating and allow for operation of TME at higher currents. Previous SDS depletion studies were conducted using dialysis membranes with MWCOs of 0.5-1 kDa, 3.5 kDa, and 6-8 kDa, and no trend in SDS depletion rate or protein yields were observed[81]. All membrane sizes successfully depleted SDS to the desired level, but no conclusions could be drawn about

the effectiveness of a particular pore size over another[81]. Theoretically, an increased pore size should also provide a larger diffusion coefficient, by increasing ε, the volume void fraction of the membrane (Equation 1.20), and decreasing φ, the reduced pore diameter (Equation 1.22 and Equation 1.23). Although, contribution to overall flux by diffusion is small and it is unlikely to provide any meaningful changes in SDS flux.

Here, TME is operated using membranes with pore sizes of 12-14 kDa MWCO and 0.5-1kDa MWCO to assess the impacts on resistance and Joule heating. As seen in Figure 3.21, the larger pore size is associated with lower observed sample cell temperatures throughout the run.

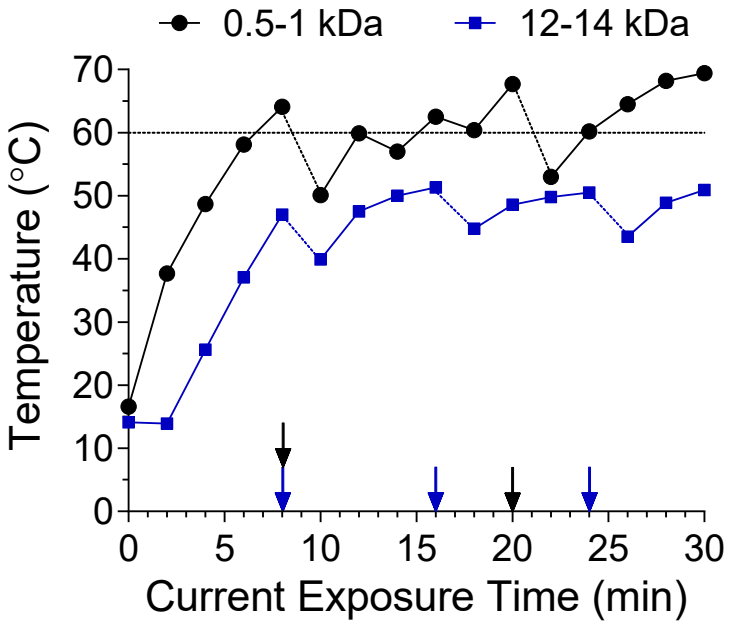

Figure 3.21 Real time temperature of the TME sample cell during SDS depletion using a 0.5-1 kDa MWCO dialysis membrane or a 12-14 kDa MWCO dialysis membrane. The black and blue arrows correspond to points where the power supply was temporarily paused.

Although, both MWCO sizes were given three pause events throughout the course of the run to allow for additional cooling, it is clear TME operated with a 12-14 kDa membrane remains cooler overall. The lower observed temperatures with the 12-14 kDa MWCO

membrane correlate to lower TME system resistance. The average resistance observed for the 0.5-1 kDa membrane was 6.3 kΩ, and 5.6 kΩ for the 12-14 kDa membrane. It should be noted these values correspond to overall system resistance (2 membranes, one on either side of the sample cell cartridge) and are not specific to resistance observed across the membrane at the anode interface. Nonetheless, the only differences between the 0.5-1 kDa membrane run and the 12-14 kDa membrane run was the pore size of the membrane, therefore the difference in resistance observed can be attributed to this change.

Perhaps in complete parallel with the membrane thickness experiments, differences in temperature and resistance were observed, but no noteworthy decreases in SDS depletion rate or sample yield were seen. Figure 3.22 depicts the SDS depletion curves for TME operated at 50 mA with a 0.5-1 kDa membrane or a 12-14 kDa membrane.

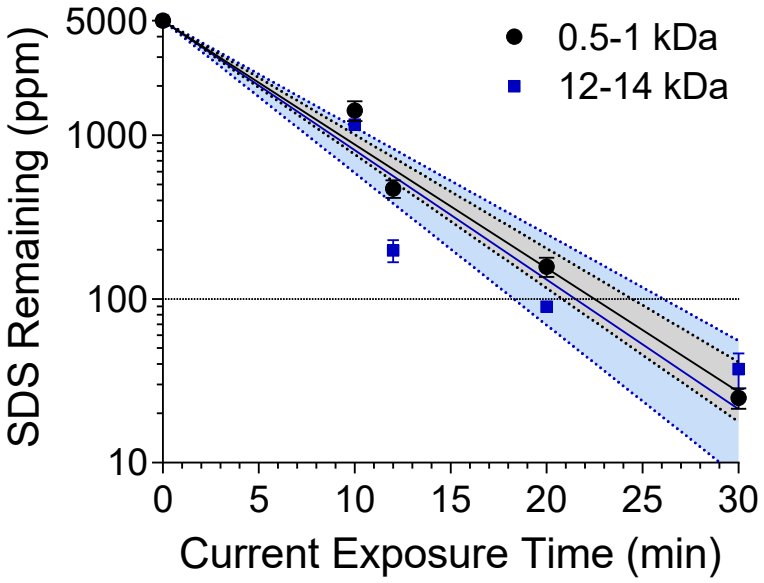

Figure 3.22 The residual SDS of a 0.1 g/L BSA solution containing 5000 ppm SDS, plotted as a function of TME run time at 50 mA constant current using a dialysis membrane with a 0.5-1 kDa MWCO or a 12-14 kDa MWCO. The data are fit to exponential decay functions with the error of the fit displayed as the shaded regions within the dotted lines. Error bars represent the standard deviation from 3 replicate measurements.

It could be hypothesized that larger pore diameter can be associated with faster movement of SDS, which would appear as an increase in depletion rate compared to 0.5-1 kDa MWCO membrane. However, the SDS depletion rates for each pore size have minimal differences between them. The final concentration of SDS at 30 min of operation time is statistically the same, whether the 0.5-1 kDa MWCO membrane or the 12-14 kDa MWCO membrane is used with final values of 25 ± 4 ppm and 38 ± 9 ppm respectively. It is known from the equation describing diffusivity at infinite dilution, D^0 (see Equation 1.24), diffusivity will increase with increasing temperature, which means the actual observed diffusivity, D, will also increase. Therefore, the slower flux seen with a smaller pore size, might be mitigated by the increase in heat throughout the run which increases the flux indirectly. An increase in Joule heating decreases viscosity and increases both ion mobility and diffusivity. This is a likely explanation as to why minimal differences are observed between the two membranes for SDS depletion. The 12-14 kDa MWCO membrane appears faster initially (t=0 to t=20), but as the run continues to 30 min, the sample with the 0.5-1 kDa MWCO membrane warms and an increase in flux is observed, hence both experiments finish at near identical residual SDS values. Future experiments assessing how membrane warming impacts SDS depletion rates could help clarify the presented hypothesis.

When employing membranes with larger pore sizes for TME it is important to consider how the retention of small MW proteins will be affected. This is especially important when considering that top down MS experiments are generally most successful with proteins <30 kDa[232]. Though, ideally the TME should be universally applicable to proteins of all sizes within a proteome. Given that BSA has a MW of 66.5 kDa, it is unlikely it will be affected by increasing the MWCO to 12-14 kDa. However, when considering a

protein like ubiquitin, which has a MW of 8.5 kDa, it is possible the retention will decrease. It should be noted the MWCO values associated with dialysis membranes are ranges based on an average Stokes radius rather than a strict cut off. Additionally, the Stoke's radii of most proteins increases after denaturing (typically by factors of 1.6-2.2 for monomeric proteins)[229]. Furthermore, the hydrodynamic radius of a protein also increases when complexed with SDS, for example the hydrodynamic radius of BSA increases by a factor of 2.7 when bound to SDS[233]. Nonetheless, Figure 3.23, displays a yield of 21 ± 7% for ubiquitin after TME using a 12-14 kDa MWCO membrane, while the yield using the 0.5-1 kDa MWCO membrane is significantly higher at 75 ± 15% (t-test, $p<0.05$).

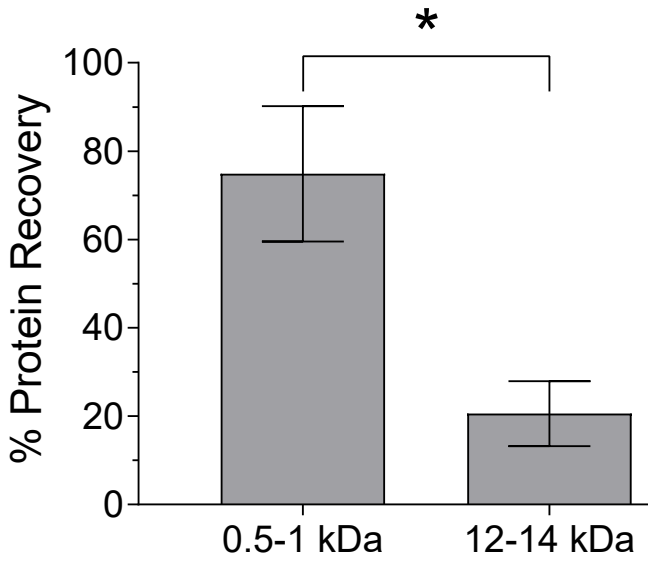

Figure 3.23 Final protein recovery for TME depletion on 0.1 g/L ubiquitin initially in 5000 ppm SDS using a 0.5-1 kDa MWCO dialysis membrane or a 12-14 kDa MWCO dialysis membrane. Error bars represent the standard deviation from 3 replicate measurements.

It is unclear whether the losses observed are due to ubiquitin passing completely through the membrane pores or being just large enough to become lodged within the pores. However, the exclusion of protein mixtures from nanoporous membranes has been observed even with a pore size more than twice as large as the protein diameter[234]. With

this in mind, another experiment was performed to try and boost the retention abilities of the membrane towards ubiquitin. A protein sample containing 0.1 g/L BSA and 0.1 g/L ubiquitin was depleted using TME with a 12-14 kDa MWCO membrane and subsequently separated using a 30 kDa MWCO centrifugal filter cartridge, which allowed ubiquitin to flow through, while the BSA was retained on the filter. Separation allowed for separate protein-specific yield measurements seen in Figure 3.24.

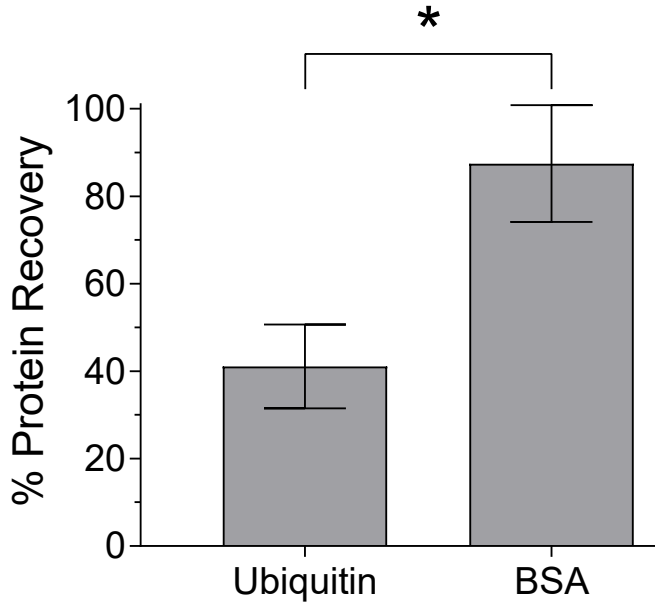

Figure 3.24 Final protein recovery for TME depletion of a mixture of 0.1 g/L BSA and 0.1 g/L ubiquitin initially in 5000 ppm SDS using a 12-14 kDa MWCO dialysis membrane. After depletion, protein samples were separated based on MW using a 30 kDa MWCO centrifugal filter cartridge, to get separate yield measurements for each protein. Error bars represent the standard deviation from 3 replicate measurements.

The final yield of ubiquitin was 41 ± 9% and the yield of BSA was 87 ± 10%. It can be seen the presence of other proteins has an impact on the ability of ubiquitin to adsorb to or pass through the membrane. The recovery of ubiquitin was approximately doubled when BSA was present in equivalent quantities. Although different to TME, the reduction in flux of one macromolecule due to the presence of another is a well understood phenomenon in nano- and ultrafiltration membrane processes and is mainly due to pore-blocking,

concentration polarization, and adsorption[133,134,140,235–238]. In short, the most retained species (here it is BSA), forms a dynamic membrane on the surface of the filtration membrane essentially creating a new membrane surface where the working pore size is dictated by the particles themselves (BSA molecules)[236]. The formation of a cake layer on the membrane surface is also the prevailing reason why there is often minimal noticeable difference in flux or purity when changing the size of the pores for most filtration procedures[239]. Although there is much less protein present in TME systems, there is evidence in the literature for dilute protein solutions also experiencing fouling phenomena[240]. Additionally, it has been proposed the initial stages of membrane flux decline can occur within seconds of the process beginning, which suggests TME is vulnerable to these mechanisms, just as other membrane filtration processes are[134].

3.8 Chapter 3 Conclusions

The experiments presented in this chapter demonstrate how changing the parameters of the membrane can have profound impacts on the levels of Joule heating experienced. A thinner membrane and a larger-pored membrane can both provide a decrease in the overall resistance observed across the system, and hence a decrease in the levels of Joule heating experienced. This could allow for safe operation of TME at higher currents. Additionally, no statistically significant change in SDS depletion rates was observed after changing the membrane thickness and pore size. Though, larger pore sizes gave poor recovery for smaller proteins. This is likely due to poor retention or enhanced adsorption and pore-blocking. This phenomenon can be lessened when a mixture of differently sized proteins is used with a larger pored membrane. It is hypothesized the larger proteins form a dynamic layer in front of the membrane (due to concentration polarization)

which aids in retention of smaller components and discourages unfavourable and/or irreversible interactions with the membrane surface. TME is designed for use on proteomic samples which contain thousands of different components that could contribute to the formation of a dynamic membrane.

Moreover, the potential for SDS depletion time to be shortened significantly is displayed by increasing the applied current up to 90 mA. Extremely fast depletion times (<15 min) and extremely low half-lives (down to 1.1 ± 1 min) are observed at 90 mA, and show large improvements over the previous studies on TME[65]. However, more strategies to combat Joule heating at these high current levels are still required to achieve optimal operation. Further discussions into the complete impacts of high current TME operation on protein recovery and other possible strategies to mitigate high levels of sample heating will be presented in the next chapter.

Chapter 4: Alleviating the Effects of Joule Heating During TME[‡]

4.1 Impacts of Joule Heating at Higher Currents

Operation of TME at higher currents brings on new challenges associated with Joule heating and protein sample solubility. Various strategies for heat dissipation, including pre-chilling the TME device and electrolyte buffer, as well as intermittent manual pausing/mixing are laborious and limited in their capacity to manage heat. This chapter presents a simple and automated solution to the problems of heat generation during TME at higher operating currents. The implications of which will be observed experimentally and correlated to mathematical expressions from Chapter 1 for SDS flux and observed resistance.

Returning to the depletion experiments seen previously in Figure 3.18, although much higher rates of depletion are observed compared to the previous study in 2016[65], the temperature and protein recovery plots illustrate the severe impacts of Joule heating. Figure 4.1 displays the real time temperature data for TME when operated at constant currents ranging from 30 to 90 mA.

‡ Portions of this chapter have been published in: Unterlander, N.; Doucette, A. A. Accelerated SDS depletion from proteins by transmembrane electrophoresis: Impacts of Joule heating. *Electrophoresis*, 2018. DOI: 10.1002/elps.201700410.

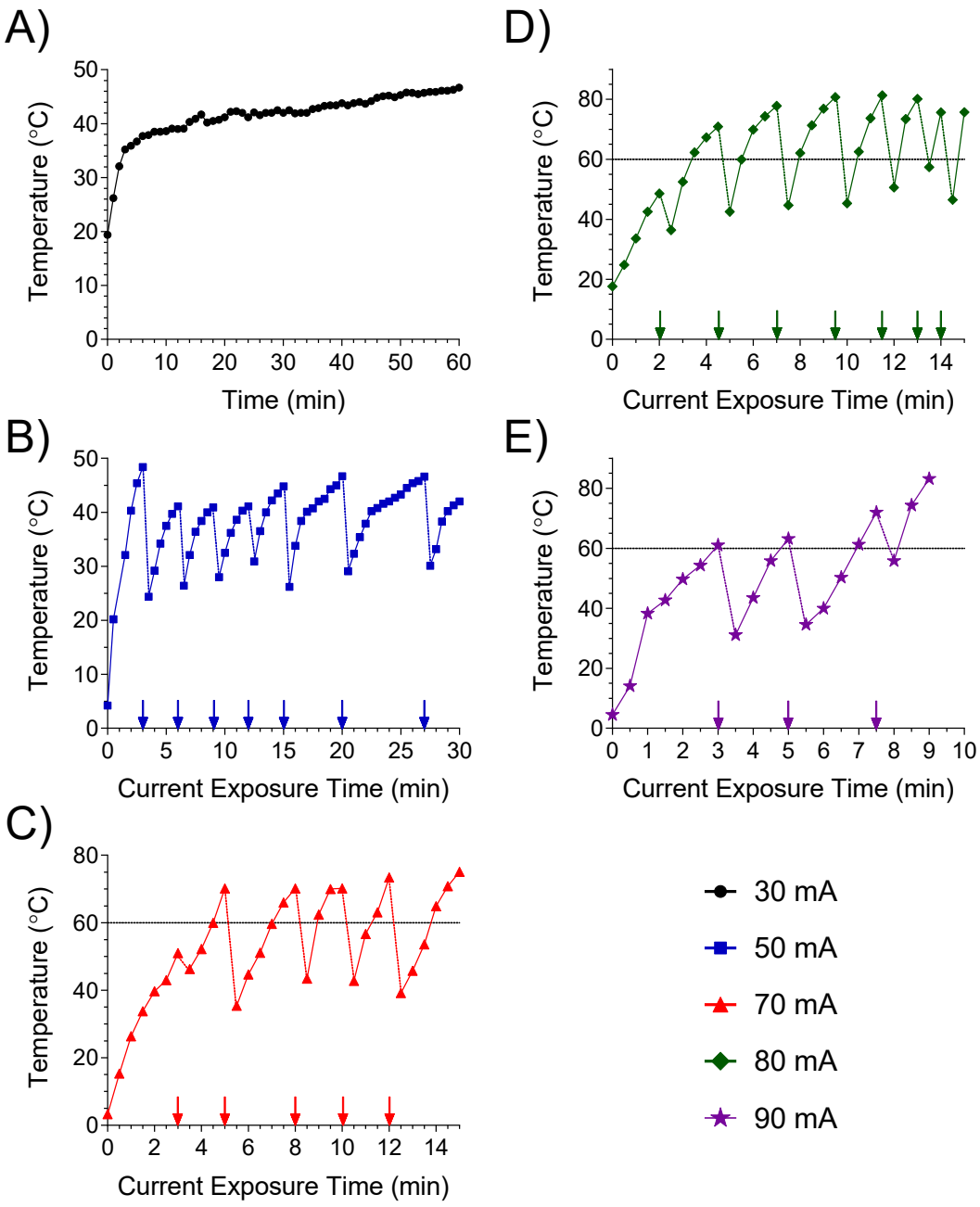

Figure 4.1 Real time temperature data for TME on 0.1 g/L BSA (initially in 5000 ppm SDS) using A) 30 mA, B) 50 mA, C) 70 mA, D) 80 mA, or E) 90 mA constant current. The arrows correspond to points where the power supply was temporarily paused. These runs correspond to those which yielded the results of Figure 3.18.

Increasing the TME current to beyond 50 mA, requires multiple pause events throughout the run, which are depicted in Figure 4.1 as arrows along the x-axis. Additionally, it can be noted, as the current is increased past 50 mA, the sample cell temperature breaches the

60°C limit multiple times throughout a run, despite many pausing events. As the current is increased from 70 mA through to 90 mA, the frequency of pausing events increases to the point where pausing is required every 1-2 min to avoid boiling the sample, making these runs impractical. With significant increases in Joule heating being experienced inside the TME sample cell, it follows that protein yields will decline. As seen in Figure 4.2, the protein yields progressively drop as the current is increased, and progressively lower as the operating time increases.

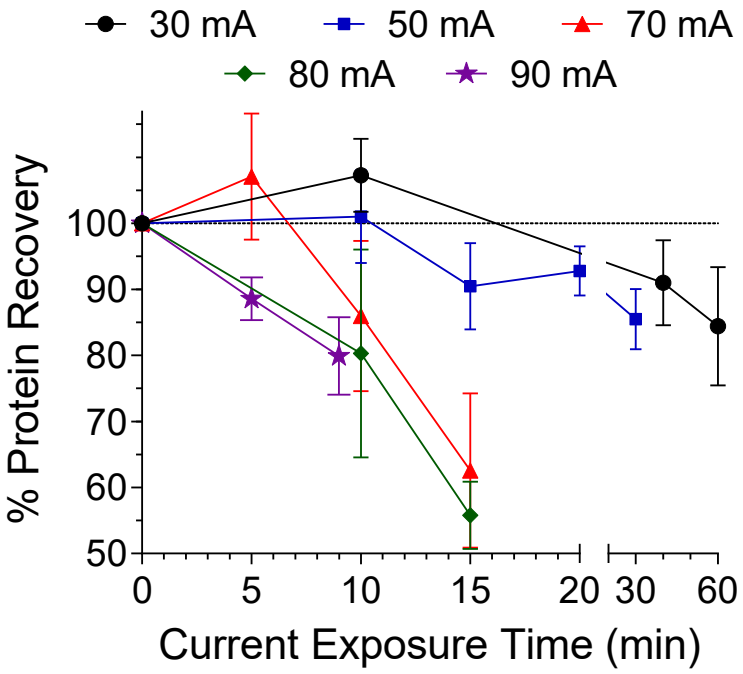

Figure 4.2 The percent protein recovery of BSA initially at 0.1 g/L in 5000 ppm SDS plotted as a function of TME run time at currents ranging from 30-90 mA. These runs correspond to those which yielded the results of Figure 3.18 and Figure 4.1. Error bars represent the standard deviation from 3 replicate measurements.

The observed results are consistent with Equation 1.7 ($H = I^2Rt$) relating heat generated to applied current and time. Interestingly, the run at 90 mA finishes with a significantly higher (t-test, $p<0.05$) overall yield than the 80 mA run and this is attributed to the fact that a run at 90 mA only requires 10 min of TME rather than 15 min. The highest final yields

are seen with the 30 mA and 50 mA constant current runs (84 ± 9% and 85 ± 5%, respectively), in which the temperature remains below 60°C for the entirety of the runs (Figure 4.1). Maintenance of temperatures below 60°C during the 30 mA and 50 mA runs gave significantly higher final yields compared to the 70 mA and 80 mA runs (t-test, $p<0.05$). It has already been shown that any "lost" protein can be recovered with a simple 80% cold formic acid rinse (see Figure 3.15) though potential for membrane fouling may decrease SDS depletion rates. In the 70 mA run, the temperature has increased well beyond 60°C 3 times within the first 10 min, demanding 3 pause points. Pause points are incorporated throughout the run, but there was still difficulty in maintaining a reasonable sample cell temperature. This explains the significantly lower (t-test, $p<0.05$) final protein yields observed at 70 mA (62 ± 12%) and those observed at 80 mA (56 ± 5%). The 90 mA run finishes with comparable yields (t-test, $p>0.05$) to the 30 mA and 50 mA runs however, the duration of the run is much shorter. The 90 mA run has ~20% loss of protein within 9 min, while the 30 mA and 50 mA runs show only a minor decrease in protein recovery over the time period of 30 to 60 min.

Some additional evidence for the importance of heat dissipation during TME comes from the previously unrealized importance of thorough mixing. Previous studies reported pausing the voltage and thoroughly mixing the sample chamber prior to sampling from TME to obtain a representative sample[65]. It was unknown at the time how important the mixing step was to overall heat dissipation as well as SDS depletion success. As seen in Figure 4.3 previously published temperature plots collected for a 50 mA TME run report much lower sample cell temperatures compared to present 50 mA temperature plots[65].

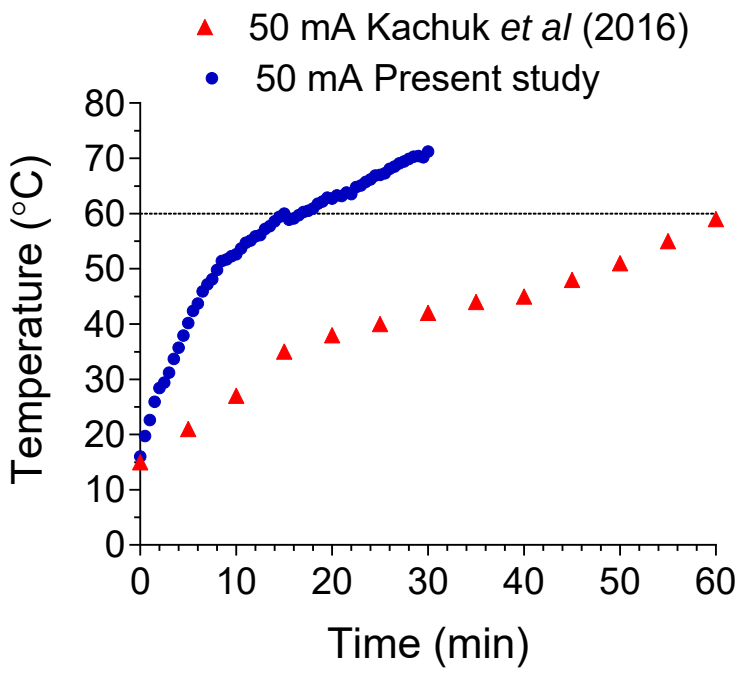

Figure 4.3 Temperature of the TME sample cell over time as measured in the previous TME study[65] which employed pausing and mixing throughout the experiment compared to the temperature measured in the present study, with no pausing or mixing. Both samples contained 0.1 g/L BSA initially at 5000 ppm SDS, both run at 50 mA constant current. Temperature in the previous study was measured using a Fisher Scientific stainless-steel thermometer probe (Cat. no. 15-077-23), whereas the present study was measured using an Omega CN7500 series temperature/process controller with attached thermocouple.

The difference between these experiments is the use of pausing and mixing throughout the course of the run. The previous study emphasized the need for pausing and mixing prior to sampling from TME in order to obtain a proper representative sample. However unknowingly, this necessity was keeping the TME sample cell much cooler. As can be seen in Figure 4.3, the temperature of the sample cell at 50 mA gets significantly hotter without any pausing or mixing, and surpasses 60°C after 15 min. Additionally, previous temperature data was obtained with a Fisher Scientific temperature probe (Cat. no. 15-077-23) which had a diameter of 40 mm, making the size of the probe inappropriately large compared to the volume being measured. It is likely the temperature probe, being so much

larger than the sample, was inadvertently cooling the sample while measuring it as well. The current studies employed a much smaller thermocouple wire attached to an Omega CN7500 series temperature/process controller.

Further evidence for the importance of mixing is given when the behaviour of the proteins within TME is examined without any form of pausing or mixing throughout the run. The proteins can be seen to localize towards one side of the sample chamber based on their charge, which is to be expected when an electric field is applied. Figure 4.4 displays hemoglobin protein (naturally red-brown coloured) samples removed from either side of the TME sample chamber after 20 min of run time at 50 mA.

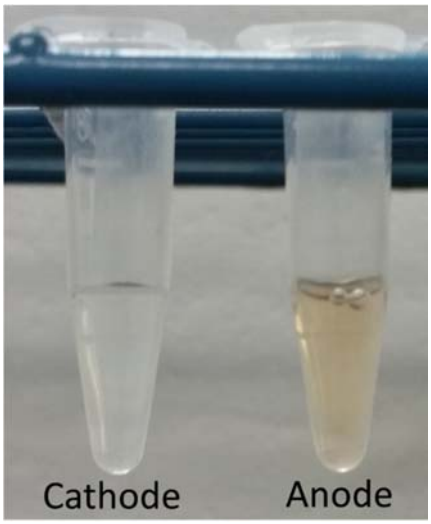

Figure 4.4 Solutions of bovine hemoglobin (0.5 g/L) removed from the TME sample cell, following SDS depletion at 50 mA for 20 min without any mixing or pausing. Both solutions come from the same TME sample cell, with the vial on the left being obtained by directing a pipet tip towards the cathode side of the sample cell, and the vial on the right towards the anode side.

It can very clearly be seen that the hemoglobin solution has localized toward the anode-side of the sample chamber. The TME electrolyte buffer is at a pH of 8.3, which would give bovine hemoglobin (pI=6.8) a net negative charge even after all SDS is depleted[241].

Upon application of an electric field, anions migrate towards the anode, which is exactly what is observed. Each sample was quantified *via* BCA assay showing 85 ± 5% of the sample was in the anode sample, while only 24 ± 4% was in the cathode sample. The build up of protein macromolecules toward one side of the sample chamber can be very detrimental to the integrity of the membrane (*i.e.* clogging, fouling) and add additional resistance across the membrane, especially considering the anode-side is also the side the SDS is migrating out through[228].

The results presented so far suggest a vital need for mitigation of Joule heating. The previous studies employed chilling of the TME disassembled pieces (-20°C) and chilling of sample and electrolyte buffer solutions (4°C) prior to assembling and running[81]. These strategies are also utilized in the studies presented in this thesis to help delay the impacts of Joule heating, but it is clear more control over temperature is still required. Although somewhat effective at permitting TME operation at higher currents, the introduction of multiple, strategically placed, pause points fails to control temperature enough to maintain sample yield. Moreover, the requirement of pausing introduces the need for human intervention, and increases the required run time. One of the main benefits of TME over the vast majority of SDS depletion techniques is automation, and that feature is being lost here. One suggestion could be a temperature program in which the TME voltage is automatically paused when a critical temperature value is reached. The main problem with this strategy is illustrated in Figure 3.17, outlining the impacts of SDS back-diffusion from the anode buffer chamber back intro the sample chamber upon removal of the electric field. In addition, automated voltage pausing still does not address the clear need for mixing during TME. Thus, a new, fully automated, simplistic, and constant approach must be

taken. A simple and automated way to increase heat dissipation is the addition of a stir bar inside the sample chamber (see Figure 2.5).

4.2 Combating Joule Heating with Mixing Strategies

The addition of a stir bar during TME positively impacted the levels of Joule heating inside the sample chamber. TME experiments at 30, 50, and 70 mA were performed with a stir bar, or with manual pausing and mixing, or with no mixing at all. Figure 4.5 depicts the corresponding temperature plots using these different mixing strategies for TME runs on 0.1 g/L BSA (initially in 5000 ppm SDS).

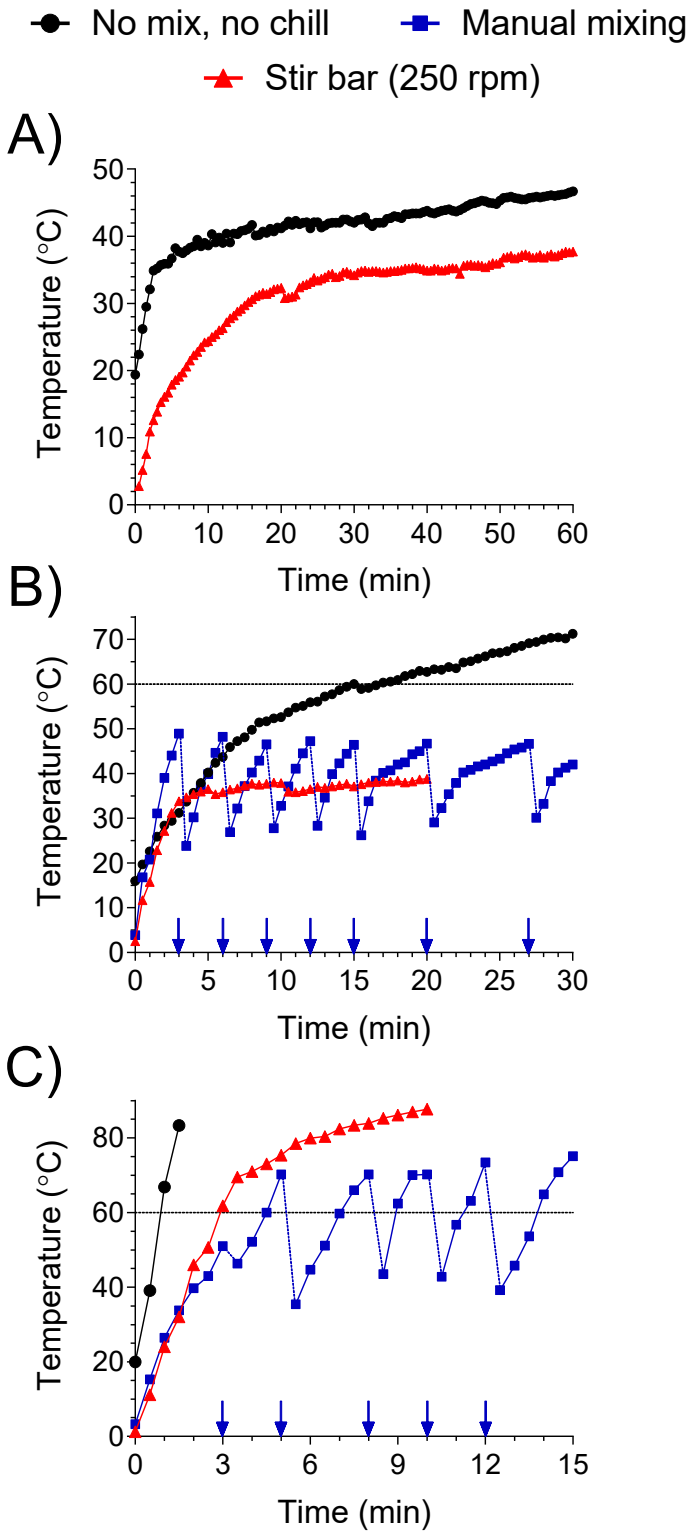

Figure 4.5 Real time temperature data for TME on 0.1 g/L BSA (initially in 5000 ppm SDS) at A) 30, B) 50, and C) 70 mA, using various mixing strategies to manage the sample cell temperature. The blue arrows correspond to times where the power supply was temporarily paused.

The 30 mA temperature plot seen in Figure 4.5 A displays the temperature for a sample with a stir bar and a sample without any mixing or pre-chilling of the TME device. Both curves reach a plateau temperature, but there is a very clear difference between the two treatments. The sample without mixing or pre-chilling plateaued at a temperature of ~40°C, while the sample with the stir bar plateaued at ~30°C. Also, the plateau is reached much slower in the sample containing the stir bar suggesting a slower build up of heat. Although a positive benefit of the stir bar was observed for the 30 mA run, there was little concern about the overall temperature during this run in the first place because sample cell temperature, even without any mixing, stays well below the 60°C threshold.

Utilization of a stir bar at 50 mA is seen to have dramatic effects on the levels of Joule heating (Figure 4.5 B). It was clearly demonstrated earlier that the 50 mA TME runs required frequent pausing events to ensure a reasonable sample cell temperature (see Figures 4.1 and 4.3). When no pausing events are employed, the temperature continues to rise for the duration of the 30 min to 71.2°C. However, when a stir bar is used for continuous mixing throughout the run, a dramatic decrease in temperature is observed. With a stir bar the temperature of the sample cell reaches a plateau at ~35°C within 4 min and remains stable for the duration of the run. Overall the sample cell stays cooler when utilizing a stir bar compared to no mixing or manual mixing.

Running the TME above 50 mA constant current was previously considered impractical because the excessive Joule heating demanded too many pause events and reduced sample yield. Additionally, before any mixing strategies, runs above 50 mA were nearly impossible because the risk of boiling the sample or burning the membrane. This is clearly demonstrated in the no mixing, no chilling temperature plot for 70 mA in Figure 4.5

C. Within 1.5 min the sample cell temperature has reached 83.3°C and would likely continue to rise to dangerous levels had the run continued. As shown earlier, with manual mixing the TME sample cell chamber remained at a more manageable temperature, but raised above 60°C several times throughout the run, with a final temperature of 75.1°C. However, with the use of a stir bar, manual intervention is no longer required. As seen in Figure 4.5 C, the generation of heat when using a stir bar is more gradual compared to no mixing. When using a stir bar, the temperature curve appears to be approaching a 'plateau-like' region. Although the observed sample cell temperatures are higher than the 60°C threshold, it has minimal effects on sample recovery. This is likely due to the run only requiring 10 min to complete, which isn't enough time to observe any significant yield losses (see Figure 3.14). Overall, the rate of heat generation when using a stir bar is smaller than that observed with manual mixing or no mixing.

It is clear from the data presented above that the use of a stir bar for constant mixing inside the sample chamber lowers Joule heating. The cooling effects of a stir bar can be explained rather simply. When a heated solution is left stagnant, the only mode of heat dissipation is transfer to the walls of the container or to the surrounding environment. This is known as pure conduction or natural convection. When stirring is introduced to a heated solution, a faster rate of cooling is observed because the rate of convection is increased. Stirring, or any form of forced convection, helps quickly bring the hottest portions of the solution towards the surface where the most heat transfer can take place. In mathematical terms, the greater the heat differential between two surfaces (the solution and the environment in this case) the faster heat will escape. Therefore, by bringing the hottest

portion towards the surface of the liquid, the temperature differential is maximized (*i.e.* the temperature difference between the solution and the environment is highest).

There is also another mechanism, specific to membrane processes, in which a stir bar can reduce the observed levels of Joule heating. As seen in Figure 4.4, with no mixing inside the TME sample chamber, there is substantial levels of protein build up on the membrane surface. This is a direct result of the membranes ability to retain protein within the sample cell, which leads to concentration polarization. This can promote protein aggregation, adsorption onto the membrane surface, and pore-blocking, which decreases the permeability of the membrane, leading to an overall increase in resistance within the system. Equation 1.7 describes the proportional relationship between resistance and heat generated. The observed levels of TME system resistance with and without a stir bar can be seen in Figure 4.6 below.

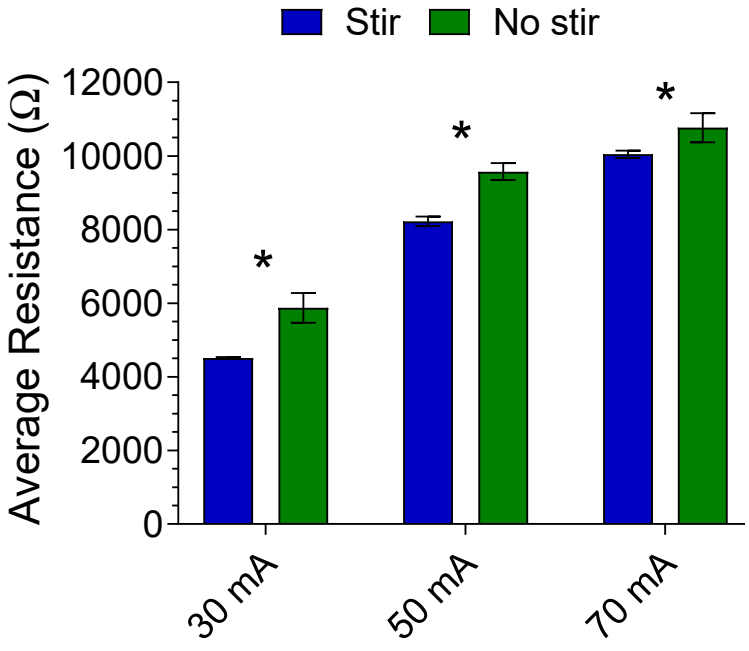

Figure 4.6 Average resistance observed across the TME system for three different applied currents with and without a stir bar. Each set of bars corresponds to a different applied current from 30 mA to 70 mA. Error bars represent the standard deviation from 3

replicate measurements. The asterisks represent statistically significant differences as determined by t-test ($p<0.05$).

There is a significant decrease in the average resistance measured across the TME system when a stir bar is utilized. At 30 mA, the average resistance without any mixing strategy is 5.9 ± 0.4 kΩ, while the average resistance with a stir bar is 4.5 ± 0.3 kΩ. Similarly, at 50 mA the average resistance across the TME system is 9.6 ± 0.2 kΩ without mixing, and 8.2 ± 0.1 kΩ with constant mixing from a stir bar. The trend follows when running at 70 mA as well, with the average resistances across the system were determined to be 10 ± 1 kΩ and 11 ± 0.4 kΩ with and without a stir bar respectively. Though, it should be noted, a 70 mA TME run without any mixing is impossible, as such, the "no stir" run at 70 mA employed a manual pause and mix strategy. The decreases in average resistance observed between these experiments is attributed to the stir bar removing high levels of build up against the membrane, which increases the porosity and hence easing the flow of current across the membrane. Stirring and other types of forced convection are well documented strategies to help boost the performance and durability of industrial membrane processes by preventing membrane fouling, adsorption, and flux decline due to concentration polarization[133,236,242–244].

4.3 Effects of Mixing Strategies on Protein Recovery

The main advantage of maintaining a lower TME sample cell temperature is preservation of sample solubility thus providing a higher total sample recovery upon completion of the run. As seen in Figure 4.7, there is a significant difference in the final protein recovery for the 50 mA and 70 mA runs when a stir bar is used for mixing (t-test, $p<0.05$).

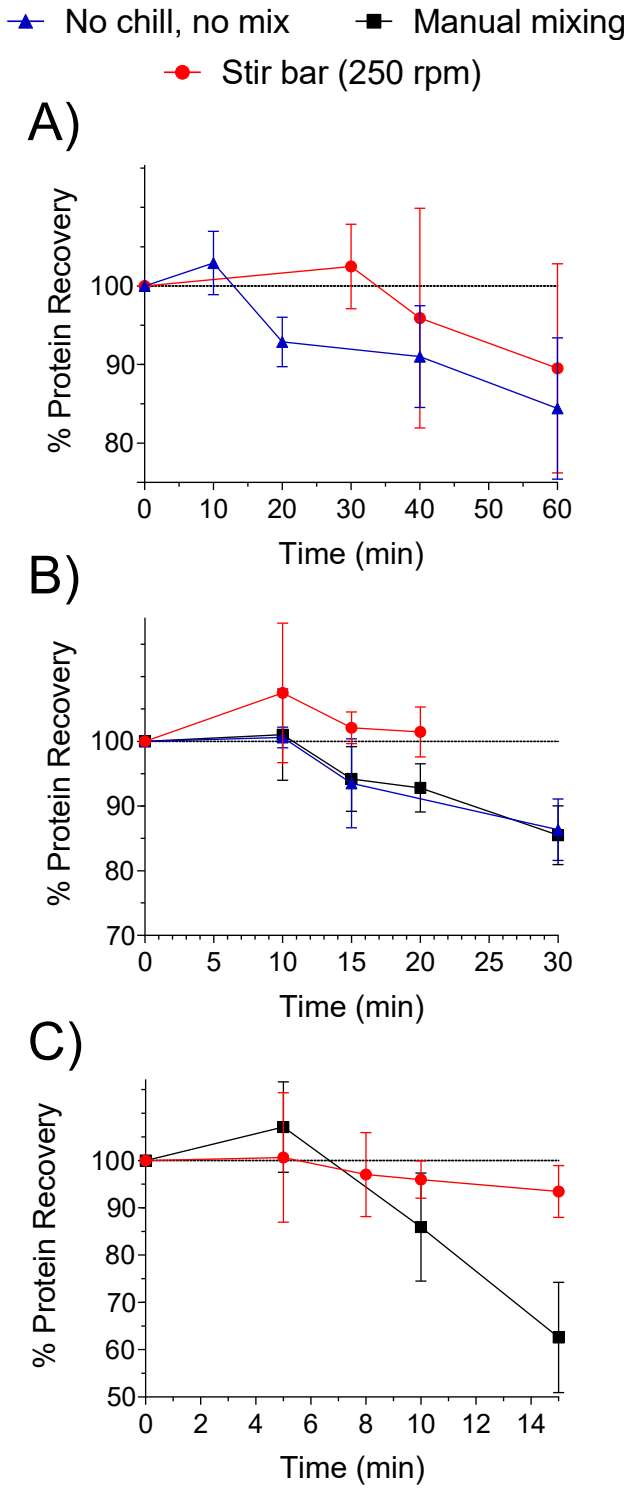

Figure 4.7 The protein recovery of BSA initially at 0.1 g/L in 5000 ppm SDS plotted as a function of TME run time at A) 30, B) 50, and C) 70 mA constant current using various mixing strategies to manage the sample cell temperature. These runs correspond to the temperature plots of Figure 4.5 and the SDS depletion plots of Figure 4.8. Each data point for the stir bar runs represents a separate TME experiment, run for the specified time. Error bars represent the standard deviation from 3 replicate measurements.

The 30 mA run also trended towards higher yields with a stir bar but show no statistically significant differences (t-test, $p>0.05$). The final yield for the 50 mA run with a stir bar showed no protein losses with a final yield of 101 ± 4% after 20 min. This result correlates nicely with the temperature plot seen in Figure 4.5 B, where the temperature remains steadily below 60°C when mixing with a stir bar. In contrast, the runs utilizing manual mixing or no mixing showed a steady decrease in yield after 10 min, with ~15% loss at the end of the runs. Perhaps the most dramatic difference can be seen in the 70 mA run seen in Figure 4.7 C, where a 30% difference in recovery is seen between the two treatments. As seen before, manual mixing at 70 mA gave a steady loss in recovery after the first 5 min, ending with ~40% sample loss. However, when a stir bar is utilized there is very minimal loss in yield, with a final recovery of 94 ± 5%. These plots illustrate the effectiveness of a stir bar at managing the Joule heating experienced inside the sample chamber enough to permit TME operation at higher currents. In addition, constant stirring reduces build up against the membrane, preventing pore blockage which has been shown to reduce observed resistance across the system. Moreover, a stir bar can reduce protein aggregation and prevents adsorption onto the membrane providing further benefits to protein recovery.

4.4 Effects of Mixing Strategies on SDS Depletion Rates

Based on the results shown thus far, it has been hypothesized the addition of a stir bar in TME promotes heat dissipation, and prevents protein build up against the membrane, hence preventing adsorption, pore-blocking, and other mechanisms of flux decline. The prominent reasons for including a stir bar in industrial membrane processes is to prevent flux decline, not temperature control. In this regard, it is reasonable to consider the rate of SDS depletion could be positively impacted by the presence of a stir bar during TME.

As seen in Figure 4.8 and Table 4.1 there are significant differences (t-test, $p<0.05$) observed in the rate of SDS depletion when a stir bar is utilized for 50 mA and 70 mA TME runs.

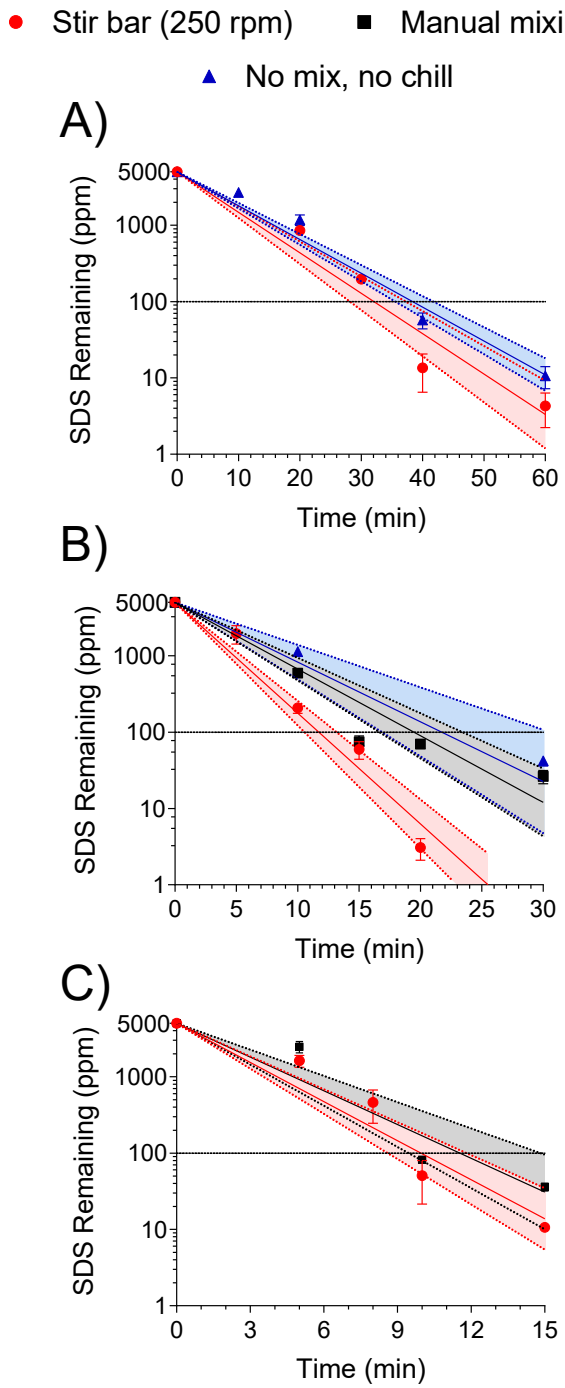

Figure 4.8 The residual SDS for TME experiments operating at A) 30, B) 50, and C) 70 mA constant current using various mixing strategies to manage the sample cell

temperature. These runs correspond to the temperature plots of Figure 4.5, and the protein recovery plots of Figure 4.7. Each data point for the stir bar runs represents a separate TME experiment, run for the specified time. The data are fit to exponential decay functions with the error of the fit displayed as the shaded regions within the dotted lines. Error bars represent the standard deviation from 3 replicate measurements.

Table 4.1 Equations for exponential decay fits and half-lives of SDS depletion of 0.1 g/L BSA (originally in 5000 ppm SDS) with TME at 30, 50, and 70 mA using various mixing strategies.

	Stir bar (250 rpm)		Manual mixing		No mix, no chill	
I (mA)	$t_{\frac{1}{2}}$	Equation	$t_{\frac{1}{2}}$	Equation	$t_{\frac{1}{2}}$	Equation
30	5.7 ± 0.8	$SDS_t = 5000e^{-0.12}$	n/a	n/a	6.8 ± 1	$SDS_t = 5000e^{-0.10}$
50	2.1 ± 1	$SDS_t = 5000e^{-0.33}$	3.4 ± 1	$SDS_t = 5000e^{-0.20}$	3.9 ± 0.6	$SDS_t = 5000e^{-0.18}$
70	1.8 ± 1	$SDS_t = 5000e^{-0.39}$	2.0 ± 1	$SDS_t = 5000e^{-0.33}$	n/a	n/a

At 30 mA the half-life is reduced from 6.8 ± 1 min to 5.7 ± 0.8 min with the incorporation of a stir bar. There is a trend towards faster depletion rates however, no statistically significant difference can be stated (t-test $p>0.05$). At 50 mA, minor differences between the rates of SDS depletion are observed when manual mixing and no mixing are utilized (half-lives of 3.4 ± 1 min and 3.9 ± 0.6 min respectively). This could suggest the implementation of more pause/mixing events to see a more pronounced difference. However, when a stir bar is utilized, the half-life reduces to 2.1 ± 1 min, and a dramatic difference can be seen in the SDS depletion plot in Figure 4.8 B. With a stir bar, SDS depletion at 50 mA only requires 20 min of TME operation rather than the 30 min originally used. When considering the 70 mA runs, the half-life drops from 2.0 ± 1 min to 1.8 ± 1 min when a stir bar replaces manual mixing. Although a decrease in the half-life observed, the

difference is less dramatic than that observed for the 50 mA runs. This could indicate another limiting factor though difficult to determine what based on the data. Nevertheless, forced convection can be seen to enhance SDS flux, and a stir bar should be utilized for best results. There are a number of reasons why a stir bar could promote SDS to cross the membrane. Concentration polarization, as discussed earlier, is a known contributing factor to flux decline in filtration processes. Bellhouse and Lewis in 1988 were the first to demonstrate improvements to permeate flux using a concept called "vortex" mixing to separate proteins from blood plasma[243]. Although different than a stir bar, creating oscillatory flow currents in their sample prevented blood cells from obstructing the membrane pores. It has been shown the effects of electrophoretic force and vortex mixing have an additive effect on the increase in flux[244], and an increase in the rate of stirring gives an increase in the flux observed[242]. A wide range of other literature sources corroborate these findings and promote protein agitation as a key strategy to membrane-based processes[120,140,146,190,228,242,245–249].

As seen above, a stir bar can act as an anti-fouling measure to prevent a significant and constant dynamic protein membrane layer from forming on the surface of the membrane and decreasing overall flux. However, a baseline SDS depletion rate without the interference from proteins has not been determined up to this point. Therefore, TME was run at 50 mA constant current with a stir bar at 250 rpm on a sample of 5000 ppm SDS with no protein (*i.e.* 0 g/L BSA). The results, seen in Figure 4.9, were unexpected, with an increase in half-life from 2.1 ± 1 min to 4.2 ± 1 min. The 0.1 g/L BSA run plotted in Figure 4.9, is from Figure 4.8 B and plotted for comparison.

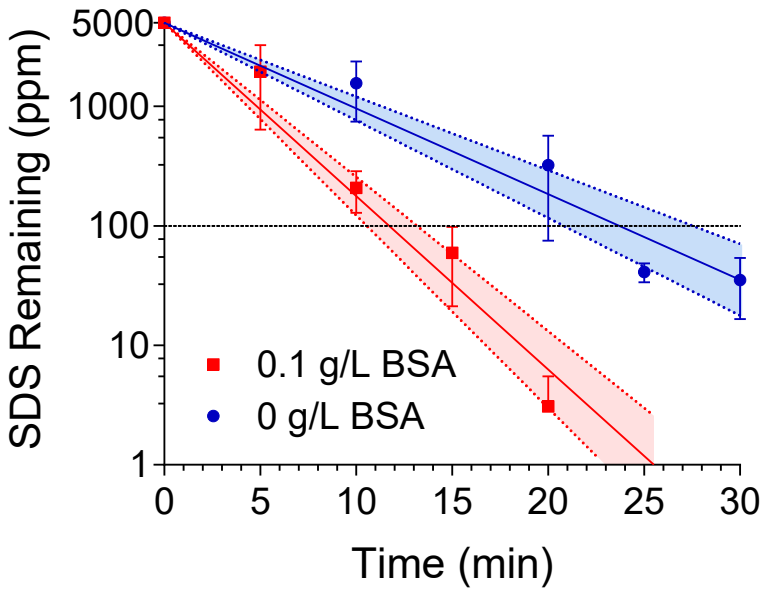

Figure 4.9 Residual SDS of a sample initially containing 5000 ppm SDS with 0 g/L BSA compared to a 0.1 g/L BSA sample also initially containing 5000 ppm SDS. Both samples were depleted at 50 mA constant current with a 250 rpm stir bar. The 0 g/L run had the equation $SDS_t = 5000e^{-0.165t}$, which gave a half-life of 4.2 ± 1 min. The data are fit to exponential decay functions with the error of the fit displayed as the shaded regions within the dotted lines. Error bars represent the standard deviation from 3 replicate measurements.

This unexpected decrease in SDS depletion rate in the absence of protein is not fully understood, however, it is hypothesized that the protein, being so much larger/heavier than SDS molecules, may act to anchor the SDS at a region near the dialysis membrane. Anchoring may help the SDS reach the diffusion layer at the membrane surface instead of being constantly pushed around the sample cell by the forces of the stir bar. It should be noted this is just a hypothesis and further experiments should be considered (see Chapter 6).

An increase in stirring rates during industrial protein filtration processes tends to give an increase in overall permeate flux[242]. With that in mind, it is plausible to believe that flux of SDS in TME can be enhanced simply by increasing the speed of stirring from the lowest setting (250 rpm) to a higher setting. Considering this hypothesis, TME was used to

deplete a 0.1 g/L BSA sample initially at 5000 ppm SDS with a stir bar at 250 rpm, or a stir bar at 2500 rpm. Figure 4.10 displays the SDS depletion curves for the BSA sample with normal stirring and fast stirring, and Table 4.2 depicts the calculated half-lives and corresponding exponential decay equations.

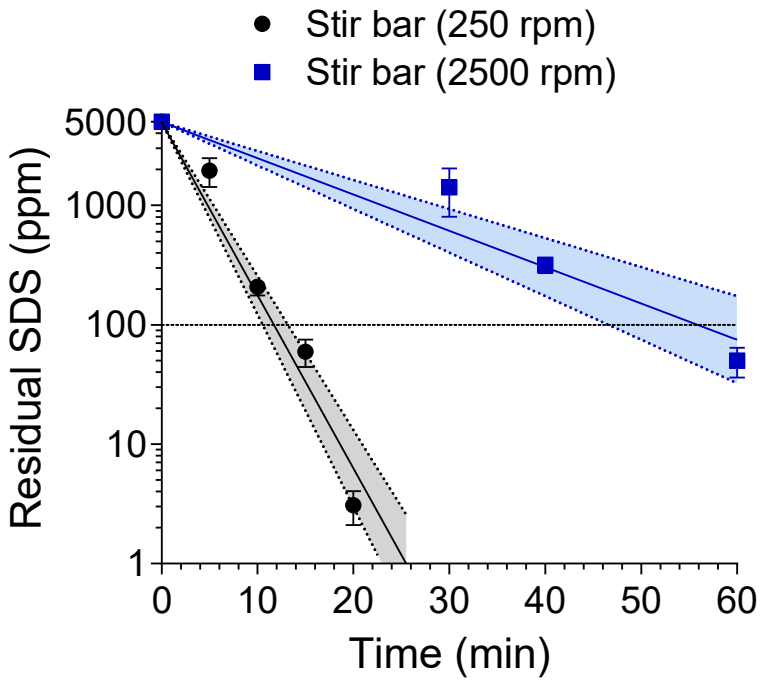

Figure 4.10 The residual SDS for TME experiments operating at 50 mA on a sample of 0.1 g/L BSA initially at 5000 ppm SDS with a stir bar at a speed of 250 rpm or 2500 rpm. The data are fit to exponential decay functions with the error of the fit displayed as the shaded regions within the dotted lines. Error bars represent the standard deviation from 3 replicate measurements.

Table 4.2 Equations for exponential decay fits and half lives of SDS depletion at 50 mA on 0.1 g/L BSA initially at 5000 ppm SDS using TME with a stir bar at a speed of 250 rpm or 2500 rpm.

Treatment	$t_{\frac{1}{2}}$	Equation
Stir bar 250 rpm	2.1 ± 1	$SDS_t = 5000e^{-0.122t}$
Stir bar 2500 rpm	8.9 ± 0.4	$SDS_t = 5000e^{-0.078t}$

Unexpectedly, the rate in SDS depletion is seen to decrease significantly (t-test, $p<0.05$) with a faster stirring speed. With a stir speed of 2500 rpm, the half-life increases from 2.1

± 1 min to 8.9 ± 0.4 min (~5 times higher). In a study done by Do and Elhassadi in 1985 it was found an increase in stirring from 300 rpm to 1600 rpm gave increases in overall permeate flux when using an Amicon stir cell ultrafiltration device on BSA samples. What differs in this study to TME is the Amicon stir cell is pressurized giving an overall bulk flow of sample towards the ultrafiltration membrane, while the stir bar sits directly above the membrane continuously reducing concentration polarization and removing any cake layer that forms. TME lacks this force pushing a bulk flow of solvent towards the membrane, so any significant motion pushing/pulling SDS away from the membrane could have a negative effect on flux. The forces created by a stir bar at 2500 rpm (at 90° to the membrane) could be preventing SDS from reaching the membrane, therefore negatively impacting SDS flux.

4.5 Chapter 4 Conclusions

The results presented in this chapter clearly highlight the benefits of constant stirring during TME. The stir bar helps to maximize heat dissipation through simple forced convection mechanisms, providing substantial decreases in sample cell temperature and removing the requirement for manual pausing and/or mixing throughout a TME run. Additionally, the stir bar provided significant decreases in average system resistance, which correlated with the overserved decrease in Joule heating. Furthermore, a stir bar helps to continuously remove any protein build up at the membrane surface which has been shown to increase porosity, prevent adsorption and pore-blocking, which significantly increases sample yield and SDS flux out of the sample cell. Utilizing a stir bar with TME can permit operation at 70 mA, without any required pausing or supervision, completing depletion to <100 ppm in <10 min operation time while maintaining a sample yield of 94 ± 5%.

Alternate parameters such as stirring speeds and effects of the presence of protein within the system were also explored. Though, no clear conclusions can be drawn about why changing these parameters negatively impacted SDS depletion rates, and further experiments (discussed in Chapter 6) are still required.

Chapter 5: High Current TME on Complex Protein Samples[ǂ]

5.1 SDS Depletion of Proteomic Samples *via* TME with Constant Stirring

Prior results presented in this thesis concerning TME were completed on a simple system containing 1 or 2 protein standards. As mentioned, proteins are very diverse macromolecules and protein recovery can vary widely depending on amino acid content, hydrophobicity, size, *etc*. BSA is a highly water-soluble protein, so these results are not completely representative of a more complex sample, such as an entire proteome. Removing SDS from complex protein mixtures can be quite different, and highly dependent on the sample identity. Concentrations of free and protein bound SDS will vary with sample contents and complexity. Required depletion times will also vary widely depending on how strongly SDS interacts with a given protein. It has been demonstrated in the literature that SDS displays a variety of different binding rates and mechanisms for different proteins, which indicates SDS removal may occur at different rates[35–37,52,56,59,250,251].

With this in mind, a complex sample may contain a host of other materials which can negatively impact SDS flux through the membrane. Various undissolved materials or contaminants that would not be present in a single protein sample, such as cellular debris, buffer constituents, lipids, DNA, complex sugars *etc*. In fact, the intended purpose of TME is for complex proteomes with extremely variable contents, so it is appropriate to examine its performance with this type of sample. It has already been shown in Chapter 3 Section 3.7, even the addition of a single protein (ubiquitin and BSA, see Figure 3.24) can give

ǂ Portions of this chapter have been published in: Unterlander, N.; Doucette, A. A.; Membrane-based SDS Depletion Ahead of Peptide and Protein Analysis by Mass Spectrometry. *Proteomics*, 2018. DOI: https://doi.org/10.1002/pmic.201700025.

significant changes to the retention qualities of the membrane. To assess the difference in performance of TME on complex protein mixtures, unfractionated and GELFrEE fractionated *S. cerevisiae* protein extracts were TME purified and the depletion of SDS was measured over time. Additionally, to evaluate the impacts of a stir bar, the unfractionated samples were TME purified with and without the use of a stir bar. As seen in Figure 5.1 A and Table 5.1, the SDS depletion rates for a proteome sample are significantly lower than that of a 0.1 g/L BSA sample depleted at the same constant current.

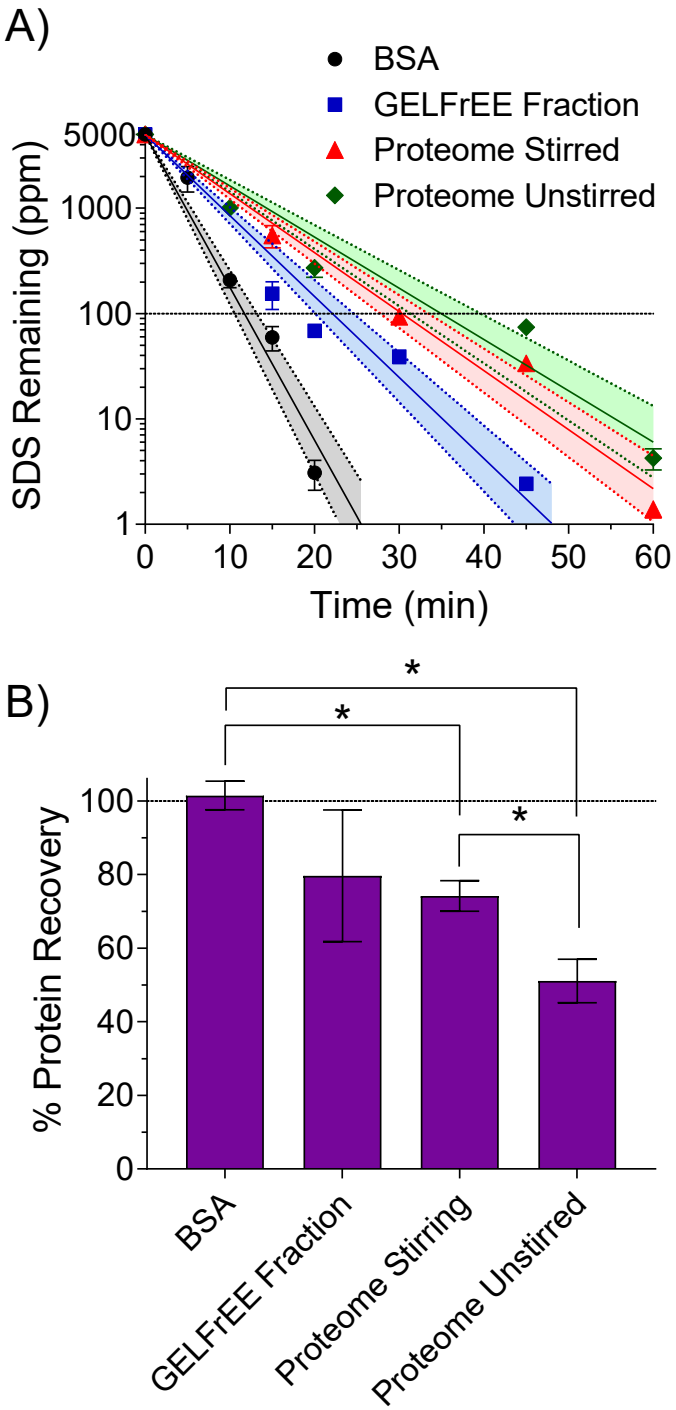

Figure 5.1 A) The residual SDS for TME experiments operating at 50 mA constant current on an unfractionated (5000 ppm SDS, 0.1 g/L) or GELFrEE fractionated (~2970 ppm SDS, 0.13 g/L) *S. cerevisiae* protein extract. The GELFrEE fraction seen above corresponds to a pooled set of protein samples with MW ranging from ~37 kDa to 50 kDa. Additionally, the unfractionated proteome samples were TME purified with and without a stir bar (250 rpm) inside the sample chamber. The data are fit to exponential decay functions with the error of the fit displayed as the shaded regions within the dotted

lines. B) Protein recovery after depletion for each sample seen in A. The asterisks signify statistically significant differences between protein yields as indicated *via* t-test ($p<0.05$).

Table 5.1 Equations for exponential decay fits and half-lives of SDS depletion at 50 mA on unfractionated and fractionated *S. cerevisiae* proteome samples with and without a stir bar.

Sample	$t_{\frac{1}{2}}$ (min)	Equation
S. cerevisiae proteome – No stir	6.2 ± 1	$SDS_t = 5000e^{-0.112t}$
S. cerevisiae proteome – Stir bar (250 rpm)	5.4 ± 1	$SDS_t = 5000e^{-0.129t}$
S. cerevisiae GELFrEE Fraction – Stir bar (250 rpm)	3.9 ± 2	$SDS_t = 5000e^{-0.177t}$

The unfractionated proteome sample without stirring required the longest time for depletion (45 min to reach <100 ppm) and had the highest half life value of 6.2 ± 1 min. The final concentration of SDS after 60 min of TME run time was 4.2 ± 1 ppm. When a stir bar is added to the unfractionated sample <100 ppm is reached within 30 min and the half-life lowers to 5.4 ± 1 min. The concentration of SDS reached 33 ± 2 ppm within 45 min, and <2 ppm within 60 min (recall: limit of quantitation for MBAS: 2 ppm). However, when compared to the half life value obtained with a BSA sample (2.1 ± 1 min), these are still significantly (t-test, $p<0.05$) slower rates of depletion. A number of factors could be contributing to the drop in SDS flux across the membrane when a more complex sample is depleted. In a proteomic sample, the build up of constituents on top of the membrane is no longer of uniform composition, and likely giving many different working pore sizes which the SDS must travel through to reach the MWCO membrane. Highly hydrophobic lipids, and large DNA pieces can also be adsorbing onto the membrane and blocking SDS from passing through. Additionally, electrostatic interactions between different proteins of opposite charge can create regions of very tight, densely packed protein layers slowing overall flux[19,22,23].

The GELFrEE fractionated proteome sample provides the fastest rate of all the proteome samples with a half life of 3.9 min. The fractionated sample required only 20 min to reach 69 ± 8 ppm and reached <2 ppm after 45 min of depletion. The faster rate observed for this sample is likely due to the extra purification achieved during GELFrEE fractionation. Many of the interfering substances (lipids, DNA, complex sugars, *etc.*), and some of the initial 5000 ppm SDS is electrophoresed out of the gel before the sample is collected. However, the proteome sample, although fractionated, still has a slower rate of SDS depletion than the BSA samples seen earlier. GELFrEE fractionated samples, are collected in running buffer (192 mM glycine, 25 mM Tris, 0.1% SDS), meaning they differ in sample composition compared to the BSA samples from Chapter 3 and 4 which were prepared in water. The slower rate of SDS depletion seen with a fractionated sample (as compared to BSA) is attributed to the extra buffer constituents. It was previously shown, the addition of excess charged species (50 – 200 mM NaCl) to the protein sample, negatively impacted SDS depletion rates[252] however, further experiments are required to fully understand these effects (see Chapter 6).

The binding mechanisms between SDS and proteins are protein-specific, sometimes requiring a multi-step process to reach equilibrium[29,30,31,9]. It was previously hypothesized that this variation in SDS interaction strength could indicate certain proteins within the proteome require more or less time to become purified[81]. However, if the applied electric field is of a magnitude sufficiently higher than the binding energy of SDS and protein, it is unknown whether a significant impact on depletion would be observed.

Interestingly, the voltage over time for a proteome sample compared to BSA sample is quite different and could help clarify some of the differences in SDS depletion observed. Figure 5.2 depicts the voltage plotted over time for the depletion experiments in Figure 5.1,

each run at 50 mA with a total initial protein concentration of 0.1 g/L. The black BSA curve is plotted for comparison purposes.

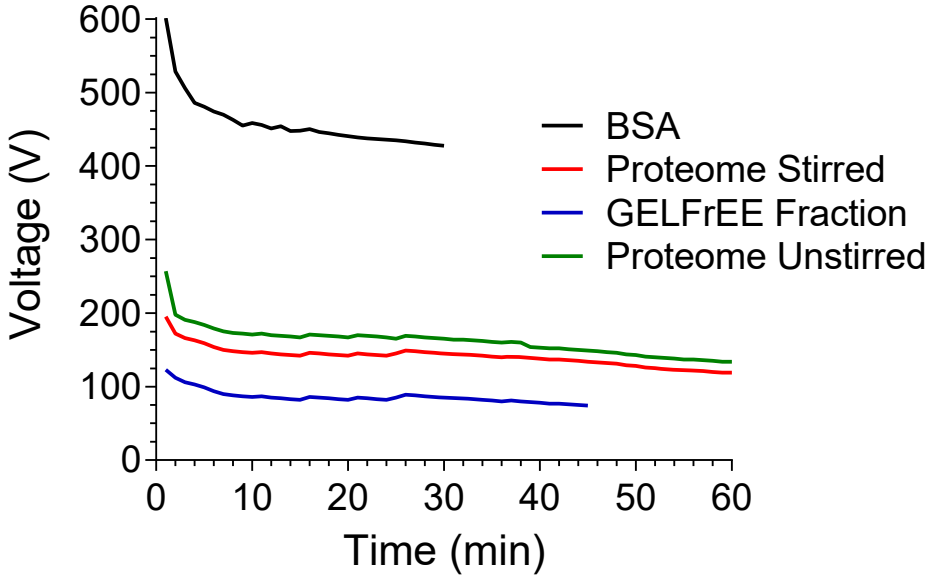

Figure 5.2 Voltage over time for TME run at 50 mA on a GELFrEE fractionated *S. cerevisiae* proteome extract with a stir bar (250 rpm), and an unfractionated *S. cerevisiae* proteome extract with and without stirring (250 rpm). The black curve represents a 0.1 g/L BSA (initially in 5000 ppm SDS and water) TME depletion experiment plotted for comparison purposes.

A significantly lower voltage is observed for all proteome samples compared to the 0.1 g/L BSA sample (prepared in 5000 ppm SDS and water). This is the expected trend when considering the difference in sample contents between a proteome and BSA. As mentioned, the GELFrEE fractionated proteome contains high levels of GELFrEE running buffer, providing an increase in ion concentration and hence an increase in conductivity. A higher conductivity gives a direct decrease in resistance, which means voltage will also decrease. This sample contains the highest concentration of ions and can be seen to have the lowest voltage. Interestingly, each curve displays a sharp drop in resistance between 0.5 and 2 min. This drop is largest for the BSA sample (in water and SDS), second largest for the proteome samples (in 50 mM Tris and SDS), and smallest for the GELFrEE fraction (in running

buffer and SDS). It is suggested this drop may represent the "equilibration" between the ions in the sample chamber and the ions in the buffer chambers. The GELFrEE fraction shows the smallest drop because the running buffer for GELFrEE very closely resembles the TME buffer.

As for SDS depletion rates, the voltage is also known as the "electromotive force", and when there is less of this "force" the SDS is depleted at a slower rate. As the concentration of ions increases, the current is "carried" through the system easier, which means less "electromotive force" is required. This translates to less force pushing on SDS anions and a lower rate of depletion.

When considering the protein yields for each sample (Figure 5.1 B), the expected trends are observed. TME on a stirred 0.1 g/L BSA sample with a recovery of 101 ± 4% is plotted as a bench mark. The stirred GELFrEE fractionated proteome sample gave the highest yield with 80 ± 18%. Some yield loss is to be expected because maintaining the solubility of relatively hydrophobic proteins within the sample is difficult upon removal of SDS. However, a yield of 80% is considered relatively high among other depletion methods[80,102]. Additionally, although trending towards lower, the yield for the GELFrEE fractionated proteome sample was not found to be statistically different when compared to the BSA sample (t-test, $p>0.05$). The unfractionated proteome sample had significantly higher (t-test, $p<0.05$) yields when a stir bar was employed (74 ± 4 %) compared to an unstirred sample (51 ± 6 %), due to the same reasons discussed in Chapter 4. The stir bar helps promote heat dissipation through forced convection which decreases overall observed Joule heating and hence overall protein aggregation/precipitation. In addition, constant sample agitation discourages protein precipitation or build up on the membrane surface, which prevents membrane fouling, adsorption and pore-blocking. This provides an overall

decrease in observed system resistance, which further decreases the amount of Joule heating generated.

As expected, the lowest yield was seen in the unfractionated, unstirred proteome sample, with nearly half the sample being lost. Overall, lower yields are observed for complex proteome samples when compared to BSA, which is to be expected. The large variation in protein solubility, thermal stability, and MW in a proteome sample speaks to the fussy nature of the sample, especially after the removal of a solubilizing/stabilizing agent like SDS. This "lost" protein can be recovered in full with the use of a formic acid rinse step (see Table 5.2).

Table 5.2 Initial recoveries and formic acid rinse recoveries for each sample SDS depleted in Figure 5.1 A.

Sample	Initial recovery (μg)	Formic acid rinse recovery (μg)	Total Combined Recovery (%)
GELFrEE Fraction	51.9	14.6	102.1 ± 2
Proteome Stirring	32.8	16.8	99.1 ± 2
Proteome Unstirred	25.5	24.7	100.5 ± 1

The formic acid rinse is utilized here to resolubilize any protein aggregates or precipitate remaining after the sample is removed from TME when depletion is complete. The formic acid provides full recovery of the proteome samples suggesting the majority of loss is due to aggregation or adsorption onto the membrane rather than lost through the membrane or irreversibly broken down. Overall yields for proteome samples ranging between ~60-80% are considered appreciable yields, when compared to the other available SDS depletion methods[80,92,93,253–255].

5.2 TME *vs* Other Membrane-based SDS Depletion Methods in BUP

As mentioned earlier, there are a wide range of SDS depletion techniques available (see Section 1.1.5.3). However, many methods lack the capacity to remove both free and

protein-bound SDS, and those that can often sacrifice sample yield to do so[80]. Despite the documented successes of TME achieving >98% SDS depletion and maintaining exceptionally high protein yields (>95%)[65,215], its implementation in the proteomics community is shadowed by more familiar/'popular' methods of depletion. For BUP workflows, FASP is the preferred method of SDS depletion, while acetone precipitation is favoured for TDP. To benchmark the performance of TME, protein recovery and residual SDS of proteome samples is compared to these two prevalent methods.

To begin any proteomic analysis of a complex biological sample, separation to reduce sample complexity is a crucial first step. Here, GELFrEE[45] is used to fractionate the extracted proteome of *C. reinhardtii* prior to depletion and MS analysis. The separation is pictured in the SDS-PAGE gel in Figure 5.3.

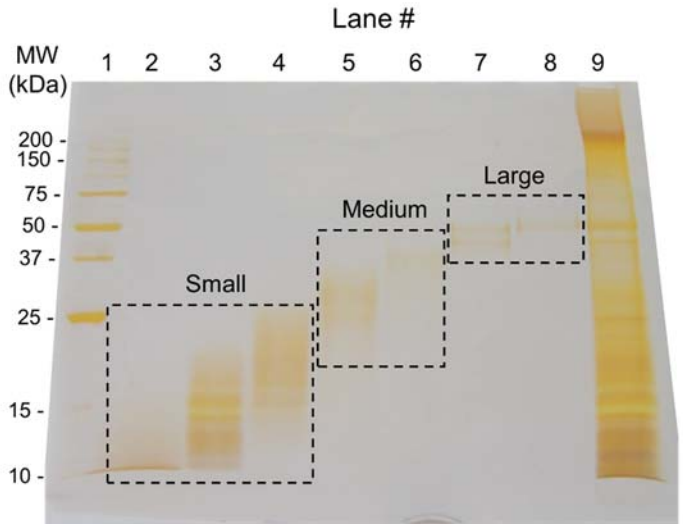

Figure 5.3 SDS-PAGE of GELFrEE fractionated *C. reinhardtii*. Lane 1 contains the labelled MW ladder. Lanes 2-8 contain the GELFrEE fractions, with boxes showing the fractions that were pooled to create the final 3 samples (small, medium, and large) for SDS purification. Lane 9 contains unfractionated *C. reinhardtii* as a control.

Fractions collected from GELFrEE were pooled to create 3 discrete samples (small, medium, and large) with MW approximately centered on 15, 25, and 50 kDa. Each sample

was divided and SDS depleted *via* TME, FASP (10 kDa or 30 kDa MWCO), or acetone precipitation in a 0.2 μm filter-based spin cartridge. The MW distribution of all MS-identified proteins in each pooled GELFrEE fraction is provided as a box and whisker plot in Figure 5.4.

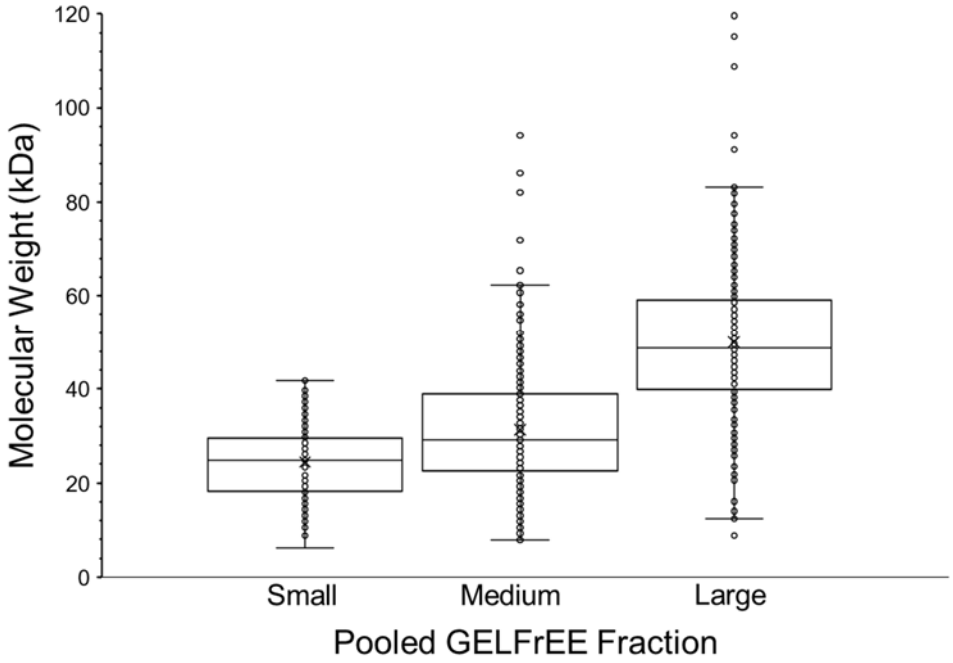

Figure 5.4 Box and whisker plot depicting the distribution of MW of all identified proteins in each pooled GELFrEE *C. reinhardtii* fraction (small, medium, and large).

The small fraction shows a median around ~24 kDa, the medium fraction ~30 kDa, and the large fraction ~50 kDa. The overlap in MW seen between the small and medium fraction in the SDS-PAGE gel in Figure 5.3 is corroborated by the overlap of the boxes for the small and medium fractions in Figure 5.4.

Although the maximal level of residual SDS which permits LC-MS analysis is often quoted at 0.01% (100 ppm)[64], there is still some MS signal suppression and SDS adducts at this level, especially with intact proteins. Additionally, the FASP and acetone precipitation protocols cannot be easily modified in response to removing more or less

SDS, unlike TME where runtime dictates the level of purity. Thus, for optimal and fair comparison across each method, 10 ppm residual SDS was the goal for these studies. As depicted in Figure 5.5, all strategies depleted SDS from ~5000 ppm to the desired level (≥99.8% removal) or lower.

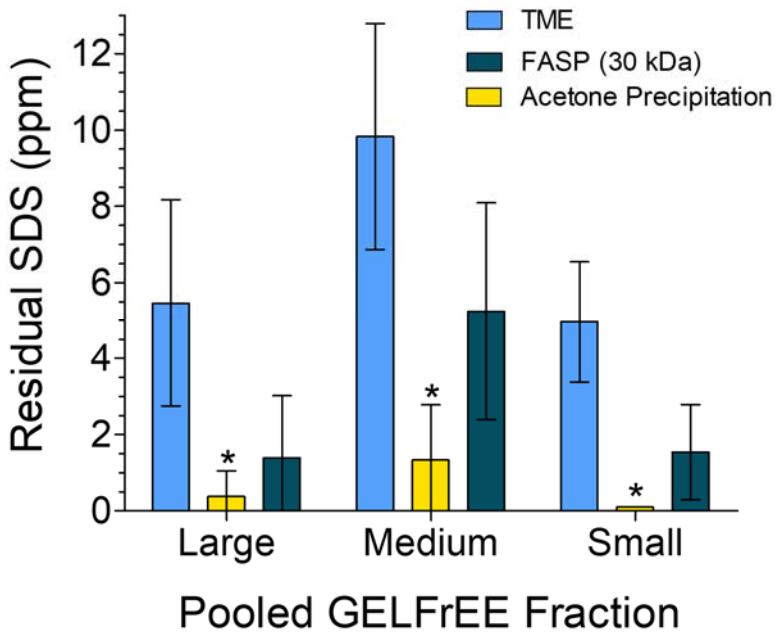

Figure 5.5 Residual SDS after purification of GELFrEE fractionated *C. reinhardtii* samples (pictured in Figure 5.3) by TME, acetone precipitation, or FASP. SDS was quantified *via* MBAS assay. The initial SDS was 5000 ppm for all samples. Error bars represent standard deviation from three replicates and the asterisks indicate statistical significance as determined by t-test ($p<0.05$).

TME depleted SDS to 5 ± 2 ppm, 10 ± 3 ppm, and 6 ± 3 ppm, for the small, medium, and large fractions respectively. While, FASP depleted SDS to 2 ± 1 ppm, 5 ± 3 ppm, and 1 ± 2 ppm, for the small, medium, and large fractions respectively. These values were not found to be statistically different from those obtained with TME (t-test, $p>0.05$). In contrast, the purity achieved *via* acetone precipitation was significantly better than the two other methods (t-test, $p<0.05$), and the residual SDS was below the MBAS assay limit of quantitation (2 ppm). Although differences between the level of purification can be seen

between the methods, it's imperative to note the magnitude of the difference is microscopic compared to the starting value of ~5000 ppm and has no impact on the capacity of MS to characterize the proteome mixture. All methods deplete SDS well below a threshold of 10 ppm, indicating that all methods are equally capable of purifying proteins.

The differences between the methods becomes much more apparent when the protein recovery is analyzed. From Figure 5.6 it is clear TME provides significantly higher sample yield of the three methods (t-test, $p<0.05$), with recoveries ranging between 89-94%.

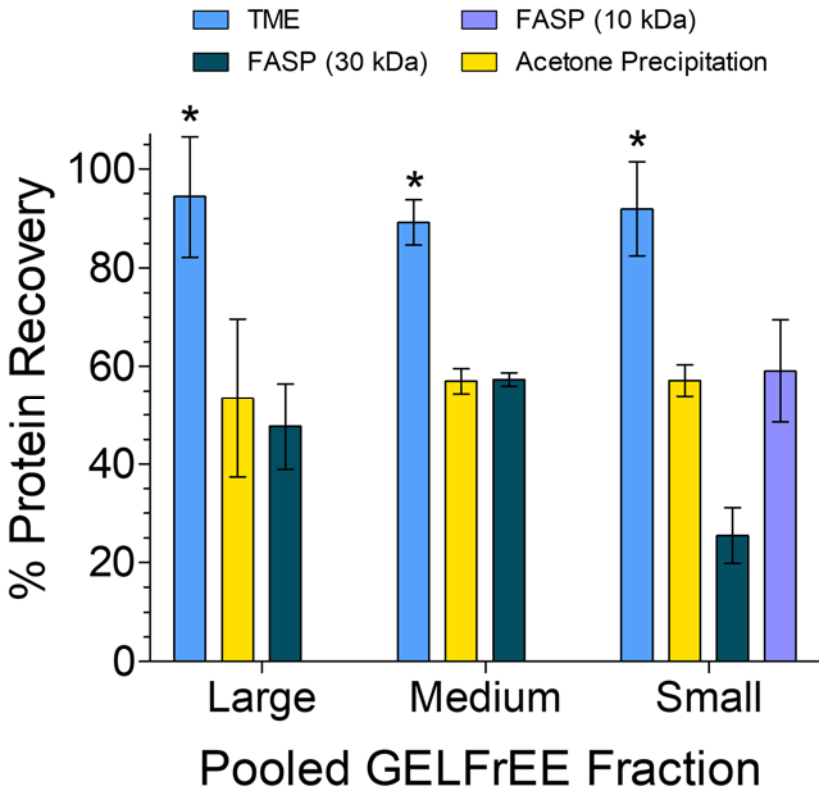

Figure 5.6 Protein recovery of GELFrEE fractionated, SDS-depleted *C. reinhardtii* samples, as quantified by LC-UV quantification. Error bars represent standard deviation from 3 replicates, and the asterisks denote statistical significance as determined by t-test ($p<0.05$).

Low and/or variable peptide yields from FASP have been previously documented[80,93,256,257], with success often depending on trivialities such as type and quantity of digestion enzyme, and brand of filter cartridge used. Using the 30 kDa MWCO FASP cartridge, moderate protein recoveries of 57 ± 1% and 48 ± 9% were achieved for the medium and large fractions respectively. Though the recovery for the small fraction was much lower, at 25 ± 6%. This was expected considering the small fraction contains many proteins with a MW <30 kDa (see Figure 5.3). Using the 10 kDa MWCO FASP cartridge a higher recovery was achieved for the small fraction, at 59 ± 10%. It should be noted, an SDS extraction (1%, 65°C) of the FASP membranes post sample elution recovered the bulk of the unrecovered sample[255]. This confirmed much of the lost yield experienced with FASP can be attributed to denatured proteins adsorbing to the filter and becoming less accessible to enzymatic digestion or resolubilization. When considering the yields for acetone precipitation, it is seen to range between 53-57%, similar to those obtained with FASP. There are a number of factors that can affect the protein recovery for both FASP and acetone precipitation inside a 0.2 μm centrifugal filter. Larger pored membranes run the risk of having proteins pass through the membrane or become so deeply embedded it becomes difficult to resolubilize them. In addition, proteins are extremely chemically diverse and show different inclinations towards precipitation. Some proteins may not precipitate as efficiently and are discarded along with the supernatant, also the 0.2 μm filter may not catch all the protein aggregates and are lost through the filter. Another limiting factor in sample recovery when conducting acetone precipitation is the re-solubilization solvent, choosing a solvent compatible to all proteins within a proteome is nearly impossible, certain proteins will solubilize much easier than others. That being said, an LC-MS compatible solvent must be chosen, which usually contain some quantity of

organic solvent, often providing poor solubilization of highly hydrophobic proteins, like membrane proteins. However, Doucette and colleagues (2014) demonstrated solubilization with 80% cold formic acid is an effective solvent for hydrophobic proteins giving yields after precipitation >90% without significant protein modification[88]. For traditional acetone precipitation (*i.e.* without a centrifugal filter), yield losses associated with imprecise pipetting techniques must also be considered. Acetone precipitation is famously known as a simple technique but it requires an experienced hand[254]. However, the employment of a spin filtration cartridge removes this problem. Although yield losses were observed for both FASP and acetone precipitation, the losses may be irrelevant if enough prototypic peptides are present to reliably make an identification for bottom-up studies. Regardless, TME gives the least loss in sample and this translates to higher confidence when making an identification of unique sets of proteins which may have been lost with other purification methods (discussed more below). Furthermore, quantitative proteomic experiments rely on the ability to obtain consistent and high sample yields[258–261].

The total numbers of identified peptides and proteins across the three methods for each GELFrEE fraction are summarized in the bar graphs in Figure 5.7 A and B.

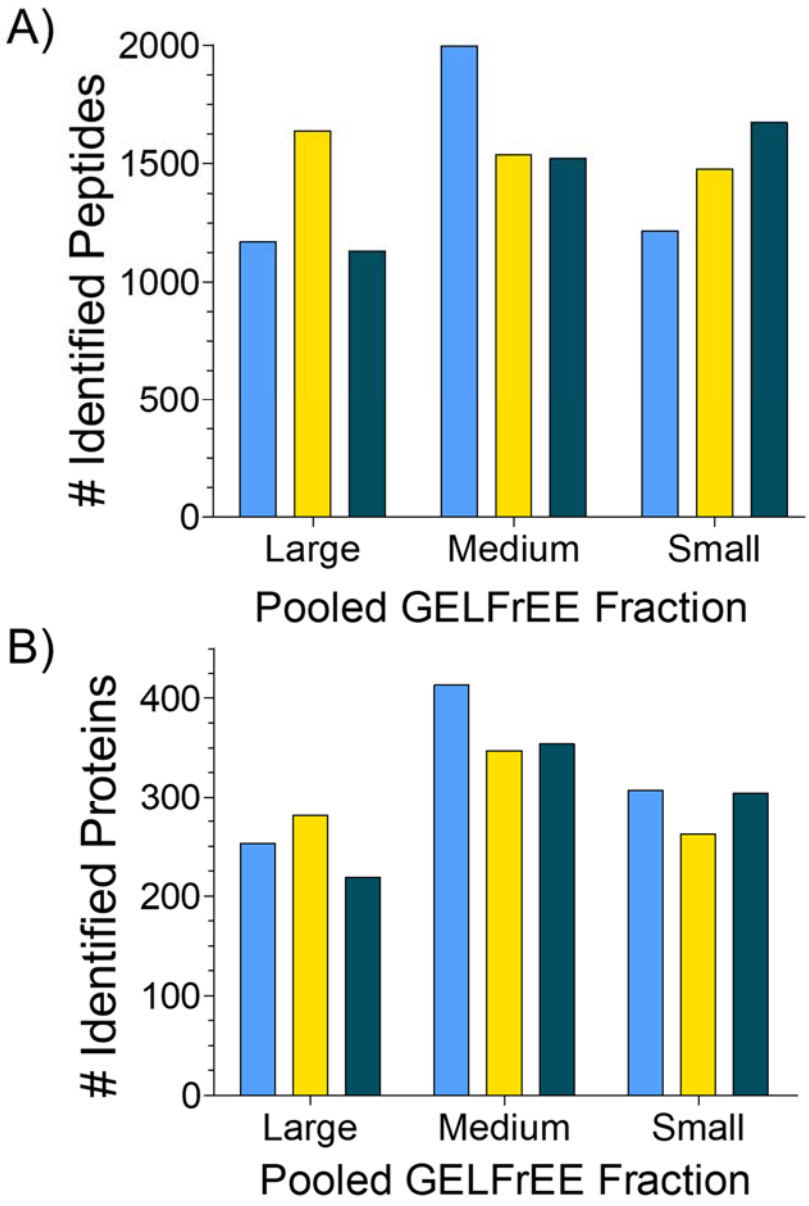

Figure 5.7 Total number of *C. reinhardtii* A) peptides and B) proteins identified from each GELFrEE fraction after SDS-depletion with TME, FASP, or acetone precipitation. It should be noted, FASP with 10 kDa MWCO was utilized for the small fraction, whereas FASP with 30 kDa MWCO was used for the medium and large fractions.

The higher yields associated with TME in Figure 5.6 translate to higher numbers of peptides and proteins identified in the medium GELFrEE fraction (1997 peptides and 413 proteins). For the small fraction, FASP identified the most peptides (1672), but when considering the proteins identified, FASP and TME had nearly identical numbers (304 and 307,

respectively). In the large fraction, acetone precipitation clearly identified the most peptides (1637), which gave an increase in the numbers of proteins identified (281, *vs* 253 TME and 219 FASP). In total, the higher yields observed with TME in Figure 5.6 gave higher total protein identifications (973), when compared to FASP (877) and acetone precipitation (890), but not to a degree proportional to the mass of protein recovered. Though, based on these bar graphs, it is difficult to distinguish any depletion method as performing better than the others. A similar trend is observed when the identity of each peptide and protein is compared across the three methods. As seen in the Venn diagrams in Figure 5.8, there is significant overlap in both the proteins (71.1%) and peptides (58.1%) identified by each method.

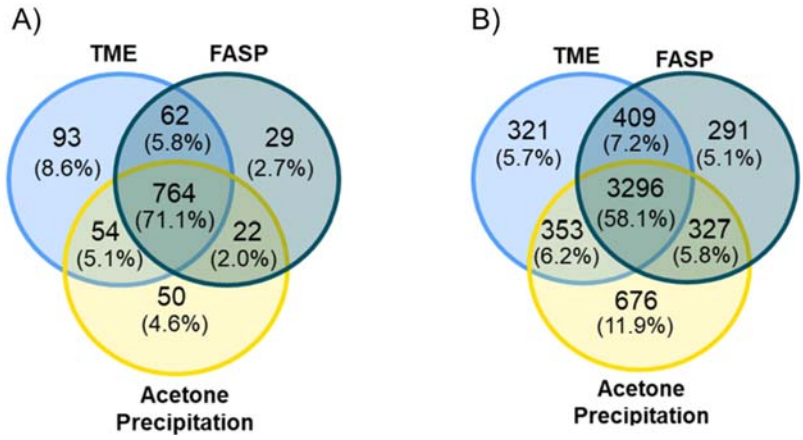

Figure 5.8 Venn diagrams comparing the identified A) proteins and B) peptides from all three *C. reinhardtii* GELFrEE fractions after SDS-depletion with TME, FASP, or acetone precipitation.

Acetone precipitation identified a much higher number of unique peptides (676), while FASP identified the lowest (291). When looking at unique proteins, TME identified 3 times more (93) compared to FASP (29), and twice as much compared to acetone precipitation (50). Although differences exist in these Venn diagrams, due to the large peptide and

protein overlap observed, the same conclusion can be drawn that all three membrane-based SDS depletion methods yield similar results.

Closer examination of the identified proteins for each method show TME provides higher yields for proteins <30 kDa compared to FASP and acetone precipitation (Figure 5.9), despite the fact that the smallest MWCO option (10 kDa) was used for the FASP samples.

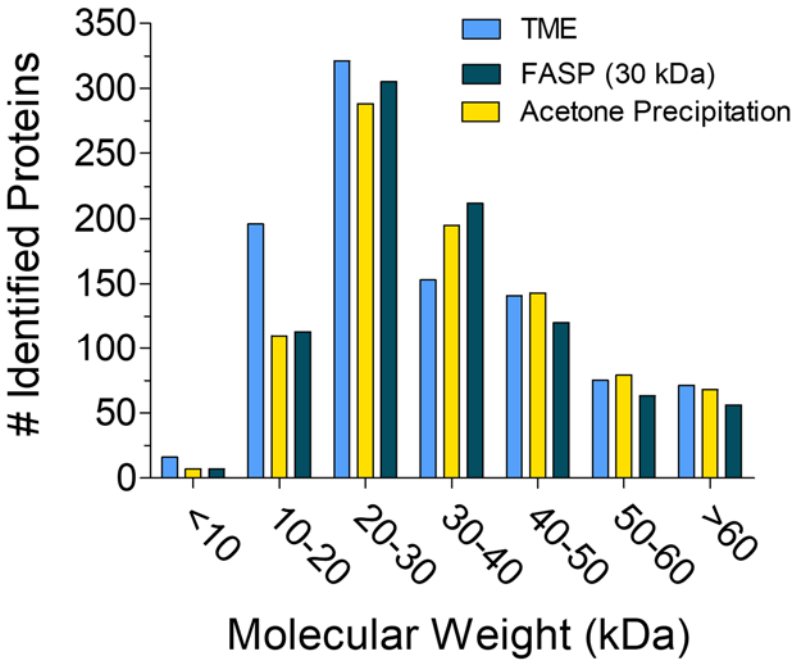

Figure 5.9 Histogram comparing SDS depletion methods (TME, FASP, and acetone precipitation in 0.2 µm centrifugal filter) according to MW range of the MS-identified proteins post clean-up.

This is attributed to the utilization of a much smaller (3 kDa) MWCO membrane in TME, allowing for the retention of many much smaller proteins that may be lost through larger FASP membranes. The inability to retain low MW proteins with FASP is a documented problem in the literature[262–264]. Consequently, as seen in Figure 5.9, FASP is more suited to proteins 30-40 kDa. However, it should be noted the methods with which SDS is carried through the membrane in FASP and TME are fundamentally different (*i.e.* centrifugal force

vs electromigration) and a comparison of their MWCO retention features is open to doubt. With FASP, it is possible for proteins smaller than the effective pore size of the membrane to be retained since a denatured protein occupies a larger hydrodynamic radius[265]. At MW >40 kDa, the number of identified proteins is comparable for each of the three methods however, FASP gives the lowest counts for each bin. When considering acetone precipitation, a similar trend is observed for low MW proteins. This can be attributed to the fact that low MW proteins do not precipitate as effectively as larger proteins. This phenomenon is documented in many precipitation procedures including acetone precipitation. For example, acetonitrile precipitation is often used to enrich protein extracts with low MW proteins by precipitating the larger proteins[266,267]. Additionally, the classic method of protein precipitation *via* "salting-out" is often used to separate protein solutions by rough MW[268]. In general, based on these results, TME performs more favourably for lower MW proteins, which are often underrepresented in proteomic studies[269–272].

Following SDS depletion with any method, a major concern is the loss of hydrophobic proteins through aggregation and precipitation. Any protein which has been denatured has a much higher propensity to aggregate and precipitate out of solution, but hydrophobic proteins are considerably less stable in aqueous solutions. This is a major concern for all methods, especially TME, where the sample is recovered in SDS-free solution. For acetone precipitation, hydrophobic proteins are much less likely to resolubilize out of the pellet into SDS-free LC-MS solvent. Similarly, for FASP, the hydrophobic proteins are much more likely to irreversibly adsorb onto the regenerated cellulose membrane, preventing resolubilization or proper digestion. Despite the potential for losses, Figure 5.10 shows successful detection of hydrophobic proteins for all three methods.

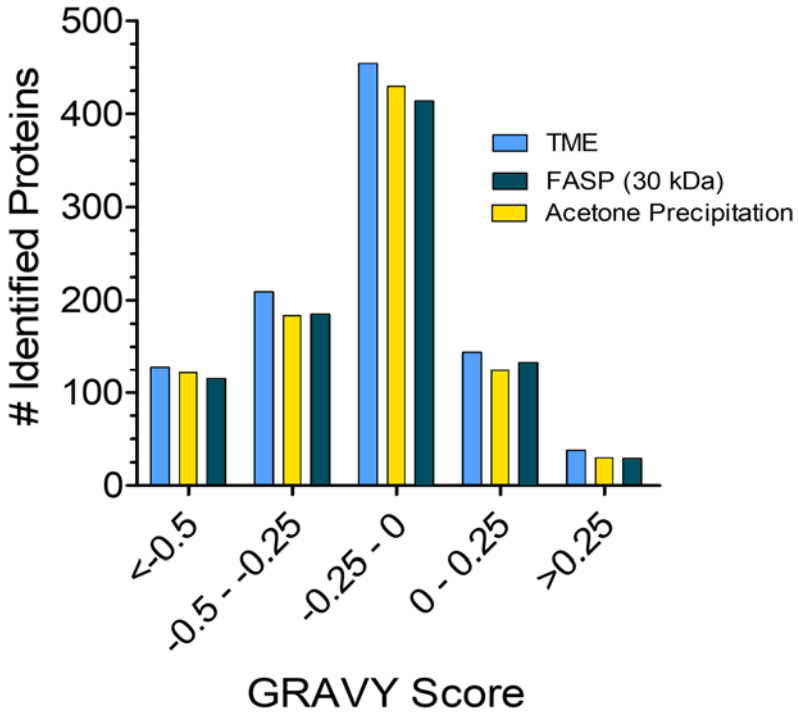

Figure 5.10 Histogram comparing the GRAVY score for the proteins identified using TME, FASP, or acetone precipitation as the SDS depletion method. A more positive score indicates a higher degree of protein hydrophobicity, while a more negative score indicates a more hydrophilic protein.

Here, hydrophobicity is determined based on GRAVY (grand average of hydropathy) score. The GRAVY score for a given protein is calculated by summing the hydropathy values of all amino acids in a protein divided by the number of residues in the protein sequence. Each amino acid is assigned a hydropathy value based on its partitioning between two immiscible liquid phases[273]. Generally speaking, the more positive a GRAVY score, the more hydrophobic a protein is. As seen in Figure 5.10, TME identified a higher number of hydrophobic proteins (182, ~19%), while FASP and acetone precipitation identified 162 (~18%) and 154 (~17%) respectively. TME maintains a temperature-controlled sample, which could translate into higher numbers of hydrophobic proteins remaining in solution throughout depletion. Although higher, the differences are minimal and it is difficult to

establish whether this result is TME-specific. When, considering the entire distribution of identified proteins, all three strategies provide similar results, covering a wide array of proteins with varying hydrophobicity levels.

Although each method performs comparably on many fronts, the higher sample yields observed with TME translated into higher PSMs per protein identified. PSMs are defined as the total number of identified peptide sequences for a single protein (including redundant ones), based on the fragment spectra[274]. Generally speaking, PSMs provide an indication of protein quantity. Each PSM is a unique event, therefore a higher PSM count for an identified protein indicates more peptides from that protein reached the MS[275]. The number of PSMs for each common protein identified between FASP and TME, and acetone precipitation and TME, were plotted in Figure 5.11 A and B.

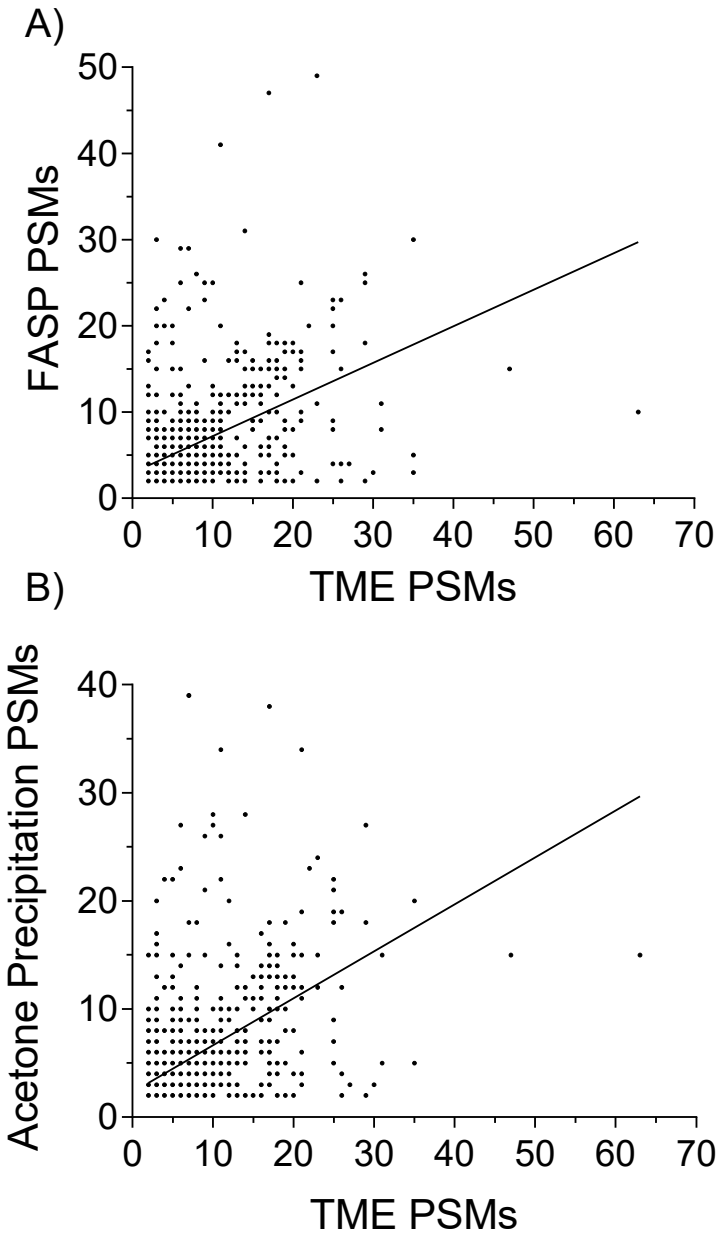

Figure 5.11 A) Peptide spectral matches of identified proteins observed for FASP *vs* TME purified samples and B) peptide spectral matches of identified proteins observed for acetone precipitation *vs* TME purified samples. A linear regression of the data is displayed for each. The equation for the regression in A) was $y = 0.4243x + 2.977$, and the equation for the regression in B) was $y = 0.4347x + 2.292$.

It is clear from the slopes of the regression lines (0.42 and 0.43) TME-purified proteins are generally detected with approximately 2.5-fold greater number of PSMs per protein. Higher protein recovery with TME gave higher PSMs per protein, but perhaps a more dramatic

difference between the methods could be elucidated if the samples were fractionated more thoroughly or more quantity/replicates were injected into the MS.

5.3 TME *vs* Other Membrane-based SDS Depletion Methods in TDP

In addition to surveying the performance of these depletion techniques in a bottom-up workflow, a top-down study was also performed. For simplicity, intact protein detection was performed on a solution of six standard proteins (see Table 2.1) ranging in MW from 9-29 kDa. TME and acetone precipitation inherently allow both bottom-up and top-down MS analysis without any further modification to the technique. In TME intact proteins are recovered in SDS-free solution, while in acetone precipitation intact proteins are resolubilized from the precipitated pellet into SDS-free solution. To perform intact protein experiments, the digestion step can simply be omitted. The digestion step in FASP is thought to be required as this is how the proteins are recovered off the filter membrane once depleted of SDS (digested peptides are small enough to penetrate the membrane and pass through). However, for the purposes of this study, a novel "intact FASP" method was created where the digestion step is omitted and the proteins are recovered off the membrane as intact proteins. Although inclusion of multiple digestion enzymes has been shown to enhance protein recovery during FASP[276], it should be known the centrifugal filters employed in FASP protocols are also routinely used for the concentration and recovery of intact proteins above a certain MWCO size.

Considering the "intact FASP" approach had not previously been reported, the possibility of being unable to recover intact proteins from the FASP membrane with LC-MS compatible solvent (5% acetonitrile, 0.1% formic acid in Milli-Q water) was considered. The sample recovery of the standard protein mixture after SDS depletion with

10 kDa and 30 kDa MWCO FASP filters was first assessed. Regardless of MWCO size, the cartridges gave statistically similar results averaging ~80%, which was found to be comparable to the performance of TME and acetone precipitation with the same standard protein mixture[255]. When using more complex samples, like *C. reinhardtii* proteome extracts, yields off the membrane were lower, but comparable to conventional bottom-up FASP (47% with 10 kDa, 20% with 30 kDa)[255]. It is hypothesized the lower yields associated with the 30 kDa MWCO membrane are resulting from the larger pores allowing intact proteins to penetrate deeper into the membrane, preventing full re-solubilization. SDS-PAGE experiments confirmed any unrecovered *C. reinhardtii* proteins were still present on the membrane, and could be recovered after a more rigorous wash of the FASP membrane with 1% SDS[255].

Once the "intact FASP" approach was confirmed to provide acceptable sample recoveries, the LC-MS of intact proteins could proceed. Following SDS purification with each strategy to a concentration of SDS ≤ 10 ppm, each sample was subject to LC separation prior to MS analysis. An equivalent sample containing the 6 protein standards (see Table 2.1) and no SDS served as a control. Figure 5.12 depicts the total ion chromatograms (TIC) containing 7 distinct protein peaks labelled (I) – (VII) (hemoglobin dissociates into α and β chains which elute independently).

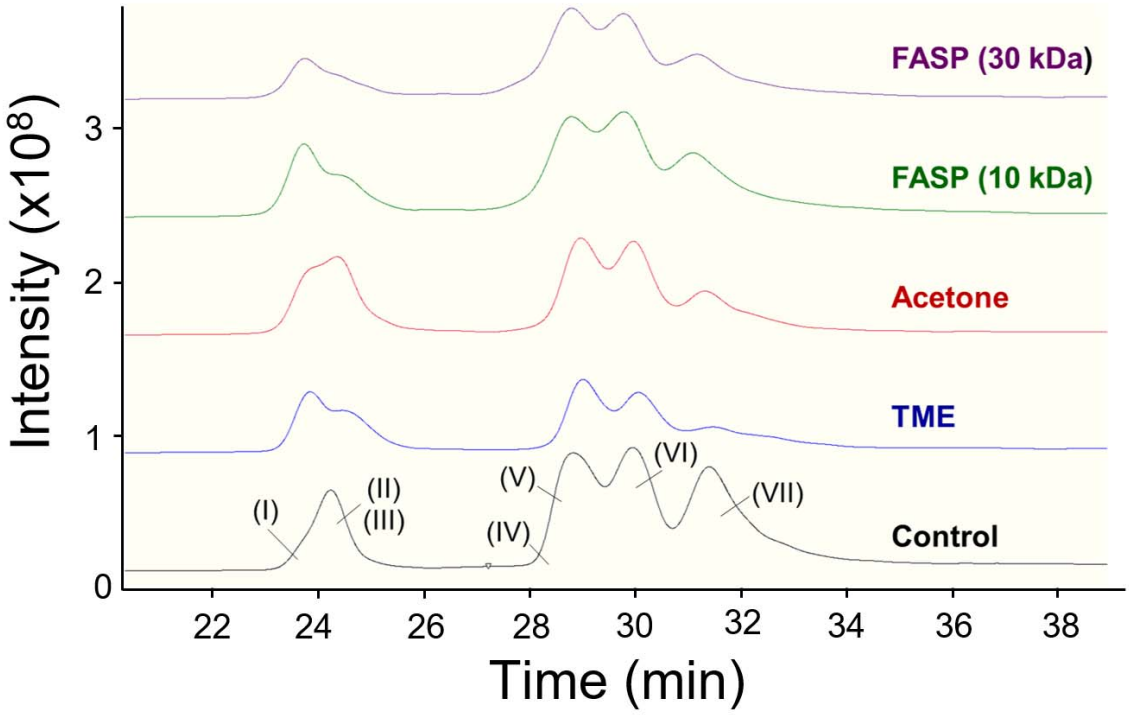

Figure 5.12 Total ion chromatograms showing the reversed phase separation and subsequent MS detection of 7 intact protein standard: (I) ubiquitin, (II) cytochrome c, (III) lysozyme, (IV) myoglobin, (V) hemoglobin α, (VI) carbonic anhydrase, (VII) hemoglobin β. The control sample was prepared in the absence of SDS, while all remaining traces were obtained following SDS removal (final SDS conc. ≤10 ppm) including the "intact FASP" purification protocol.

The intensities observed for each chromatogram apart from the control are very similar. Each method displays a small fraction of intensity decline compared to the control sample. Additionally, minor differences between each spectrum show certain proteins respond differently to each depletion method. For example, 30 kDa MWCO FASP displays the lowest intensity for the 3 smallest proteins (MW 8-14 kDa) in the standard mixture (I)-(III), which is expected considering the larger pore size. Additionally, TME and acetone precipitation show smaller intensity for hemoglobin β (VII) compared to the control, which is one of the most hydrophobic proteins out of the standard mixture (see Table 2.1). It is likely maintaining solubilization of this protein was difficult upon removal of SDS during

these methods. Alternatively, additional signal suppression could arise from increased residual SDS levels on hemoglobin β. It is possible, due to its hydrophobicity, SDS binding interactions with hemoglobin β are stronger, leading to increased signal suppression. Although minor differences were detected in the LC chromatograms, each protein can be visualized, regardless of the method, and their detection *via* MS was still successful. The MS charge state envelopes for 3 selected proteins can be found in Figure 5.13.

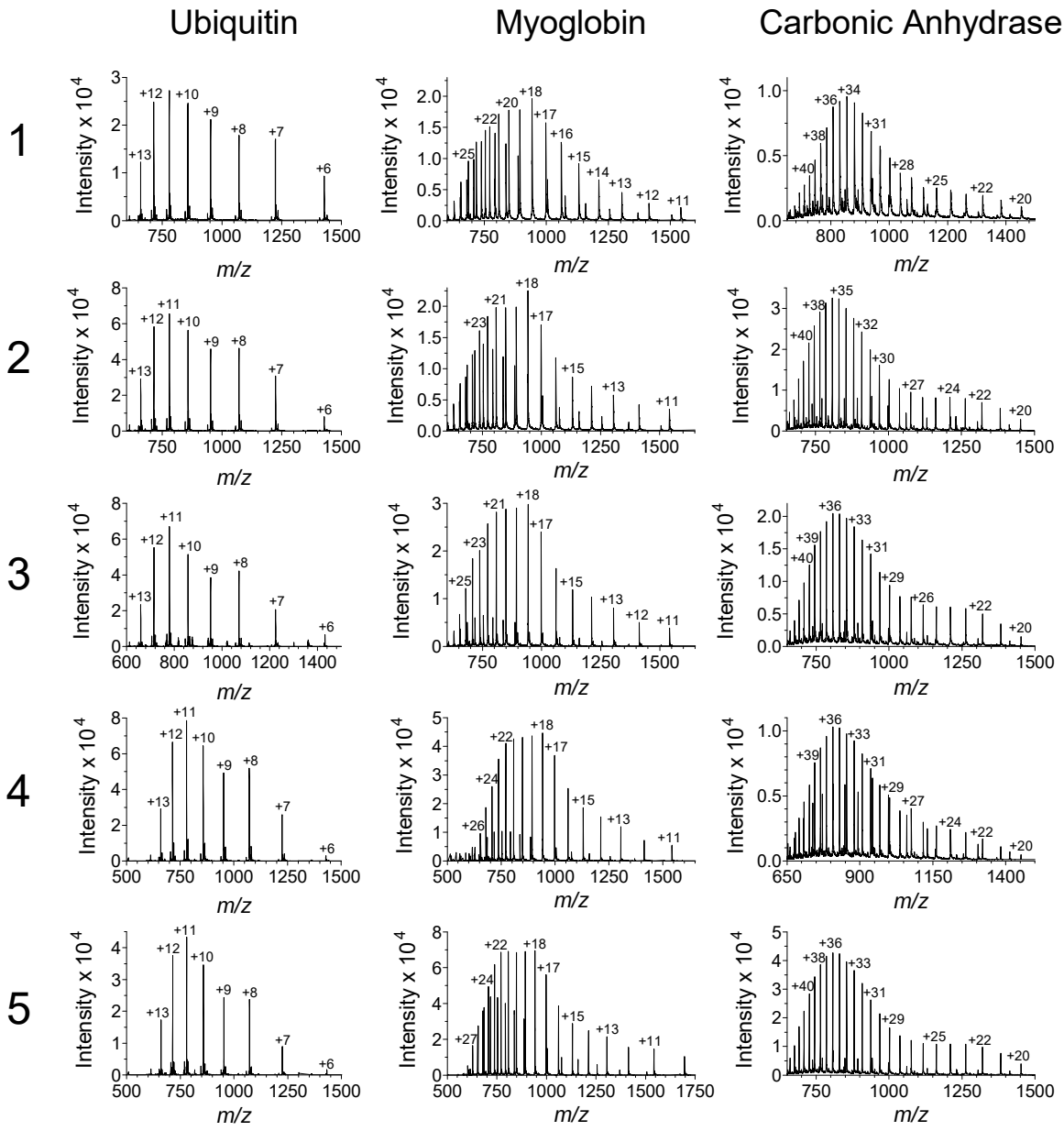

Figure 5.13 MS charge state envelopes for ubiquitin, myoglobin, and carbonic anhydrase after SDS depletion with each method as follows: row 1 = FASP (30 kDa MWCO), row 2 = FASP (10 kDa MWCO), row 3 = acetone precipitation, row 4 = TME, row 5 = control (initial SDS = 0 ppm).

It is clear from the appearance of the charge state envelopes for ubiquitin, myoglobin, and carbonic anhydrase that each SDS purification strategy yields high-quality ESI MS charge state envelopes for intact proteins. This is to be expected considering the

similar protein recovery and SDS purity (≤10 ppm SDS) across all three methods with intact proteins. Each charge state envelope is nearly indistinguishable from the control sample (5) in terms of spectra intensity and appearance. There is minimal presence of interfering SDS adducts across the three methods, and negligible levels of baseline noise. The spectra for carbonic anhydrase displays the most noise in the baseline for all methods, with FASP (30 kDa) having the highest levels. Each purification strategy successfully detected all proteins, though it should be noted, the final eluting protein (hemoglobin β) had reduced signal intensity for all purification methods, which is to be expected because it is the most hydrophobic protein (see Table 2.1). The appearance of the charge state envelopes and the successful detection of all 7 proteins validate the applicability of all these membrane-based SDS depletion methods for top-down proteomic workflows.

5.4 Chapter 5 Conclusions

SDS depletion is a key step prior to MS analysis, and there are many strategies available. Some of the more favoured methods available (FASP and acetone precipitation in a Teflon membrane filter) employ membrane filtration to achieve sample purity and set an excellent benchmark for emerging membrane-based methods like TME. An assessment of the performance of these three methods in both bottom-up and top-down proteomic workflows found successful results with all methods. However, TME generally achieves essentially surfactant-free samples with consistently higher yields over those observed with FASP and acetone precipitation. All three methods identified similar numbers of peptides and proteins and displayed significant overlap in the identity of each. Perhaps larger differences between the three methods could be revealed if more GELFrEE fractions were analyzed or replicate MS/MS runs were performed. Nonetheless, higher yields with TME

translated to grater PSMs per protein and higher detection of low MW proteins. In the top-down studies, all three methods performed comparably, with minimal differences between them. The work shown in this chapter, shows TME performs just as well, if not better, as the favoured methods of SDS depletion in the field, and its use will promote incorporation of SDS in proteomics workflows for both BUP and TDP studies.

Chapter 6: Conclusion

6.1 Conclusions

The speed, sensitivity, and high-throughput capabilities of modern MS instruments have made them essential tools in proteomics workflows. In addition, SDS is undoubtedly the most favoured reagent in protein extraction and separation/fractionation, but its detriments to downstream analysis (LC-MS) are unfortunately evident (see Section 1.1.5.2). As such the development of SDS-depletion techniques has become a relevant and active research area. There are many methods available for the removal of SDS (see Section 1.1.5.3), but many fail to remove both the free and protein-bound SDS while maintaining high sample yields. Recently, this group developed a novel electrophoretic, membrane-based SDS removal method called TME (see Section 1.1.5.4). The technique is robust and reproducible, successfully depleting SDS from both simple and complex protein samples to levels acceptable for LC-MS analysis (≤100 ppm) while maintaining >90% protein yield[65]. In addition, SDS depletion from samples enriched with hydrophobic membrane proteins has been demonstrated with TME. The originally developed TME was successful, but it required lengthy (1 hour) operation times, along with rigorous sample mixing throughout the depletion process to prevent overheating. The requirement for sample mixing lengthened the time required for depletion, necessitated manual intervention, and contributed to error/sample loss. In addition, little was understood about the electrophoretic properties of TME, and how Joule heating (a feature common to all electrophoretic processes) effects depletion and sample yield.

Initial investigations on TME highlighted the necessity for a theoretical model of SDS depletion over time. The variable nature of each TME experiment and the existing history of data, made comparison between experiments difficult and unreliable. Chapter 3 begins by proposing an exponential decay approximation derived from a simplified NP equation, relating the flux of an ion to the strength of the applied electric field. The exponential decay function is commonly used to model flux decline in other membrane processes and allows for direct comparison between TME experiments with varying initial conditions (*via* half-lives). As an example, a similar electrophoretic device reported by Tuszynski and Warren in 1975, demonstrated SDS depletion to below 10 ppm, similar to the present study[103]. However, their approach demonstrates an SDS depletion half-life of 60 min. From the results reported by Kachuk and colleagues, a half-life of 5.9 min was calculated[65]. In this thesis, the lowest half-life was seen to be 1.1 min.

It is understood from previous studies that high levels of Joule heating limits TME operation to lower current (≤40 mA) and contributes to protein aggregation and yield loss. It was initially thought that different TME operation modes (*i.e.* constant power, current, or voltage) had little impact on performance. It was demonstrated here that operation at constant current gives a decrease in the heat generated over time, whereas constant voltage gives an increase, and constant power remains uniform. Thus, it can be concluded that constant current is in fact the preferred method of TME operation.

Protein aggregation during TME is a significant problem that is worsened when SDS is removed and Joule heating increases temperatures to above 60°C. SDS-depleted protein samples were demonstrated to aggregate and precipitate more readily upon heating, and at lower temperatures than native BSA, or SDS-containing BSA. This demonstrated the

importance of maintaining a continuous low sample cell temperature during TME operation. Although potentially problematic, multiple experiments show that a simple formic acid re-extraction of the sample cell can retrieve any unrecovered proteins after SDS depletion (lost to aggregation/adsorption). However, it is still the preferred alternative that proteins remain in solution throughout the TME run; protein aggregation on the membrane likely increases the resistance by restricting the pores, thus lowering the rate of SDS depletion.

Reducing the overall system resistance is also an important step in minimizing the levels of Joule heating, and the region with the highest resistance in TME is the membrane. By halving the membrane thickness and increasing the pore size, a significant decrease in the TME cell resistance was observed in the system, which directly correlated to the sample cell temperature becoming much lower. Additionally, these changes to the membrane gave no significant changes to SDS depletion rates nor protein recovery. Though smaller proteins showed diminished recovery with larger-pored membranes, this effect could be lessened by the addition of other differently-sized proteins to the sample cell. Lower temperature and system resistance can allow for safe operation of TME at higher currents (*i.e.* +50 mA). However, manual mixing was also shown to be ineffective at regulating temperature at high operating currents, and frequent pausing of the power supply leaves samples vulnerable to significant levels of SDS-back diffusion. More strategies to combat Joule heating at these high current levels are still required to achieve optimal operation.

Chapter 4 begins by establishing that the TME sample cell temperatures were severely underestimated in previous studies. This result was followed by an illustration of protein localization against the membrane surfaces within the TME sample cell when no

mixing is performed. Constant stirring with a stir bar inside the TME sample cell was proposed to help dissipate heat, and prevent significant protein build up against the membrane surface. A stir bar was shown to significantly reduce observed sample cell temperatures for 30, 50, and 70 mA runs, completely removing the requirement for manual pausing/mixing events. Lower sample cell temperature also correlated to significantly lower levels of system resistance, and significant improvements to sample yield. A stir bar helps to increase porosity, prevent adsorption, and pore-blocking by continuously removing any protein build up at the membrane surface, which has been shown to increase sample yield and SDS flux out of the sample cell. TME with a stir bar permits operation at 70 mA, without any required pausing or supervision, completing depletion to below 100 ppm in fewer than 10 min while maintaining a sample yield of 94 ± 5%. It was also shown that the absence of protein and fast stir speeds can be detrimental to SDS depletion rates. Though, no clear conclusions can be drawn about why changing these parameters gave negative effects on SDS depletion rates, and further experiments (discussed below) are still required.

The results presented in Chapters 3 and 4 were completed on simple systems containing 1 or 2 protein standards, but proteins are very chemically diverse and these results are not completely representative of an entire proteome. With this in mind, the performance of TME on unfractionated and GELFrEE fractionated *S. cerevisiae* protein extracts was assessed. As expected, TME operates less effectively with a complex proteome mixture, likely due to the high levels of buffer constituents, lipids, biopolymers, cellular debris, *etc.* In addition, protein-protein interactions can strongly influence the "working" pore size experienced by SDS. The most successful sample was the fractionated *S. cerevisiae* with a stir bar, owing to this sample containing the lowest level of

contaminants. In addition, large decreases in voltage as compared to BSA (made in water) were observed for these samples. The decrease in voltage was attributed to differences in solvent components (*i.e.* running buffer or Milli-Q water), and likely contributed to the lower depletion rates observed.

For the remainder of Chapter 5, TME performance was compared to two more favoured and well-established depletion methods, acetone precipitation and FASP. To maximize reliability and reproducibility, acetone precipitation was performed inside a custom two-stage centrifugal filter cartridge for this study. Additionally, a novel "intact FASP" protein clean-up method was proposed and successfully utilized during the TDP study. Comparison to these methods sets an excellent benchmark for emerging membrane-based methods like TME. An assessment of the performance of these three methods in a BUP study on *C. reinhardtii* and a TDP workflow with a standard protein mixture was presented. All three methods reliably depleted SDS to ≤ 10 ppm, and TME consistently maintained significantly higher sample yields. All three methods gave very similar numbers of peptides and proteins identified, as well as significant overlap in the identity of each. Nonetheless, higher yields with TME translated to a greater number of PSMs per protein and increased detection of low MW proteins. Despite potential for losses, all three methods displayed successful detection of hydrophobic proteins, as determined by GRAVY score, with TME identifying the greatest number. In the intact protein studies, all three methods performed comparably, with minimal differences in quality/appearance of TIC and charge envelopes observed. The work presented in this chapter, shows TME performs just as well, if not better, than the favoured methods of SDS depletion in the field.

As MS instrumentation continues to develop, its implementation in proteomics workflows is becoming more commonplace. This necessitates the development of new and effective front-end protein sample processing techniques. The introduction of TME by this group in 2016 demonstrated its success as an SDS-depletion method, but also revealed limitations in terms of depletion time (1 hour), and management of high levels of Joule heating. This thesis presents multiple different strategies to improve temperature management during TME. Changes to the membrane, operating mode, and addition of a stir bar significantly reduced the levels of Joule heating allowing for TME operation at higher currents. Proper temperature management with a stir bar also gave significantly improved sample yields, as well as increased SDS depletion rates. The improvements to TME presented in this thesis put forward a reliable and completely automated platform for SDS removal. Its demonstrated success (as compared to other popular methods) will promote incorporation of SDS in proteomics workflows for both BUP and TDP studies in the future.

6.2 Suggested Future Work

This thesis presents an improved understanding of the fundamental variables governing SDS-depletion in TME as well as significant improvements to TME performance over the original. Nonetheless, there are some questions that remain unanswered, as well as new possible research paths revealed.

First, further investigations into the effect temperature has on voltage, system resistance, and membrane porosity are required. In general, it is understood, high levels of heating promote protein aggregation, membrane fouling, and a decline in flux/yield which is undesirable for TME. Conversely, moderate warming can decrease solution viscosity,

which decreases resistance (and heat generation), which increases ion velocity. In addition, warming could increase the porosity of the membrane, further aiding overall flux and further reducing resistance. The impacts of heating during TME are still not fully understood, and experiments in which the temperature of TME is held constant (cold *vs* warm) could help provide insights on how SDS flux is influenced.

Further studies are also required in regards to larger-pore membranes. A clear decrease in both system resistance and temperature are observed when a larger pored membrane is utilized. Though no effect on SDS depletion rates were observed, and diminished protein yields for low MW proteins was observed. Proteins have a significantly larger hydrodynamic radii when denatured and there are many industrial processes which successfully retain proteins of sizes much smaller than the designated MWCO. With that, it is unclear whether the diminished yields of ubiquitin (8 kDa) during TME with a 12-14 kDa MWCO are from lack of retention or large levels of membrane adsorption. Perhaps a formic acid rinse of the sample cell could recover the missing yield, and a more definitive conclusion could be drawn about the retention qualities of larger-pored membranes with small proteins in TME.

Next, some questions about the performance of TME with a stir bar were left unanswered. It is unclear why TME performance changes on a SDS sample which contains no protein. A depletion experiment with no protein and no stirring could identify whether the observed result is related to the stir bar. In addition, an experiment comparing SDS depletion on a very small protein *vs* a very large protein could provide merit for the proposed “anchoring” hypothesis. Moreover, a TME experiment on an extremely dilute

protein sample (approaching 0 g/L) could also help to understand why the presence of protein increases depletion rates.

Furthermore, a better understanding of TME performance on complex protein mixtures is warranted. It is hypothesized the differences occur due to multiple different interfering contaminants, but this requires further experiments to confirm. Perhaps an experiment comparing SDS-depletion of a BSA sample made in running buffer (instead of Milli-Q water) to a GELFrEE fractionated sample could help identify if these buffer constituents slow SDS depletion rates. Although the samples being compared would still be a proteome *vs* a single protein. An alternative experiment could be comparison of SDS depletion rates on a GELFrEE fractionated sample and a GELFrEE fractionated acetone precipitated sample. The acetone precipitation step would remove any contaminants and buffer constituents, allowing for resolubilization in Milli-Q water with SDS. Additionally, large differences in voltage were observed between a single protein and a complex proteome sample. It is hypothesized this also comes from the high levels of buffer constituents in the proteome samples. However, an experiment comparing SDS-depletion rates and voltages of BSA prepared in Milli-Q *vs* BSA prepared in TME electrolyte buffer could help identify if the buffer constituents are influencing the results.

Finally, there are some TME parameters that were not evaluated in this thesis but merit exploration including modifying the overall dimensions of the system to increase the surface area:volume ratio. This could provide improvements to heat dissipation (like CE) and increases in SDS flux by increasing the proportion of the sample exposed to the membrane surface. Other modifications could include overall miniaturization of the system to accommodate small sample volumes and reduce the consumption of electrolyte buffer

and membrane. Modifications to the electrolyte buffer volume, buffer components, pH, and concentration may provide ability to operate at higher currents and increase temperature tolerances. Lastly, modification of the off-line TME system presented in this thesis to an "on-line" flow through system could help increase heat dissipation, prevent SDS back diffusion, further remove any human intervention, and promote interfacing between downstream technologies like GELFrEE or LC-MS.

Bibliography

(1) Sanger, F.; Tuppy, H. The Amino-acid Sequence in the Phenylalanyl Chain of Insulin 1. The identification of lower peptides from partial hydrolysates. *Biochem. J.* **1951**, *49* (4), 463–481.

(2) Sanger, F.; Tuppy, H. The Amino-acid Sequence in the Phenylalanyl Chain of Insulin 2. The investigation of peptides from enzymic hydrolysates. *Biochem. J.* **1951**, *49* (4), 481–490.

(3) Perutz, M. F.; Rossmann, M. G.; Cullis, A. F.; Muirhead, H.; Will, G.; North, A. C. T. Structure of Hæmoglobin: A three-dimensional fourier synthesis at 5.5-Å resolution, obtained by X-ray analysis. *Nature* **1960**, *185*, 416–422.

(4) Kendrew, J. C.; Dickerson, R. E.; Strandberg, B. E.; Hart, R. G.; Davies, D. R.; Phillips, D. C.; Shore, V. C. Structure of Myoglobin: A three-dimensional fourier synthesis at 2 Å resolution. *Nature* **1960**, *185*, 422–427.

(5) Lander, E. S.; Linton, L. M.; Birren, B.; Nusbaum, C.; Zody, M. C.; Baldwin, J.; Devon, K.; Dewar, K.; Doyle, M.; FitzHugh, W.; et al. Initial sequencing and analysis of the human genome. *Nature* **2001**, *409*, 860–921.

(6) The C. elegans Sequencing Consortium. Genome Sequence of the Nematode C. elegans: A platform for Investigating Biology. *Science (80-.).* **1998**, *282* (5396), 2012–2019.

(7) Wasinger, V. C.; Cordwell, S. J.; Cerpa-poljak, A.; Yan, J. X.; Gooley, A. A.; Wilkins, M. R.; Duncan, M. W.; Harris, R.; Williams, K. L.; Humphery-smith, I. Progress with gene-product mapping of the Mollicutes: Mycoplasma genitalium. *Electrophoresis* **1995**, *16*, 1090–1094.

(8) Smith, L. M.; Kelleher, N. L. Proteoform: a single term describing protein complexity. *Nat. Methods* **2013**, *10* (3), 186–187.

(9) Toyama, B. H.; Savas, J. N.; Park, S. K.; Harris, M. S.; Ingolia, N. T.; Yates, J. R.; Hetzer, M. W. Identification of long-lived proteins reveals exceptional stability of essential cellular structures. *Cell* **2013**, *154* (5), 971–982.

(10) Karve, T. M.; Cheema, A. K. Small Changes Huge Impact: The Role of Protein Posttranslational Modifications in Cellular Homeostasis and Disease. *J. Amino Acids* **2011**, *2011*, 1–13.

(11) Yoshida, M.; Loo, J. A.; Lepley, R. A. Proteomics as a Tool in the Pharmaceutical Drug Design Process. *Curr. Pharm. Des.* **2001**, *7* (4), 293–312.

(12) Mokou, M.; Lygirou, V.; Vlahou, A.; Mischak, H. Proteomics in cardiovascular disease: recent progress and clinical implication and implementation. *Expert Rev. Proteomics* **2017**, *14* (2), 117–136.

(13) Lacerda, C. M. R.; Kenneth, F. Environmental proteomics: applications of proteome profiling in environmental microbiology and biotechnology. *Briefings Funct. Genomics Proteomics* **2009**, *8* (1), 75–87.

(14) Kenrick, K. G.; Margolis, J. Isoelectric Focusing and Gradient Gel Electrophoresis: A Two-Dimensional Technique. *Anal. Biochem.* **1970**, *33* (1), 204–207.

(15) O'Farrell, P. H. High resolution two-dimensional electrophoresis of proteins. *J. Biol. Chem.* **1975**, *250* (10), 4007–4021.

(16) Klose, J.; Kobalz, U. Two-dimensional electrophoresis of proteins: An updated protocol and implications for a functional analysis of the genome. *Electrophoresis* **1995**, *16* (6), 1034–1059.

(17) Rogowska-Wrzesinska, A.; Le Bihan, M.; Thaysen-Andersen, M.; Roepstorff, P. 2D gels still have a niche in proteomics. *J. Proteomics* **2013**, *88*, 4–13.

(18) Gross, J. H. *Mass Spectrometry: A Textbook*, 2nd ed.; Springer-Verlag: Heidelberg, 2011.

(19) Karas, M.; Bachmann, D.; Bahr, U.; Hillenkamp, F. Matrix-Assisted Ultraviolet Laser Desorption of Non-Volatile Compounds. *Int. J. Mass Spectrom. Ion Process.* **1987**, *78* (C), 53–68.

(20) Tanaka, K.; Waki, H.; Ido, Y.; Akita, S.; Yoshida, Y.; Yoshida, T. Protein and Polymer Analyses up to m/z 100 000 by Laser Ionization Time-of-flight Mass Spectrometry. *Rapid Commun. Mass Spectrom.* **1988**, *2* (8), 151–153.

(21) Caprioli, R. M.; Farmer, T. B.; Gile, J. Molecular Imaging of Biological Samples: Localization of Peptides and Proteins Using MALDI-TOF MS. *Anal. Chem.* **1997**, *69* (23), 4751–4760.

(22) Dole, M.; Mack, L. L.; Hines, R. L.; Mobley, R. C.; Ferguson, L. D.; Alice, M. B. Molecular Beams of Macroions. *J. Chem. Phys.* **1968**, *49* (5), 2240–2249.

(23) Fenn, J. B.; Mann, M.; Meng, C. K.; Wong, S. F.; Whitehouse, C. M. Electrospray Ionization for Mass Spectrometry of Large Biomolecules. *Science (80-.).* **1989**, *246* (4926), 64–71.

(24) Konermann, L.; Ahadi, E.; Rodriguez, A. D.; Vahidi, S. Unraveling the mechanism of electrospray ionization. *Anal. Chem.* **2013**, *85* (1), 2–9.

(25) Wilm, M.; Mann, M. Analytical Properties of the Nanoelectrospray Ion Source. *Anal. Chem.* **1996**, *68* (1), 1–8.

(26) El-Aneed, A.; Cohen, A.; Banoub, J. Mass Spectrometry, Review of the Basics: Electrospray, MALDI, and Commonly Used Mass Analyzers. *Appl. Spectrosc. Rev.* **2009**, *44* (3), 210–230.

(27) Whitelegge, J. Intact protein mass spectrometry and top-down proteomics. *Expert Rev. Proteomics* **2013**, *10* (2), 127–129.

(28) Qi, Y.; Volmer, D. A. Electron-Based Fragmentation Methods in Mass Spectrometry: An Overview. *Mass Spectrom. Rev.* **2017**, *36* (1), 4–15.

(29) Forbes, A. J.; Mazur, M. T.; Patel, H. M.; Walsh, C. T.; Kelleher, N. L. Toward efficient analysis of >70 kDa proteins with 100% sequence coverage. *Proteomics* **2001**, *1* (8), 927–933.

(30) Wu, C.; Tran, J. C.; Zamdborg, L.; Durbin, K. R.; Li, M.; Ahlf, D. R.; Early, B. P.; Thomas, P. M.; Sweedler, J. V; Kelleher, N. L. A protease for "middle-down" proteomics. *Nat. Methods* **2012**, *9* (8), 822–826.

(31) Switzar, L.; Giera, M.; Niessen, W. M. A. Protein Digestion: An Overview of the Available Techniques and Recent Developments. *J. Proteome Res.* **2013**, *12*, 1067–1077.

(32) Kinter, M.; Sherman, N. E. *Protein Sequencing and Identification Using Tandem Mass Spectrometry*; Desiderio, D. M., Nibbering, N. M. M., Eds.; John Wiley & Sons, Inc.: New York, NY, 2000.

(33) Kelleher, N. L.; Lin, H. Y.; Valaskovic, G. A.; Aaserud, D. J.; Fridriksson, E. K.; Mclafferty, F. W. Top Down versus Bottom Up Protein Characterization by Tandem High-Resolution Mass Spectrometry. *J. Am. Chem. Soc.* **1999**, *121* (4), 806–812.

(34) Laemmli, U. K. Cleavage of Structural Proteins during the Assembly of the Head of Bacteriophage T4. *Nature* **1970**, *227* (5259), 680–685.

(35) Reynolds, J. A.; Tanford, C. Binding of Dodecyl Sulfate to Proteins at High Binding Ratios. Possible Implications for the State of Proteins in Biological Membranes. *Proc. Natl. Acad. Sci. U. S. A.* **1970**, *66* (3), 1002–1007.

(36) Otzen, D. Protein–surfactant interactions: A tale of many states. *Biochim. Biophys. Acta* **2011**, *1814* (5), 562–591.

(37) Nelson, C. A. The Binding of Detergents to Proteins. *J. Biol. Chem.* **1971**, *246* (12), 3895–3901.

(38) Rabilloud, T.; Chevallet, M.; Luche, S.; Lelong, C. Two-dimensional gel electrophoresis in proteomics: Past, present and future. *J. Proteomics* **2010**, *73*, 2064–2077.

(39) Reinders, J.; Zahedi, R. P.; Pfanner, N.; Meisinger, C.; Sickmann, A. Toward the Complete Yeast Mitochondrial Proteome: Multidimensional Separation Techniques for Mitochondrial Proteomics. *J. Proteome Res.* **2006**, *5* (7), 1543–1554.

(40) Li, X.; Gerber, S. A.; Rudner, A. D.; Beausoleil, S. A.; Haas, W.; Villén, J.; Elias, J. E.; Gygi, S. P. Large-Scale Phosphorylation Analysis of α-Factor-Arrested Saccharomyces cerevisiae. *J. Proteome Res.* **2007**, *6*, 1190–1197.

(41) Gautier, V.; Mouton-barbosa, E.; Bouyssié, D.; Delcourt, N.; Beau, M.; Girard, J.; Cayrol, C.; Burlet-Schiltz, O.; Monsarrat, B.; Gonzalez de Peredo, A. Label-free Quantification and Shotgun Analysis of Complex Proteomes by One-dimensional SDS-PAGE/NanoLC-MS. *Mol. Cell. Proteomics* **2012**, *11* (8), 527–539.

(42) Young, B. L.; Mlamla, Z.; Gqamana, P. P.; Smit, S.; Roberts, T.; Peter, J.; Theron, G.; Govender, U.; Dheda, K.; Blackburn, J. The identification of tuberculosis biomarkers in human urine samples. *Eur. Respir. J.* **2014**, *43* (6), 1719–1729.

(43) Colgrave, M. L.; Goswami, H.; Byrne, K.; Blundell, M.; Howitt, C. A.; Tanner, G. J. Proteomic Profiling of 16 Cereal Grains and the Application of Targeted Proteomics To Detect Wheat Contamination. *J. Proteome Res.* **2015**, *14*, 2659–2668.

(44) Kuljanin, M.; Dieters-Castator, D. Z.; Hess, D. A.; Postovit, L.-M.; Lajoie, G. A. Comparison of sample preparation techniques for large-scale proteomics. *Proteomics* **2017**, *17* (1–2), 1600337.

(45) Tran, J. C.; Doucette, A. A. Gel-eluted Liquid Fraction Entrapment Electrophoresis: An Electrophoretic Method for Broad Molecular Weight Range Proteome Separation. *Anal. Chem.* **2008**, *80* (5), 1568–1573.

(46) Speers, A. E.; Wu, C. C. Proteomics of Integral Membrane Proteins -- Theory and Application. *Chem. Rev.* **2007**, *107* (8), 3687–3714.

(47) Seddon, A. M.; Curnow, P.; Booth, P. J. Membrane proteins, lipids and detergents: not just a soap opera. *Biochim. Biophys. Acta - Biomembr.* **2004**, *1666*, 105–117.

(48) Rajendran, L.; Knölker, H.-J.; Simons, K. Subcellular targeting strategies for drug design and delivery. *Nat. Rev.* **2010**, *9*, 29–42.

(49) Almén, M. S.; Nordström, K. J. V; Fredriksson, R.; Schiöth, H. B. Mapping the human membrane proteome: a majority of the human membrane proteins can be classified according to function and evolutionary origin. *BioMed Cent. Biol.* **2009**, *7* (50), 1–14.

(50) Koebnik, R.; Locher, K. P.; Van Gelder, P. Structure and function of bacterial outer membrane proteins: barrels in a nutshell. *Mol. Microbiol.* **2000**, *37* (2), 239–253.

(51) Kumar, A.; Agarwal, S.; Heyman, J. A.; Matson, S.; Heidtman, M.; Piccirillo, S.; Umansky, L.; Drawid, A.; Jansen, R.; Liu, Y.; et al. Subcellular localization of the yeast proteome. *Genes Dev.* **2002**, *16*, 707–719.

(52) Andersen, K. K.; Oliveira, C. L.; Larsen, K. L.; Poulsen, F. M.; Callisen, T. H.; Westh, P.; Pedersen, J. S.; Otzen, D. The Role of Decorated SDS Micelles in Sub-CMC Protein Denaturation and Association. *J. Mol. Biol.* **2009**, *391* (1), 207–226.

(53) Ibel, K.; May, R. P.; Kirschner, K.; Szadkowski, H.; Mascher, E.; Lundhal, P. Protein-decorated micelle structure of sodium-dodecyl-sulfate–protein complexes as determined by neutron scattering. *Eur. J. Biochem.* **1990**, *190* (2), 311–318.

(54) Otzen, D. E. Protein Unfolding in Detergents: Effect of Micelle Structure, Ionic Strength, pH, and Temperature. *Biophys. J.* **2002**, *83* (4), 2219–2230.

(55) Nielsen, M. M.; Andersen, K. K.; Westh, P.; Otzen, D. E. Unfolding of β-Sheet Proteins in SDS. *Biophys. J.* **2007**, *92* (10), 3674–3685.

(56) Andersen, K. K.; Westh, P.; Otzen, D. E. Global Study of Myoglobin-Surfactant Interactions. *Langmuir* **2008**, *24* (2), 399–407.

(57) Otzen, D. E.; Sehgal, P.; Westh, P. α-Lactalbumin is unfolded by all classes of surfactants but by different mechanisms. *J. Colloid Interface Sci.* **2009**, *329* (2), 273–283.

(58) Jones, M. N. A Theoretical Approach to the Binding of Amphipathic Molecules to Globular Proteins. *Biochem. J.* **1975**, *151*, 109–114.

(59) Valstar, A. N. K. Protein-Surfactant Interactions, Uppsala University, 2000.

(60) Tanford, C. *The Hydrophobic Effect: Formation of Micelles and Biological Membranes*; John Wiley & Sons, Inc.: New York, NY, 1980.

(61) Turro, N. J.; Lei, X.-G.; Ananthapadmanabhan, K. P.; Aronson, M. Spectroscopic Probe Analysis of Protein-Surfactant Interactions: The BSA/SDS System. *Langmuir* **1995**, *11* (7), 2525–2533.

(62) Shirahama, K.; Tsujii, K.; Takagi, T. Free-boundary Electrophoresis of Sodium Dodecyl Sulfate-Protein Polypeptide Complexes with Special Reference to SDS-Polyacrylamide Gel Electrophoresis. *J. Biochem.* **1974**, *75* (2), 309–319.

(63) Kachuk, C.; Doucette, A. A. The benefits (and misfortunes) of SDS in top-down proteomics. *J. Proteomics* **2018**, *175*, 75–86.

(64) Botelho, D.; Wall, M. J.; Vieira, D. B.; Fitzsimmons, S.; Liu, F.; Doucette, A. Top-Down and Bottom-Up Proteomics of SDS-Containing Solutions Following Mass-Based Separation. *J. Proteome Res.* **2010**, *9* (6), 2863–2870.

(65) Kachuk, C.; Faulkner, M.; Liu, F.; Doucette, A. A. Automated SDS Depletion for Mass Spectrometry of Intact Membrane Proteins though Transmembrane Electrophoresis. *J. Proteome Res.* **2016**, *15* (8), 2634–2642.

(66) Ogorzalek Loo, R. R.; Dales, N.; Andrews, P. C. Surfactant effects on protein structure examined by electrospray ionization mass spectrometry. *Protein Sci.* **1994**, *3*, 1975–1983.

(67) Chapman, J. R. *Methods in Molecular Biology: Protein and Peptide Analysis by Mass Spectrometry*; Walker, J. M., Ed.; Humana Press: Totowa, NJ, 1996.

(68) Ghosh, S. Interaction of trypsin with sodium dodecyl sulfate in aqueous medium: A conformational view. *Colloids Surfaces B Biointerfaces* **2008**, *66* (2), 178–186.

(69) Arribas, J.; Castaño, J. G. Kinetic studies of the Differential Effect of Detergents on the Peptidase Activities of the Multicatalytic Proteinase from Rat Liver. *J. Biol. Chem.* **1990**, *265* (23), 13969–13973.

(70) Yu, Y.-Q.; Gilar, M.; Lee, P. J.; Bouvier, E. S. P.; Gebler, J. C. Enzyme-Friendly, Mass Spectrometry-Compatible Surfactant for In-Solution Enzymatic Digestion of Proteins. *Anal. Chem.* **2003**, *75* (21), 6023–6028.

(71) Lowry, O. H.; Rosebrough, N. J.; Farr, A. L.; Randall, R. J. Protein Measurement with the Folin Phenol Reagent. *J. Biol. Chem.* **1951**, *193* (1), 265–275.

(72) Bradford, M. M. A Rapid and Sensitive Method for the Quantitation of Microgram Quantities of Protein Utilizing the Principle of Protein-Dye Binding. *Anal. Biochem.* **1976**, *72* (1–2), 248–254.

(73) Steinberg, T. H. Protein Gel Staining Methods: An Introduction and Overview. In *Methods in Enzymology*; Burgess, R. R., Deutscher, M. P., Eds.; Elsevier Inc.: Oxford, UK, 2009; Vol. 463, pp 541–563.

(74) Marshall, T.; Williams, K. M. Interference in the Coomassie Brilliant Blue and Pyrogallol Red protein dye-binding assays is increased by the addition of sodium dodecyl sulfate to the dye reagents. *Anal. Biochem.* **2004**, *331* (2), 255–259.

(75) Chertov, O.; Biragyn, A.; Kwak, L. W.; Simpson, J. T.; Boronina, T.; Hoang, V. M.; Prieto, D. A.; Conrads, T. P.; Veenstra, T. D.; Fisher, R. J. Organic solvent extraction of proteins and peptides from serum as an effective sample preparation for detection and identification of biomarkers by mass spectrometry. *Proteomics* **2004**, *4* (4), 1195–1203.

(76) Wang, H.; Qian, W.-J.; Mottaz, H. M.; Clauss, T. R. W.; Anderson, D. J.; Moore, R. J.; Camp, D. G.; Pallavicini, M.; Smith, D. J.; Smith, R. D. Development and Evaluation of a Micro- and Nano-Scale Proteomic Sample Preparation Method. *J Proteome Res* **2005**, *4* (6), 2397–2403.

(77) Rey, M.; Mrázek, H.; Pompach, P.; Novák, P.; Pelosi, L.; Brandolin, G.; Forest, E.; Havlíček, V.; Man, P. Effective Removal of Nonionic Detergents in Protein Mass Spectrometry, Hydrogen/Deuterium Exchange, and Proteomics. *Anal. Chem.* **2010**, *82* (12), 5107–5116.

(78) Chang, Y.-H.; Gregorich, Z. R.; Chen, A. J.; Hwang, L.; Guner, H.; Yu, D.; Zhang, J.; Ge, Y. A New Mass Spectrometry-compatible Degradable Surfactant for Tissue Proteomics. *J. Proteome Res.* **2015**, *14* (3), 1587–1599.

(79) Vieira, D. B.; Crowell, A. M. J.; Doucette, A. A. Perfluorooctanoic acid and ammonium perfluorooctanoate: volatile surfactants for proteome analysis? *Rapid Commun. Mass Spectrom.* **2012**, *26* (5), 523–531.

(80) Kachuk, C.; Stephen, K.; Doucette, A. Comparison of sodium dodecyl sulfate depletion techniques for proteome analysis by mass spectrometry. *J. Chromatogr. A* **2015**, *1418*, 158–166.

(81) Kachuk, C. Assessment, Development, and Improvement of SDS Depletion Strategies in Mass Spectrometry Proteomic Workflows, Dalhousie, 2016.

(82) Rosenfeld, J.; Capdevielle, J.; Guillemot, J. C.; Ferrara, P. In-gel Digestion of Proteins for Internal Sequence Analysis after One- or Two-Dimensional Gel Electrophoresis. *Anal. Biochem.* **1992**, *203*, 173–179.

(83) Wiśniewski, J. R.; Zougman, A.; Nagaraj, N.; Mann, M. Universal sample preparation method for proteome analysis. *Nat. Methods* **2009**, *6* (5), 359–363.

(84) Lahm, H.-W.; Langen, H. Mass spectrometry: A tool for the identification of proteins separated by gels. *Electrophoresis* **2000**, *21* (11), 2105–2114.

(85) Granvogl, B.; Plöscher, M.; Eichacker, L. A. Sample preparation by in-gel digestion for mass spectrometry-based proteomics. *Anal. Bioanal. Chem.* **2007**, *389* (4), 991–1002.

(86) Jiang, L.; He, L.; Fountoulakis, M. Comparison of protein precipitation methods for sample preparation prior to proteomic analysis. *J. Chromatogr. A* **2004**, *1023*, 317–320.

(87) Barritault, D.; Expert-Bezancon, A.; Guérin, M.-F.; Hayes, D. The Use of Acetone Precipitation in the Isolation of Ribosomal Proteins. *Eur. J. Biochem.* **1976**, *63* (1), 131–135.

(88) Doucette, A. A.; Vieira, D. B.; Orton, D. J.; Wall, M. J. Resolubilisation of Precipitated Intact Membrane Proteins with Cold Formic Acid for Analysis by Mass Spectrometry. *J. Proteome Res.* **2014**, *13*, 6001–6012.

(89) Puchades, M.; Westman, A.; Blennow, K.; Davidsson, P. Removal of Sodium Dodecyl Sulfate from Protein Samples Prior to Matrix-assisted Laser Desorption/ionization Mass Spectrometry. *Rapid Commun. mass Spectrom.* **1999**, *13* (5), 344–349.

(90) Crowell, A. M. J.; MacLellan, D. L.; Doucette, A. A. A two-stage spin cartridge for integrated protein precipitation, digestion and SDS removal in a comparative bottom-up proteomics workflow. *J. Proteomics* **2015**, *118*, 140–150.

(91) Zhou, J.; Dann, G. P.; Shi, T.; Wang, L.; Gao, X.; Su, D.; Nicora, C. D.; Shukla, A. K.; Moore, R. J.; Liu, T.; et al. Simple Sodium Dodecyl Sulfate-Assisted Sample Preparation Method for LC-MS-Based Proteomics Applications. *Anal. Chem.* **2012**, *84* (6), 2862–2867.

(92) Wisniewski, J. R. Quantitative Evaluation of Filter Aided Sample Preparation (FASP) and Multienzyme Digestion FASP Protocols. *Anal. Chem.* **2016**, *88* (10), 5438–5443.

(93) Wiśniewski, J. R.; Zielinska, D. F.; Mann, M. Comparison of ultrafiltration units for proteomic and N-glycoproteomic analysis by the filter-aided sample preparation method. *Anal. Biochem.* **2011**, *410* (2), 307–309.

(94) Bereman, M. S.; Egertson, J. D.; MacCoss, M. J. Comparison between procedures using SDS for shotgun proteomic analyses of complex samples. *Proteomics* **2011**, *11* (14), 2931–2935.

(95) Jenö, P.; Scherer, P. E.; Manning-Krieg, U.; Horst, M. Desalting Electroeluted Proteins with Hydrophilic Interaction Chromatogrpahy. *Anal. Biochem.* **1993**, *215* (2), 292–298.

(96) Sun, D.; Wang, N.; Li, L. Integrated SDS Removal and Peptide Separation by Strong-Cation Exchange Liquid Chromatography for SDS-Assisted Shotgun Proteome Analysis. *J. Proteome Res.* **2012**, *11* (2), 818–828.

(97) Kawasaki, H.; Suzuki, K. Separation of peptides dissolved in a sodium dodecyl sulfate solution by reversed-phase liquid chromatography: Removal of sodium dodecyl sulfate from peptides using an lon-exchange precolumn. *Anal. Biochem.* **1990**, *186* (2), 264–268.

(98) Van Der Zee, R.; Welling-Wester, S.; Welling, G. W. Purification of Detergent-Extracted Sendai Virus Proteins by Reversed-Phase High-Performance Liquid Chromatography. *J. Chromatogr.* **1983**, *266*, 577–584.

(99) Kapp, O. H.; Vinogradov, S. N. Removal of Sodium Dodecyl Sulfate from Proteins. *Anal. Biochem.* **1978**, *91* (1), 230–235.

(100) Hengel, S. M.; Floyd, E.; Baker, E. S.; Zhao, R.; Wu, S.; Paša-Tolić, L. Evaluation of SDS depletion using an affinity spin column and IMS-MS detection. *Proteomics* **2012**, *12* (21), 3138–3142.

(101) Lenard, J. Rapid and Effective Removal of Sodium Dodecyl Sulfate from Proteins. *Biochem. Biophys. Res. Commun.* **1971**, *45* (3), 662–668.

(102) Tanca, A.; Biosa, G.; Pagnozzi, D.; Addis, M. F.; Uzzau, S. Comparison of detergent-based sample preparation workflows for LTQ-Orbitrap analysis of the Escherichia coli proteome. *Proteomics* **2013**, *13* (17), 2597–2607.

(103) Tuszynski, G. P.; Warren, L. Removal of Sodium Dodecyl Sulfate from Proteins. *Anal. Biochem.* **1975**, *67*, 55–65.

(104) Bhaskar, S.; Dutt, S.; Mukherjee, R. A Simple Method of Electroelution of Individual Protein Bands from SDS Polyacrylamide Gels for Direct Study in Cellular Assays. *J. Immunoassay* **2000**, *21* (4), 355–375.

(105) Wang, H. B.; Zhang, Y.; Gui, S. Q.; Feng, Y. R.; Han, H. C.; Mao, S. H.; Lu, F. P. Electro-ultrafiltration to remove sodium dodecyl sulfate in proteins extracted for proteomics. *RSC Adv.* **2017**, *7* (40), 25144–25148.

(106) Hegyi, G.; Kardos, J.; Kovacs, M.; Malnasi-Csizmadia, A.; Nyitray, L.; Pal, G.; Radnai, L.; Remenyi, A.; Venekei, I. *Introduction to Practical Biochemistry*; Reményi, A., Ed.; Eötvös Loránd University: Budapest, 2013.

(107) Maex, R. On the Nernst-Planck equation. *J. Integr. Neurosci.* **2017**, *16* (1), 73–91.

(108) Rathore, A. S. Joule heating and determination of temperature in capillary electrophoresis and capillary electrochromatography columns. *J. Chromatogr. A* **2004**, *1037*, 431–443.

(109) Evenhuis, C. J.; Haddad, P. R. Joule heating effects and the experimental determination of temperature during CE. *Electrophoresis* **2009**, *30* (5), 897–909.

(110) Cao, J.; Cheng, P.; Hong, F. J. Applications of electrohydrodynamics and Joule heating effects in microfluidic chips: A review. *Sci. China, Ser. E Technol. Sci.* **2009**, *52* (12), 3477–3490.

(111) Xuan, X.; Li, D. Joule heating effects on peak broadening in capillary zone electrophoresis. *J. Micromechanics Microengineering* **2004**, *14* (8), 1171–1180.

(112) Cetin, B.; Li, D. Effect of Joule heating on electrokinetic transport. *Electrophoresis* **2008**, *29* (5), 994–1005.

(113) Tang, G. Y.; Yang, C.; Gong, H. Q.; Chai, C. J.; Lam, Y. C. On Electrokinetic Mass Transport in a Microchannel With Joule Heating Effects. *J. Heat Transfer* **2005**, *127* (6), 660–663.

(114) Xuan, X. Joule heating in electrokinetic flow. *Electrophoresis* **2008**, *29* (1), 33–43.

(115) Dutta, D. Effect of Channel Sidewalls on Joule Heating Induced Sample Dispersion in Rectangular Ducts. *Int. J. Heat Mass Transf.* **2016**, *93*, 529–537.

(116) Chattoraj, D. K.; Biswas, S. C.; Mahapatra, P. K.; Chatterjee, S. Standard free energies of binding of solute to proteins in aqueous medium. Part 2. Analysis of data obtained from equilibrium dialysis and isopiestic experiments. *Biophys Chem* **1999**, *77* (1), 9–25.

(117) Pawliszyn, J.; Wu, J. Ampholyte-free Isoelectric Focusing of Proteins in Cone Shaped Capillaries. *J. Microcolumn Sep.* **1993**, *5* (5), 397–401.

(118) Ross, D.; Locascio, L. E. Microfluidic Temperature Gradient Focusing. *Anal. Chem.* **2002**, *74* (11), 2556–2564.

(119) Hu, G.; Xiang, Q.; Fu, R.; Xu, B.; Venditti, R.; Li, D. Electrokinetically controlled real-time polymerase chain reaction in microchannel using Joule heating effect. *Anal. Chim. Acta* **2006**, *557* (1–2), 146–151.

(120) Taylor, R.; Krishna, R. *Multicomponent Mass Transfer*; John Wiley & Sons, Inc.: New York, NY, 1993.

(121) Wesselingh, J. A.; Krishna, R. *Mass transfer in multicomponent mixtures*, 1st ed.; VSSD: Delft, The Netherlands, 2000.

(122) Gjelstad, A.; Rasmussen, K. E.; Pedersen-Bjergaard, S. Simulation of flux during electro-membrane extraction based on the Nernst-Planck equation. *J. Chromatogr. A* **2007**, *1174*, 104–111.

(123) Qian, N.; Sejnowski, T. J. An Electro-Diffusion Model for Computing Membrane Potentials and Ionic Concentrations in Branching Dendrites, Spines and Axons. *Biol. Cybern.* **1989**, *62* (1), 1–15.

(124) Galier, S.; Balmann, H. R. De. The electrophoretic membrane contactor: A mass-transfer-based methodology applied to the separation of whey proteins. *Sep. Purif. Technol.* **2011**, *77* (2), 237–244.

(125) Huang, C.; Jensen, H.; Seip, K. F.; Gjelstad, A.; Pedersen-Bjergaard, S. Mass transfer in electromembrane extraction - The link between theory and experiments. *J. Sep. Sci.* **2016**, *39* (1), 188–197.

(126) Kasting, G. B. Theoretical models for iontophoretic delivery. *Adv. Drug Deliv. Rev.* **1992**, *9* (2–3), 177–199.

(127) Song, C.; Corry, B. Testing the Applicability of Nernst-Planck Theory in Ion Channels: Comparisons with Brownian Dynamics Simulations. *PLoS One* **2011**, *6* (6), e21204.

(128) Boda, D.; Gillespie, D. Steady-state Electrodiffusion from the Nernst-Planck Equation Coupled to Local Equilibrium Monte Carlo Simulations. *J. Chem. Theory Comput.* **2012**, *8* (3), 824–829.

(129) Schuss, Z.; Eisenberg, R. S.; Nadler, B. Derivation of Poisson and Nernst-Planck equations in a bath and channel from a molecular model. *Phys. Rev. E* **2001**, *64* (3), 14.

(130) Song, Z.; Cao, X.; Huang, H. Electroneutral models for dynamic Poisson-Nernst-Planck systems. *Phys. Rev. E* **2018**, *97* (1), 16.

(131) R. Welty, J.; E. Wicks, C.; E. Wilson, R.; Rorrer, G. *Fundamentals of momentum, heat and mass transfer*, 5th ed.; Welter, J., Sapira, L., McFadden, P., Eds.; John Wiley & Sons, Inc.: Hoboken, NJ, 2000.

(132) Etzel, M. R. Charged Ultrafiltration and Microfiltration Membranes in Antibody Purification. In *Process Scale Purification of Antibodies*; Gottschalk, U., Ed.; John Wiley & Sons, Inc., 2008; pp 325–347.

(133) van den Berg, G. B.; Smolders, C. A. Flux Decline in Ultrafiltration Processes. *Desalination* **1990**, *77* (C), 101–133.

(134) Marshall, A. D.; Munro, P. A.; Trägårdh, G. The effect of protein fouling in microfiltration and ultrafiltration on permeate flux, protein retention and selectivity: A literature review. *Desalination* **1993**, *91* (1), 65–108.

(135) Makardij, A. A.; Farid, M. M.; Chen, X. D. A Simple and Effective Model for Cross-Flow Microfiltration and Ultrafiltration. *Can. J. Chem. Eng.* **2002**, *80* (1), 28–36.

(136) Fu, R. Q.; Xu, T. W.; Yang, W. H.; Pan, Z. X. Fundamental studies on the intermediate layer of a bipolar membrane Part II. Effect of bovine serum albumin (BSA) on water dissociation at the interface of a bipolar membrane. *J. Colloid Interface Sci.* **2004**, *278* (2), 318–324.

(137) Turker, M.; Hubble, J. Membrane Fouling in a Constant-Flux Ultrafiltration Cell. *J. Memb. Sci.* **1987**, *34* (3), 267–281.

(138) Matthiasson, E. The role of macromolecular adsorption in fouling of ultrafiltration membranes. *J. Memb. Sci.* **1983**, *16* (C), 23–36.

(139) Çetinkaya, Ö.; Gökmen, V. Assessment of an exponential model for ultrafiltration of apple juice. *J. Food Process Eng.* **2006**, *29* (5), 508–518.

(140) Ko, M. K.; Pellegrino, J. J.; Nassimbene, R.; Marko, P. Characterization of the adsorption-fouling layer using globular proteins on ultrafiltration membranes. *J. Memb. Sci.* **1993**, *76* (2–3), 101–120.

(141) Dosmar, M. Could Membrane Fouling Be a Thing of the Past? *BioProcess International*. Edgewood, NY February 2005, pp 62–66.

(142) Lee, D. N.; Merson, R. L. Examination of Cottage Cheese Whey Proteins by Scanning Electron Microscopy: Relationship to Membrane Fouling During Ultrafiltration. *J. Dairy Sci.* **1975**, *58* (10), 1423–1432.

(143) Vetier, C.; Bennasar, M.; Torodo de la Fuente, B. Study of the fouling of a mineral microfiltration membrane using scanning electron microscopy and physicochemical analyses in the processing of milk. *J. Dairy Res.* **1988**, *55* (3), 381–400.

(144) Howell, J. H.; Velicangi, O. *Ultrafiltration Membranes and Applications*, 1st ed.; Cooper, A. R., Ed.; Plenum Press: New York, NY, 1980.

(145) Cheryan, M. *Ultrafiltration and Microfiltration Handbook*, 2nd ed.; CRC Press: Boca Raton, 1998.

(146) Blonigen, S. J. Ultrafiltration behavior of polyelectrolyte and protein mixtures, Iowa State University, 1994.

(147) Stalikas, C. D. Extraction, separation, and detection methods for phenolic acids and flavonoids. *J. Sep. Sci.* **2007**, *30* (18), 3268–3295.

(148) Hristozov, D.; Domini, C. E.; Kmetov, V.; Stefanova, V.; Georgieva, D.; Canals, A. Direct ultrasound-assisted extraction of heavy metals from sewage sludge samples for ICP-OES analysis. *Anal. Chim. Acta* **2004**, *516* (1–2), 187–196.

(149) Woldemichael, G.; Tulu, T.; Flechsig, G. U. Solar UV-treatment of water samples for stripping-voltammetric determination of trace heavy metals in Awash river, Ethiopia. *Heliyon* **2016**, *2* (3), e00091.

(150) Gjelstad, A.; Pedersen-Bjergaard, S. Recent developments in electromembrane extraction. *Anal. Methods* **2013**, *5* (18), 4549–4557.

(151) Gjelstad, A.; Rasmussen, K. E.; Pedersen-Bjergaard, S. Electrokinetic migration across artificial liquid membranes. Tuning the membrane chemistry to different types of drug substances. *J. Chromatogr. A* **2006**, *1124* (1–2), 29–34.

(152) Pedersen-Bjergaard, S.; Rasmussen, K. E. Extraction across supported liquid membranes by use of electrical fields. *Anal. Bioanal. Chem.* **2007**, *388* (3), 521–523.

(153) Gjelstad, A.; Andersen, T. M.; Rasmussen, K. E.; Pedersen-Bjergaard, S. Microextraction across supported liquid membranes forced by pH gradients and electrical fields. *J. Chromatogr. A* **2007**, *1157* (1–2), 38–45.

(154) Yamini, Y.; Seidi, S.; Rezazadeh, M. Electrical field-induced extraction and separation techniques: Promising trends in analytical chemistry - A review. *Anal. Chim. Acta* **2014**, *814*, 1–22.

(155) Stichlmair, J.; Schmidt, J.; Proplesch, R. Electroextraction: A novel separation technique. *Chem. Eng. Sci.* **1992**, *47* (12), 3015–3022.

(156) Pedersen-Bjergaard, S.; Rasmussen, K. E. Electrokinetic migration across artificial liquid membranes. New concept for rapid sample preparation of biological fluids. *J. Chromatogr. A* **2006**, *1109* (2), 183–190.

(157) Collins, C. J.; Arrigan, D. W. M. A review of recent advances in electrochemically modulated extraction methods. *Anal. Bioanal. Chem.* **2009**, *393* (3), 835–845.

(158) Breadmore, M. C.; Wuethrich, A.; Li, F.; Phung, S. C.; Kalsoom, U.; Cabot, J. M.; Tehranirokh, M.; Shallan, A. I.; Abdul Keyon, A. S.; See, H. H.; et al. Recent advances in enhancing the sensitivity of electrophoresis and electrochromatography in capillaries and microchips (2014–2016). *Electrophoresis* **2017**, *38* (1), 33–59.

(159) Sekhon, B. S. An overview of capillary electrophoresis: Pharmaceutical, biopharmaceutical and biotechnology applications. *J Pharm Educ Res* **2011**, *2* (2), 2–36.

(160) Song, Y.; Xu, C.; Kuroki, H.; Liao, Y.; Tsunoda, M. Recent trends in analytical methods for the determination of amino acids in biological samples. *J. Pharm. Biomed. Anal.* **2018**, *147*, 35–49.

(161) Deinhammer, R. S.; Ting, E. Y.; Porter, M. D. Electrochemically modulated liquid chromatography (EMLC): a new approach to gradient elution separations. *J. Electroanal. Chem.* **1993**, *362* (1–2), 295–299.

(162) Deng, H.; Van Berkel, G. J.; Takano, H.; Gazda, D.; Porter, M. D. Electrochemically Modulated Liquid Chromatography Coupled On-Line with Electrospray Mass Spectrometry. *Anal. Chem.* **2000**, *72* (11), 2641–2647.

(163) Besra, L.; Liu, M. A review on fundamentals and applications of electrophoretic deposition (EPD). *Prog. Mater. Sci.* **2007**, *52* (1), 1–61.

(164) Boccaccini, A. R.; Keim, S.; Ma, R.; Li, Y.; Zhitomirsky, I. Electrophoretic deposition of biomaterials. *J. R. Soc. Interface* **2010**, *7* (Suppl 5), S581–S613.

(165) Buonomenna, M. G.; Golemme, G.; Perrotta, E. Membrane Operations for Industrial Applications. In *Advances in Chemical Engineering*; InTech: Rijeka, Croatia, 2012; pp 543–562.

(166) Zydney, A. L. Membrane Technology for Purification of Therapeutic Proteins. *Biotechnol. Bioeng.* **2009**, *103* (2), 227–230.

(167) Saxena, A.; Tripathi, B. P.; Kumar, M.; Shahi, V. K. Membrane-based techniques for the separation and purification of proteins: An overview. *Adv. Colloid Interface Sci.* **2009**, *145* (1–2), 1–22.

(168) Vesterberg, O. History of Electrophoretic Methods. *J. Chromatogr.* **1989**, *480*, 3–19.

(169) Shaposhnik, V. A.; Kesore, K. An early history of electrodialysis with permselective membranes. *J. Memb. Sci.* **1997**, *136*, 35–39.

(170) Grebenyuk, V. D.; Grebenyuk, O. V. Electrodialysis: From an Idea to Realization. *Russ. J. Electrochem.* **2002**, *38* (8), 806–809.

(171) Mattson, S. Electrodialysis of the colloidal soil material and the exchangeable bases. *J. Agric. Res.* **1926**, *33* (6), 553–567.

(172) Juda, W.; McRae, W. A. Coherent ion-exchange gels and membranes. *J. Am. Chem. Soc.* **1950**, *72* (2), 1044.

(173) Joseph, N. R.; Stadie, W. C. The simultaneous determination of total base and chloride on the same sample of serum by electrodialysis. *J. Biol. Chem.* **1938**, *125*, 795–799.

(174) Locke, A.; Hirsch, E. F. The fractionation of insulin protein by electrodialysis. *J. Am. Med. Assoc.* **1924**, *83* (24), 1913–1914.

(175) Beaver, J. J.; Bernhard, A. The Electrodialysis of Blood Serum. *J. Biol. Chem.* **1926**, *69* (6), 113–124.

(176) Locke, A.; Hirsch, E. F. The Isolation of Substances with Immune Properties: I. The Fractionation of Iso-Electric Amboceptor Pseudoglobulin by Electrodialysis. *J. Infect. Dis.* **1924**, *35* (6), 519–525.

(177) Öğütveren, Ü. B.; Koparal, S.; Özel, E. Electrodialysis for the removal of copper ions from wastewater. *J. Environ. Sci. Heal. Part A* **1997**, *32* (3), 749–761.

(178) Kesore, K.; Janowski, F.; Shaposhnik, V. A. Highly effective electrodialysis for selective elimination of nitrates from drinking water. *J. Memb. Sci.* **1997**, *127* (1), 17–24.

(179) Ottosen, L. M.; Hansen, H. K.; Laursen, S.; Villumsen, A. Electrodialytic Remediation of Soil Polluted with Copper from Wood Preservation Industry. *Environ. Sci. Technol.* **1997**, *31* (6), 1711–1715.

(180) Mazrou, S.; Kerdjoudj, H.; Cherif, A. T.; Molenat, J. Sodium hydroxide and hydrochloric acid generation from sodium chloride and rock salt by electro-electrodialysis. *J. Appl. Electrochem.* **1997**, *27* (5), 558–567.

(181) Novič, M.; Dovžan, A.; Pihlar, B.; Hudnik, V. Determination of chlorine, sulphur and phosphorus in organic materials by ion chromatography using electrodialysis sample pretreatment. *J. Chromatogr. A* **1995**, *704* (2), 530–534.

(182) Buscher, B. A. P.; Tjadenz, U. R.; van der Greef, J. Three-compartment electrodialysis device for on-line sample clean-up and enrichment prior to capillary electrophoresis. *J. Chromatogr. A* **1997**, *788* (1–2), 165–172.

(183) Debets, A. J. J.; Kok, W. T.; Hupe, K.-P.; Brinkman, U. A. T. Electrodialytic Sample Treatment Coupled On-Line with High-Performance Liquid Chromatography. *Chromatographia* **1990**, *30* (7/8), 361–366.

(184) Kamphorst, J. J.; Tjaden, U. R.; van der Heijden, R.; DeGroot, J.; van der Greef, J.; Hankemeier, T. Feasibility of electrodialysis as a fast and selective sample preparation method for the profiling of low-abundant peptides in biofluids. *Electrophoresis* **2009**, *30* (13), 2284–2292.

(185) Morales-Cid, G.; Cárdenas, S.; Simonet, B. M.; Valcárcel, M. Sample treatments improved by electric fields. *TrAC - Trends Anal. Chem.* **2010**, *29* (2), 158–165.

(186) Daufin, G.; Kerhervé, F. L.; Aimar, P.; Mollé, D.; Léonll, J.; Nau, F. Electrofiltration of solutions of amino acids or peptides. *Lait* **1995**, *75* (2), 105–115.

(187) Gözke, G.; Posten, C. Electrofiltration of Biopolymers. *Food Eng. Rev.* **2010**, *2* (2), 131–146.

(188) Ptasinski, K. J.; Kerkhof, P. J. A. M. Electric Field Driven Separations: Phenomena and Applications. *Sep. Sci. Technol.* **1992**, *27* (8–9), 995–1021.

(189) Weber, K.; Stahl, W. Improvement of filtration kinetics by pressure electrofiltration. *Sep. Purif. Technol.* **2002**, *26* (1), 69–80.

(190) Hofmann, R.; Posten, C. Improvement of dead-end filtration of biopolymers with pressure electrofiltration. *Chem. Eng. Sci.* **2003**, *58* (17), 3847–3858.

(191) Wakeman, R. J.; Sabri, M. N. Utilizing Pulsed Electric-Fields in Cross-Flow Microfiltration of Titania Suspensions. *Chem. Eng. Res. Des.* **1995**, *73* (4), 455–463.

(192) Pesch, G. R.; Du, F.; Schwientek, U.; Gehrmeyer, C.; Maurer, A.; Thöming, J.; Baune, M. Recovery of submicron particles using high-throughput dielectrophoretically switchable filtration. *Sep. Purif. Technol.* **2014**, *132*, 728–735.

(193) Seip, K. F.; Gjelstad, A.; Pedersen-Bjergaard, S. The potential of electromembrane extraction for bioanalytical applications. *Bioanalysis* **2015**, *7* (4), 463–480.

(194) Marothu, V. K.; Gorrepati, M.; Vusa, R. Electromembrane Extraction — A Novel Extraction Technique for Pharmaceutical, Chemical, Clinical and Environmental Analysis. *J. Chromatogr. Sci.* **2013**, *51* (7), 619–631.

(195) Petersen, N. J.; Rasmussen, K. E.; Pedersen-Bjergaard, S.; Gjelstad, A. Electromembrane Extraction from Biological Fluids. *Anal. Sci.* **2011**, *27* (10), 965–972.

(196) Kjelsen, I. J. Ø.; Gjelstad, A.; Rasmussen, K. E.; Pedersen-Bjergaard, S. Low-voltage electromembrane extraction of basic drugs from biological samples. *J. Chromatogr. A* **2008**, *1180* (1–2), 1–9.

(197) Petersen, N. J.; Jensen, H.; Hansen, S. H.; Foss, S. T.; Snakenborg, D.; Pedersen-Bjergaard, S. On-chip electro membrane extraction. *Microfluid. Nanofluidics* **2010**, *9* (4–5), 881–888.

(198) Rezazadeh, M.; Yamini, Y.; Seidi, S. Electromembrane extraction of trace amounts of naltrexone and nalmefene from untreated biological fluids. *J. Chromatogr. B Anal. Technol. Biomed. Life Sci.* **2011**, *879* (15–16), 1143–1148.

(199) Gjelstad, A.; Rasmussen, K. E.; Pedersen-Bjergaard, S. Electromembrane extraction of basic drugs from untreated human plasma and whole blood under physiological pH conditions. *Anal. Bioanal. Chem.* **2009**, *393* (3), 921–928.

(200) Roche, M. E.; Anderson, M. A.; Oda, R. P.; Riggs, B. L.; Strausbauch, M. A.; Okazaki, R.; Wettstein, P. J.; Landers, J. P. Capillary Electrophoresis of Insulin-like Growth Factors: Enhanced Ultraviolet Detection Using Dynamically Coated Capillaries and On-Line Solid-Phase Extraction. *Anal Biochem* **1998**, *258* (1), 87–95.

(201) Strausbauch, M. A.; Xu, S. J.; Ferguson, J. E.; Nunez, M. E.; Machacek, D.; Lawson, G. M.; Wettstein, P. J.; Landers, J. P. Concentration and separation of hypoglycemic drugs using solid-phase extraction-capillary electrophoresis. *J. Chromatogr. A* **1995**, *717* (1–2), 279–291.

(202) Bailes, P. J. Solvent Extraction in an Electrostatic Field. *Ind. Eng. Chem. Process Des. Dev.* **1981**, *20* (3), 564–570.

(203) Campos, C. D. M.; Park, J. K.; Neužil, P.; da Silva, J. A. F.; Manz, A. Membrane-free electroextraction using an aqueous two-phase system. *RSC Adv.* **2014**, *4* (90), 49485–49490.

(204) Orlando, R. M.; Rohwedder, J. J. R.; Rath, S. Electric Field-Assisted Solid Phase Extraction: Devices, Development and Application with a Cationic Model Compound. *Chromatographia* **2014**, *77* (1–2), 133–143.

(205) Orlando, R. M.; Rath, S.; Rohwedder, J. J. R. Semiautomated solid-phase extraction manifold with a solvent-level sensor. *Talanta* **2013**, *116*, 39–44.

(206) Ribeiro, C. C.; Orlando, R. M.; Rohwedder, J. J. R.; Reyes, F. G. R.; Rath, S. Electric field-assisted solid phase extraction and cleanup of ionic compounds in complex food matrices: Fluoroquinolones in eggs. *Talanta* **2016**, *152*, 498–503.

(207) Orlando, R. M.; Rohwedder, J. J. R.; Rath, S. Electric Field-Assisted Solid Phase Extraction: Study of Electrochromatographic Parameters with an Anionic Model Compound. *J. Braz. Chem. Soc.* **2015**, *26* (2), 310–318.

(208) Fang, R.; Yi, L.-X.; Shao, Y.-X.; Zhang, L.; Chen, G.-H. On-line preconcentration in capillary electrophoresis for analysis of agrochemical residues. *J. Liq. Chromatogr. Relat. Technol.* **2014**, *37* (10), 1465–1497.

(209) Bagheri, H.; Piri-Moghadam, H.; Rastegar, S. Magnetic and electric fields assisted electrospun polyamide nanofibers for on-line μ-solid phase extraction and HPLC. *RSC Adv.* **2014**, *4* (94), 52590–52597.

(210) Ramautar, R.; Somsen, G. W.; de Jong, G. J. Recent developments in coupled SPE-CE. *Electrophoresis* **2010**, *31* (1), 44–54.

(211) Eskandari, M.; Yamini, Y.; Fotouhi, L.; Seidi, S. Microextraction of mebendazole across supported liquid membrane forced by pH gradient and electrical field. *J. Pharm. Biomed. Anal.* **2011**, *54* (5), 1173–1179.

(212) He, W.; Baird, M. H. 1.; Chang, J. S. The Effect of Electric Field on Mass Transfer From Drops Dispersed in a Viscous Liquid. *Can. J. Chem. Eng.* **1993**, *71* (3), 366–376.

(213) Campos, C. D. M.; de Campos, R. P. S.; da Silva, J. A. F.; Jesus, D. P.; Orlando, R. M. Sample Preparation Assisted by Electric Field: Foundations, Advances, Applications and Trends. *Quim. Nova* **2015**, *38* (8), 1093–1106.

(214) Wuethrich, A.; Haddad, P. R.; Quirino, J. P. The electric field - An emerging driver in sample preparation. *TrAC - Trends Anal. Chem.* **2016**, *80*, 604–611.

(215) Unterlander, N.; Doucette, A. A. Accelerated SDS depletion from proteins by transmembrane electrophoresis: Impacts of Joule heating. *Electrophoresis* **2018**.

(216) Sueoka, N. Mitotic Replication of Deoxyribonucleic Acid in Chlamydomonas Reinhardi. *Proc. Natl. Acad. Sci. U. S. A.* **1960**, *46* (1), 83–91.

(217) Smith, P. K.; Krohn, R. I.; Hermanson, G. T.; Mallia, A. K.; Gartner, F. H.; Provenzano, M. D.; Fujimoto, E. K.; Goeke, N. M.; Olson, B. J.; Klenk, D. C. Measurement of Protein Using Bicinchoninic Acid. *Anal. Biochem.* **1985**, *150* (1), 76–85.

(218) Arand, M.; Friedberg, T.; Oesch, F. Colorimetric quantitation of trace amounts of sodium lauryl sulfate in the presence of nucleic acids and proteins. *Anal. Biochem.* **1992**, *207* (1), 73–75.

(219) Stephen, K. A liquid chromatography/mass spectrometry approach to quantify sodium dodecyl sulfate in protein containing samples, Dalhousie University, 2014.

(220) Jones, J. T.; Esposito, F. M. An assay evaluation of the methylene blue method for the detection of anionic surfactants in urine. *J. Anal. Toxicol.* **2000**, *24* (5), 323–327.

(221) Orton, D. J.; Doucette, A. A. A universal, high recovery assay for protein quantitation through temperature programmed liquid chromatography (TPLC). *J. Chromatogr. B Anal. Technol. Biomed. Life Sci.* **2013**, *921–922*, 75–80.

(222) Chevallet, M.; Luche, S.; Rabilloud, T. Silver staining of proteins in polyacrylamide gels. *Nat. Protoc.* **2006**, *1* (4), 1852–1858.

(223) Borzova, V. A.; Markossian, K. A.; Chebotareva, N. A.; Kleymenov, S. Y.; Poliansky, N. B.; Muranov, K. O.; Stein-Margolina, V. A.; Shubin, V. V.; Markov, D. I.; Kurganov, B. I. Kinetics of Thermal Denaturation and Aggregation of Bovine Serum Albumin. *PLoS One* **2016**, *11* (4), e0153495.

(224) Kern, R.; Malki, A.; Abdallah, J.; Liebart, J. C.; Dubucs, C.; Yu, M. H.; Richarme, G. Protein Isoaspartate Methyltransferase Is a Multicopy Suppressor of Protein Aggregation in Escherichia coli. *J. Bacteriol.* **2005**, *187* (4), 1377–1383.

(225) Bischof, J. C.; He, X. Thermal Stability of Proteins. *Ann. N. Y. Acad. Sci.* **2005**, *1066* (1), 12–33.

(226) Kumar, S.; Tsai, C.-J.; Nussinov, R. Factors enhancing protein thermostability. *Protein Eng. Des. Sel.* **2000**, *13* (3), 179–191.

(227) Szilágyi, A.; Závodszky, P. Structural differences between mesophilic, modrately thermophiic and exremely thermophilic protein subunits: results of a comprehensive survey. *Structure* **2000**, *8* (5), 493–504.

(228) Sheldon, J. M.; Reed, I. M.; Hawes, C. R. The fine-structure of ultrafiltration membranes. II. Protein fouled membranes. *J. Memb. Sci.* **1991**, *62* (1), 87–102.

(229) Dutta, S.; Bhattacharyya, D. Size of Unfolded and Dissociated Subunits versus that of Native Multimeric Proteins. *J. Biol. Phys.* **2001**, *27* (1), 59–71.

(230) Chaiet, L.; Wolf, F. J. The Properties of Streptavidin, a Biotin-Binding Protein Produced by Streptomycetes. *Arch. Biochem. Biophys.* **1964**, *106*, 1–5.

(231) Kang, W.; Cannon, J. L. A Membrane-Based Electro-Separation Method (MBES) for Sample Clean-Up and Norovirus Concentration. *PLoS One* **2015**, *10* (10), e0141484.

(232) Garcia, B. A. What Does the Future Hold for Top Down Mass Spectrometry? *J. Am. Soc. Mass Spectrom.* **2010**, *21* (2), 193–202.

(233) Tanner, R. E.; Herpigny, B.; Chen, S. H.; Rha, C. K. Conformational change of protein sodium dodecylsulfate complexes in solution: A study of dynamic light scattering. *J. Chem. Phys.* **1982**, *76* (8), 3866–3872.

(234) Sun, X.; Su, X.; Wu, J.; Hinds, B. J. Electrophoretic Transport of Biomolecules through Carbon Nanotube Membranes. *Langmuir* **2011**, *27* (6), 3150–3156.

(235) Wang, Y.; Tang, C. Y. Fouling of Nanofiltration, Reverse Osmosis, and Ultrafiltration Membranes by Protein Mixtures: The Role of Inter-Foulant-Species Interaction. *Environ. Sci. Technol.* **2011**, *45* (15), 6373–6379.

(236) Choe, T. B.; Masse, P.; Verdier, A.; Clifton, M. J. Flux decline in batch ultrafiltration: Concentration polarization and cake formation. *J. Memb. Sci.* **1986**, *26* (1), 1–15.

(237) Ingham, K. C.; Busby, T. F.; Sahlestrom, Y.; Castino, F. Separation of Macromolecules by Ultrafiltration: Influence of Protein Adsorption, Protein-Protein Interactions, and Concentration Polarization. In *Ultrafiltration Membranes and Applications*; Cooper, A. R., Ed.; Plenum Press: New York, NY, 1980; pp 141–158.

(238) Fell, C. J. D.; Kim, K. J.; Chen, V.; Wiley, D. E.; Fane, A. G. Factors Determining Flux and Rejection of Ultrafiltration Membranes. *Chem. Eng. Process.* **1990**, *27* (3), 165–173.

(239) Yoon, S. H. *Membrane Bioreactor Processes: Principles and Applications*, 1st ed.; Advances in Water and Wastewater Transport and Treatment; CRC Press: Boca Raton, 2015.

(240) Jamal, S.; Chang, S.; Zhou, H. Filtration Behaviour and Fouling Mechanisms of Polysaccharides. *Membranes (Basel).* **2014**, *4* (3), 319–332.

(241) Conway-Jacobs, A.; Lewin, L. M. Isoelectric Focusing in Acrylamide Gels: Use of Amphoteric Dyes as Internal Markers for Determination of Isoelectric Points. *Anal. Biochem.* **1971**, *43* (2), 394–400.

(242) Do, D. D.; Elhassadi, A. A. A theory of limiting flux in a stirred batch cell. *J. Memb. Sci.* **1985**, *25* (2), 113–132.

(243) Bellhouse, B. J.; Lewis, R. W. H. A High Efficiency Membrane Separator for Donor Plasmapheresis. *Trans. Am. Soc. Artifical Intern. Organs* **1988**, *34* (3), 747–754.

(244) Jurado, J.; Bellhouse, B. J. Application of Electric Fields and Vortex Mixing for Enhanced Ultrafiltration. *Filtr. Sep.* **1994**, *31* (3), 273–281.

(245) Lee, Y.; Clark, M. M. Modeling of flux decline during crossflow ultrafiltration of colloidal suspensions. *J. Memb. Sci.* **1998**, *149* (2), 181–202.

(246) Shan, H. Membrane Fouling During the Microfiltration of Primary and Secondary Wastewater Treatment Plant Effluents, University of Pittsburgh, 2004.

(247) Quintana, J. B.; Ramil, M.; Rodil, R.; Rodriguez, I.; Cela, R. New Sample Preparation Strategies for Analytical Determinations. In *Encyclopedia of Analytical Chemistry*; Meyers, R. A., Ed.; John Wiley & Sons, Ltd.: Chinchester, UK, 2014; pp 1–98.

(248) Wakeman, R. J. Electrically Enhanced Microfiltration of Albumin Suspensions. *Food Bioprod. Process. Trans. Inst. Chem. Eng. Part C* **1998**, *76* (1), 53–59.

(249) Iritani, E.; Mukai, Y.; Murase, T. Separation of Binary Protein Mixtures by Ultrafiltration. *Filtr. Sep.* **1997**, *34* (9), 967–973.

(250) Nielsen, A. D.; Borch, K.; Westh, P. Thermochemistry of the specific binding of C12 surfactants to bovine serum albumin. *Biochim. Biophys. Acta* **2000**, *1479* (1–2), 321–331.

(251) Bhuyan, A. K. On the Mechanism of SDS-Induced Protein Denaturation. *Biopolymers* **2009**, *93* (2), 186–199.

(252) Unterlander, N.; Abbott, R.; Doucette, A. A. 100th Canadian Chemistry Conference and Exhibition. In *Developing the optimal buffer system for protein purification via transmembrane electrophoresis.*; Toronto, ON, 2017.

(253) Crowell, A. M. J. Methods to Isolate Protein from Detergent-containing Solutions for Proteome Analysis, Dalhousie University, 2014.

(254) Crowell, A. M. J.; Wall, M. J.; Doucette, A. A. Maximizing recovery of water-soluble proteins through acetone precipitation. *Anal. Chim. Acta* **2013**, *796*, 48–54.

(255) Unterlander, N.; Doucette, A. A. Membrane-based SDS depletion ahead of peptide and protein analysis by mass spectrometry. *Proteomics* **2018**.

(256) Hustoft, H. K.; Malerod, H.; Wilson, S. R.; Reubsaet, L.; Lundanes, E.; Greibrokk, T. A Critical Review of Trypsin Digestion for LC-MS Based Proteomics. In *Integrative Proteomics*; Leung, H.-C., Ed.; InTech, 2012; pp 73–93.

(257) Zappacosta, F.; Scott, G. F.; Huddleston, M. J.; Annan, R. S. An Optimized Platform for Hydrophilic Interaction Chromatography-Immobilized Metal Affinity Chromatography Enables Deep Coverage of the Rat Liver Phosphoproteome. *J. Proteome Res.* **2015**, *14* (2), 997–1009.

(258) Ntai, I.; Kim, K.; Fellers, R. T.; Skinner, O. S.; Smith, A. D.; Early, B. P.; Savaryn, J. P.; LeDuc, R. D.; Thomas, P. M.; Kelleher, N. L. Applying Label-Free Quantitation to Top Down Proteomics. *Anal. Chem.* **2014**, *86* (10), 4961–4968.

(259) Schubert, O. T.; Röst, H. L.; Collins, B. C.; Rosenberger, G.; Aebersold, R. Quantitative proteomics: challenges and opportunities in basic and applied research. *Nat. Protoc.* **2017**, *12* (7), 1289–1294.

(260) Bantscheff, M.; Lemeer, S.; Savitski, M. M.; Kuster, B. Quantitative mass spectrometry in proteomics: critical review update from 2007 to the present. *Anal. Bioanlayitical Chem.* **2012**, *404* (4), 939–965.

(261) Van Oudenhove, L.; Devreese, B. A review on recent developments in mass spectrometry instrumentation and quantitative tools advancing bacterial proteomics. *Appl. Microbiol. Biotechnol.* **2013**, *97* (11), 4749–4762.

(262) Colnoe, S. Development of sample preparation methods for shotgun proteomic studies of white adipose tissue, University of Tromso, 2016.

(263) Manza, L. L.; Stamer, S. L.; Ham, A.-J. L.; Codreanu, S. G.; Liebler, D. C. Sample preparation and digestion for proteomic analyses using spin filters. *Proteomics* **2005**, *5* (7), 1742–1745.

(264) Tang, Y.; Underwood, A.; Gielbert, A.; Woodward, M. J.; Petrovska, L. Metaproteomics Analysis Reveals the Adaptation Process for the Chicken Gut Microbiota. *Appl. Environ. Microbiol.* **2014**, *80* (2), 478–485.

(265) Batas, B.; Jones, H. R.; Chaudhuri, J. B. Studies of the hydrodynamic volume changes that occur during refolding of lysozyme using size-exclusion chromatography. *J. Chromatogr. A* **1997**, *766* (1–2), 109–119.

(266) Kay, R.; Barton, C.; Ratcliffe, L.; Matharoo-Ball, B.; Brown, P.; Roberts, J.; Teale, P.; Creaser, C. Enrichment of low molecular weight serum proteins using acetonitrile precipitation for mass spectrometry based proteomic analysis. *Rapid Commun. mass Spectrom.* **2008**, *22* (20), 3255–3260.

(267) Jain, R. K.; Jawade, A. A.; Pingle, S. K.; Tumane, R. G.; Thakkar, L. R. Separation of low molecular weight serum proteins using acetonitrile precipitation assessed by one dimensional gel electrophoresis. *Eur. J. Exp. Biol.* **2015**, *5* (5), 18–23.

(268) Wingfield, P. T. Protein Precipitation Using Ammonium Sulfate. *Curr. Protoc. Protein Sci.* **2001**, *Appendix 3* (Appendix-3F).

(269) Chertov, O.; Simpson, J. T.; Biragyn, A.; Conrads, T. P.; Veenstra, T. D.; Fisher, R. J. Enrichment of low-molecular-weight proteins from biofluids for biomarker discovery. *Expert Rev. Proteomics* **2005**, *2* (1), 139–145.

(270) Klein, C.; Aivaliotis, M.; Olsen, J. V.; Falb, M.; Besir, H.; Scheffer, B.; Bisle, B.; Tebbe, A.; Konstantinidis, K.; Siedler, F.; et al. The Low Molecular Weight Proteome of Halobacterium salinarum. *J. Proteome Res.* **2007**, *6* (4), 1510–1518.

(271) Harper, R. G.; Workman, S. R.; Schuetzner, S.; Timperman, A. T.; Sutton, J. N. Low-molecular-weight human serum proteome using ultrafiltration, isoelectric focusing, and mass spectrometry. *Electrophoresis* **2004**, *25* (9), 1299–1306.

(272) Müller, S. A.; Kohajda, T.; Findeiß, S.; Stadler, P. F.; Washietl, S.; Kellis, M.; von Bergen, M.; Kalkhof, S. Optimization of parameters for coverage of low molecular weight proteins. *Anal. Bioanal. Chem.* **2010**, *398* (7–8), 2867–2881.

(273) Kyte, J.; Doolittle, R. F. A Simple Method for Displaying the Hydropathic Character of a Protein. *J. Mol. Biol.* **1982**, *157* (1), 105–132.

(274) Frank, A. M. A Ranking-Based Scoring Function For Peptide-Spectrum Matches. *J. Proteome Res.* **2009**, *8* (5), 2241–2252.

(275) Liu, H.; Sadygov, R. G.; Yates, J. R. A Model for Random Sampling and Estimation of Relative Protein Abundance in Shotgun Proteomics. *Anal. Chem.* **2004**, *76* (14), 4193–4201.

(276) Wiśniewski, J. R.; Mann, M. Consecutive Proteolytic Digestion in an Enzyme Reactor Increases Depth of Proteomic and Phosphoproteomic Analysis. *Anal. Chem.* **2012**, *84* (6), 2631–2637.

Appendix A: Electronic Supplements*

File S1: Complete list of peptides identified from *C. reinhardtii* with each SDS depletion method

File S2: Complete list of proteins identified from *C. reinhardtii* with each SDS depletion method.

* These files can be accessed through DalSpace

Appendix B: Copyright Agreement Letters

ELSEVIER LICENSE
TERMS AND CONDITIONS

Jun 08, 2018

This Agreement between Dalhousie University ("You") and Elsevier ("Elsevier") consists of your license details and the terms and conditions provided by Elsevier and Copyright Clearance Center.

License Number	4364340009444
License date	Jun 08, 2018
Licensed Content Publisher	Elsevier
Licensed Content Publication	Journal of Molecular Biology
Licensed Content Title	The Role of Decorated SDS Micelles in Sub-CMC Protein Denaturation and Association
Licensed Content Author	Kell K. Andersen,Cristiano L. Oliveira,Kim L. Larsen,Flemming M. Poulsen,Thomas H. Callisen,Peter Westh,Jan S. Pedersen,Daniel Otzen
Licensed Content Date	Aug 7, 2009
Licensed Content Volume	391
Licensed Content Issue	1
Licensed Content Pages	20
Start Page	207
End Page	226
Type of Use	reuse in a thesis/dissertation
Portion	figures/tables/illustrations
Number of figures/tables/illustrations	1
Format	both print and electronic
Are you the author of this Elsevier article?	No
Will you be translating?	No
Original figure numbers	Figure 7
Title of your thesis/dissertation	Investigations of Parameters Impacting Transmembrane Electrophoresis for Improved SDS Depletion of Proteome Samples for Mass Spectrometry
Expected completion date	Jun 2018
Estimated size (number of pages)	250

https://s100.copyright.com/CustomerAdmin/PLF.jsp?ref=6c69dd47-8c8d-42c4-8327-f45a0b563301

JOHN WILEY AND SONS LICENSE TERMS AND CONDITIONS

Jun 08, 2018

This Agreement between Dalhousie University ("You") and John Wiley and Sons ("John Wiley and Sons") consists of your license details and the terms and conditions provided by John Wiley and Sons and Copyright Clearance Center.

License Number	4364340714551
License date	Jun 08, 2018
Licensed Content Publisher	John Wiley and Sons
Licensed Content Publication	Wiley Books
Licensed Content Title	Charged Ultrafiltration and Microfiltration Membranes in Antibody Purification
Licensed Content Date	Aug 15, 2008
Licensed Content Pages	23
Type of use	Dissertation/Thesis
Requestor type	University/Academic
Format	Print and electronic
Portion	Figure/table
Number of figures/tables	1
Original Wiley figure/table number(s)	Figure 16.1
Will you be translating?	No
Title of your thesis / dissertation	Investigations of Parameters Impacting Transmembrane Electrophoresis for Improved SDS Depletion of Proteome Samples for Mass Spectrometry
Expected completion date	Jun 2018
Expected size (number of pages)	250

https://s100.copyright.com/CustomerAdmin/PLF.jsp?ref=3c076dab-cb4c-444d-98c2-ae21c040fd64

JOHN WILEY AND SONS LICENSE TERMS AND CONDITIONS

Jul 12, 2018

This Agreement between Dalhousie University ("You") and John Wiley and Sons ("John Wiley and Sons") consists of your license details and the terms and conditions provided by John Wiley and Sons and Copyright Clearance Center.

License Number	4386511328728
License date	Jul 12, 2018
Licensed Content Publisher	John Wiley and Sons
Licensed Content Publication	Electrophoresis
Licensed Content Title	Accelerated SDS depletion from proteins by transmembrane electrophoresis: Impacts of Joule heating
Licensed Content Author	Nicole Unterlander, Alan Austin Doucette
Licensed Content Date	Mar 1, 2018
Licensed Content Volume	39
Licensed Content Issue	11
Licensed Content Pages	8
Type of use	Dissertation/Thesis
Requestor type	Author of this Wiley article
Format	Electronic
Portion	Full article
Will you be translating?	No
Title of your thesis / dissertation	Investigations of Parameters Impacting Transmembrane Electrophoresis for Improved SDS Depletion of Proteome Samples for Mass Spectrometry
Expected completion date	Jun 2018
Expected size (number of pages)	250

https://s100.copyright.com/AppDispatchServlet

JOHN WILEY AND SONS LICENSE TERMS AND CONDITIONS

Jul 12, 2018

This Agreement between Dalhousie University ("You") and John Wiley and Sons ("John Wiley and Sons") consists of your license details and the terms and conditions provided by John Wiley and Sons and Copyright Clearance Center.

License Number	4386520099273
License date	Jul 12, 2018
Licensed Content Publisher	John Wiley and Sons
Licensed Content Publication	Proteomics
Licensed Content Title	Membrane-Based SDS Depletion Ahead of Peptide and Protein Analysis by Mass Spectrometry
Licensed Content Author	Nicole Unterlander, Alan A. Doucette
Licensed Content Date	Apr 16, 2018
Licensed Content Volume	18
Licensed Content Issue	9
Licensed Content Pages	8
Type of use	Dissertation/Thesis
Requestor type	Author of this Wiley article
Format	Electronic
Portion	Full article
Will you be translating?	No
Title of your thesis / dissertation	Investigations of Parameters Impacting Transmembrane Electrophoresis for Improved SDS Depletion of Proteome Samples for Mass Spectrometry
Expected completion date	Jun 2018
Expected size (number of pages)	250

https://s100.copyright.com/AppDispatchServlet